BRICS
Workshop on Biophotonics-2021

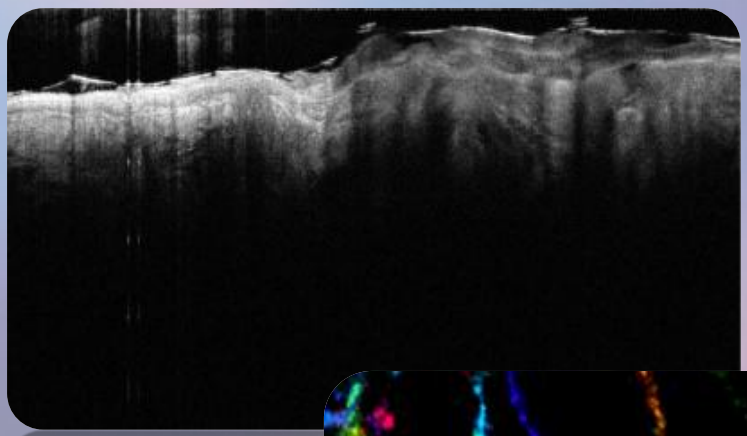

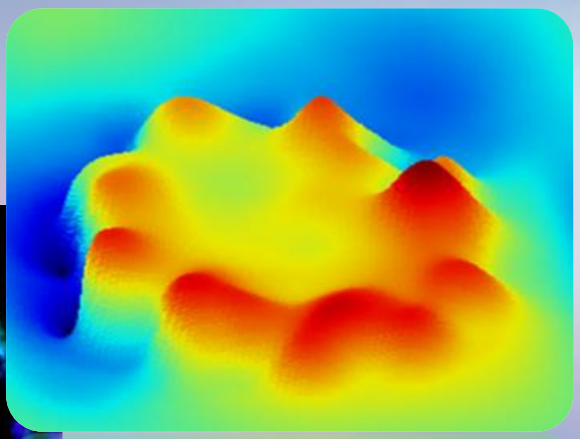

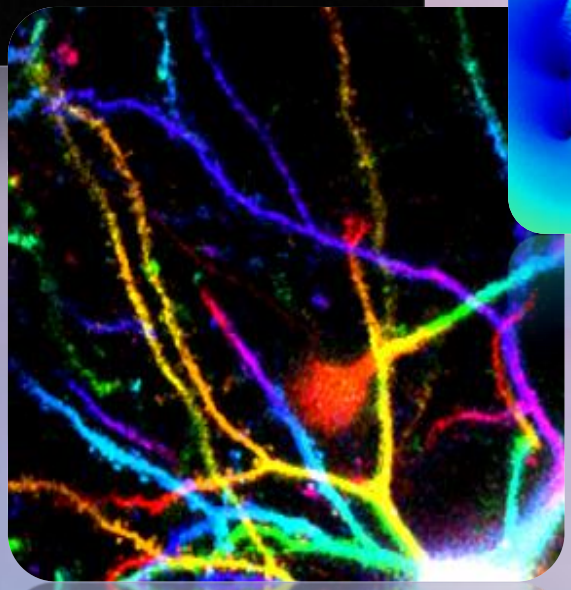

SEPTEMBER 27 – 29, 2021
UNIVERSITY OF SÃO PAULO, BRAZIL
SARATOV STATE UNIVERSITY, SARATOV, RUSSIA
MANIPAL ACADEMY OF HIGHER EDUCATION, INDIA
HAINAN UNIVERSITY, CHINA
UNIVERSITY OF JOHANNESBURG, RSA

SARATOV FALL MEETING
BRICS workshop'21

MANIPAL ACADEMY of HIGHER EDUCATION
(Deemed to be University under Section 3 of the UGC Act, 1956)

OPTICA Formerly OSA

UNIVERSITY OF JOHANNESBURG

Universidade de São Paulo

SPIE.

BRICS Workshop on Biophotonics - 2021
Book of Abstracts

Edited by Polina A. Dyachenko, Qingming Luo,
Vanderlei Salvador Bagnato, Santhosh Chidangil,
Heidi Abrahamse and Valery V. Tuchin

SEPTEMBER 27 – 29, 2021

SARATOV

УДК 535.8
ББК 22.34
С 23

BRICS Workshop on Biophotonics -2021. Book of Abstracts/ Edited by P.A. Dyachenko – Russian Federation, Qingming Luo – China, Vanderlei Salvador Bagnato – Brazil, Santhosh Chidangil – India, Heidi Abrahamse – RSA, V.V. Tuchin – Russian Federation. – 85 p.

The collection includes extended abstracts of lectures and reports of the participants of the BRICS Workshop on Biophotonics - 2021, held online as part of the Saratov Fall Meeting 2021.

ISBN 978-5-6048070-2-6

Content

BRICS Workshop on Biophotonics - 2021
SEPTEMBER 27 –29, 2021, SARATOV, RUSSIA

BRICS Workshop on Biophotonics - 2021 was held online, on 27-29, Sept. 2021, and was intended to bring together scientists, engineers and clinical researchers from the BRICS countries of various fields of science involved in the application of optics, photonics and imaging technologies to solve urgent problems of biology and medicine. The scope of this Forum ranges from basic research to instrumentation, preclinical and clinical research, mainly in those areas where researchers from the BRICS countries are world leaders. The topics are extensive and cover (but are not limited to) the following:

- ✓ **Optical Interactions in Tissue and Cells**
- ✓ **Biomedical Spectroscopy, Microscopy and Imaging**
- ✓ **Advanced Optical Techniques for Clinical Medicine**
- ✓ **Multimodal Biomedical Imaging**
- ✓ **Nano/Biophotonics**
- ✓ **Photonic Therapeutics, Diagnostics and Instrumentations**
- ✓ **Tissue Optical Clearing and Drug Delivery**
- ✓ **Antimicrobial and Antiviral Phototherapy**

Chairs:

Valery V Tuchin, Saratov State University, Russia
Qingming Luo, Hainan University, China
Vanderlei Salvador Bagnato, University of São Paulo, Brazil
Santhosh Chidangil, Manipal Academy of Higher Education, India
Heidi Abrahamse, University of Johannesburg, RSA

Secretaries:

Polina A. Dyachenko, SSU, Russia
Dongyu Li, HUST, China
Lilian Moriyama & Natalia M. Inada, University of São Paulo, Brazil
Renu John, Indian Institute of Technology, Hyderabad, India

ORGANIZED BY

- **SARATOV STATE UNIVERSITY (NATIONAL RESEARCH UNIVERSITY OF RUSSIA) (SSU)**
- **SKOLKOVO INSTITUTE OF SCIENCE & TECHNOLOGY, SKOLKOVO INNOVATION CENTRE, MOSCOW, RUSSIA**
- **HAINAN UNIVERSITY, CHINA**
- **HUAZHONG UNIVERSITY OF SCIENCE AND TECHNOLOGY (HUST), CHINA**
- **BIOMEDICAL PHOTONICS COMMITTEE OF CHINESE OPTICAL SOCIETY**
- **NATIONAL INSTITUTE OF SCIENCE AND TECHNOLOGY OF OPTICS AND PHOTONICS (INOF), UNIVERSITY OF SÃO PAULO, BRAZIL**
- **CENTRE OF EXCELLENCE FOR BIOPHOTONICS, DEPARTMENT OF ATOMIC AND MOLECULAR PHYSICS, MANIPAL ACADEMY OF HIGHER EDUCATION, INDIA**
- **UNIVERSITY OF JOHANNESBURG, THE REPUBLIC OF SOUTH AFRICA (RSA)**
- **SCIENCE MEDICAL CENTER, SSU**
- **INTERNATIONAL RESEARCH-EDUCATIONAL CENTER OF OPTICAL TECHNOLOGIES FOR INDUSTRY AND MEDICINE “PHOTONICS”, SSU**
- **SPIE STUDENT CHAPTER OF SSU**
- **OPTICA STUDENT CHAPTER OF SSU**

OPTIMIZE THE PERFORMANCE OF STIMULATED EMISSION DEPLETION (STED) NANOSCOPY THROUGH OPTICAL METHODS AND PROBES

DOI 10.24412/cl-36896-2021-1-7-7

JUNLE QU, ZHIGANG YANG, WEI YAN, LUWEI WANG, JIA LI, JIA ZHANG, JIALIN WANG

Center for Biomedical Optics and Photonics & College of Physics and Optoelectronic Engineering, Shenzhen University, China

jlqu@szu.edu.cn

ABSTRACT

Stimulated emission depletion (STED) nanoscopy is an advanced super-resolution imaging technique which can provide a lateral resolution of 10-80 nm and longitudinal resolution of 30-600 nm with high imaging speed. These abilities stimulated its increasing contribution in visualizing and understanding many complex biological structures and dynamic functions at nanoscale level. However, for live cell STED imaging, the use of intense STED laser could be detrimental as it can cause severe photodamage to live cells, tissues and even fluorophores. Moreover, use of intense STED laser is likely to accelerate photobleaching process of fluorophores which may impede long-term STED imaging. We proposed two strategies to optimize STED imaging performance with reduced STED laser power. The first method relies on the development of novel STED imaging techniques such as adaptive optics, phasor analysis, digital enhancement and temporal and spatial modulation to lower the depletion power. The other method relies upon the development of new dedicated STED probes with better photostability and lower saturation intensity, including perovskite quantum dots, carbon dots, organosilicon nanohybrids and enhanced squaraine variant probe. Furthermore, a dual-color STED microscope with a single laser source is developed and demonstrated for simultaneous STED imaging of mitochondria and tubulin in HeLa cells.

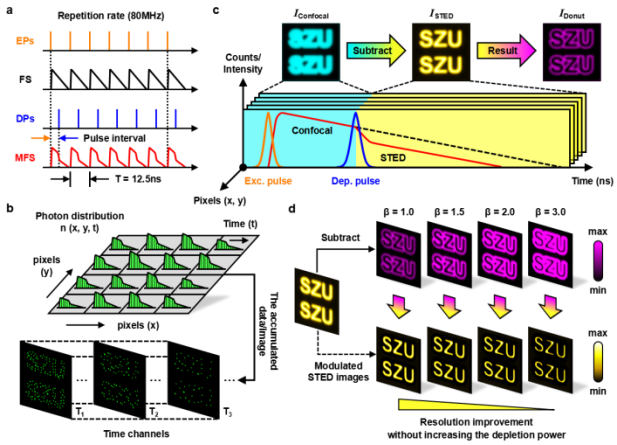

(a)

Figure: *A space-time modulation method (modulated STED) based on FLIM technique*

REFERENCES

[1] W. Yan, Y. Yang, Y. Tan, X. Chen, Y. Li, J. Qu, T. Ye, Coherent optical adaptive technique improves the spatial resolution of STED microscopy in thick samples, Photonics Res., 5:176-181(2017).

[2] L. Wang, W. Yan, R. Li, X. Weng, J. Zhang, Z. Yang, L. Liu, J. Qu, Aberration correction for improving the image quality in STED microscopy using the genetic Algorithm, Nanophotonics, 7:1971-1980(2018).

[3] Y. Chen, L. Wang, W. Yan, X. Peng, J. Qu, J. Song, Elimination of Re-excitation in Stimulated Emission Depletion Nanoscopy Based on Photon Extraction in a Phasor Plot, Laser Photonics Rev., 14: 1900352(2020).

[4] S. Ye, W. Yan, M. Zhao, X. Peng, J. Song, J. Qu, Low-Saturation-Intensity, High-Photostability, and High-Resolution STED Nanoscopy Assisted by CsPbBr3 Quantum Dots, Adv. Mater., 30:201800167(2018).

[5] X. Yang, Z. Yang, Z. Wu, Y. He, C. Shan, P. Chai, C. Ma, M. Tian, J. Teng, D. Jin, W. Yan, P. Das, J. Qu, P. Xi, Mitochondrial dynamics quantitatively revealed by STED nanoscopy with an enhanced squaraine variant probe, Nature Communications, 11, 1:1-9(2020).

[6] J. Wang, J. Zhang, L. Wang, X. Gao, Y. Shao, L. Liu, Z. Yang, W. Yan, J. Qu, Dual-color STED super-resolution microscope using a single laser source, J. Biophotonics, 13: e202000057(2020).

CLINICAL APPLICATIONS OF OCT IN GASTROENTEROLOGY

DOI 10.24412/cl-36896-2021-1-8-12

NIJAS MOHAMED[1], PAWAN KUMAR[1], RENU JOHN1*, S. ANURADHA SEKARAN[2], R. PRADEEP[3], D. NAGESHWAR REDDY[4]

[1]Medical Optics and Sensors Laboratory, Department of Biomedical Engineering, Indian Institute of Technology Hyderabad, Telangana-502285,
[2]Pathology & Lab. Medicine, Asian Institute of Gastroenterology Hyderabad
[3]Surgical Gastroenterology, Asian Institute of Gastroenterology Hyderabad
[4]Medical Gastroenterology, Asian Institute of Gastroenterology Hyderabad
**Email address for correspondence: renujohn@bme.iith.ac.in*

ABSTRACT

Optical coherence tomography (OCT) has emerged as an important tool in bio-imaging. Being a non-invasive and real-time imaging technique, it offers many promising applications in the medical field. OCT is very effective for imaging micro-scale internal structures of the various biological samples up to a depth of 2-3 mm. The invention of this near-infrared light-based, low coherence interferometric imaging technique has revolutionized the field of three-dimensional and cross-sectional tissue imaging by bridging the resolution gap between microscopy and ultrasound imaging techniques. In recent times, OCT has been established as a reliable standard procedure for diagnosing ophthalmic anomalies like Age-related macular degeneration (AMD), diabetic retinopathy, corneal edema etc. The highly sensitive subsurface imaging capability of the OCT system makes it a potential tool for the diagnosis of gastrointestinal (GI) tract cancer at the very beginning stage. The micro-scale lateral and axial resolution of the OCT system provides an edge to it on the other GI tract imaging modalities in detecting early neoplastic changes in the mucosa of the GI tract. We report this study with the prime focus on morphological differentiation and clear margin assessment of the tissue to exhibit the potential of the OCT system for early diagnosis and guided surgery in the case of gastric cancer.

Keywords: Optical coherence tomography, Cancer imaging, Gastric cancer, Gastrointestinal tract imaging.

Introduction:

OCT was derived from the low coherence interferometry imaging concept based on a Michelson interferometer and shown for the first time in 1990 by Huang et al. At the Massachusetts Institute of Technology in Prof James Fujimoto's laboratory [1]. It was quickly discovered to be a useful tool for retinal imaging. The field of OCT imaging is now much more diversified, with systems used in medical imaging, art restoration, non-destructive testing, thin-film analysis, and other applications. Real-time processing of OCT data is now possible thanks to advances in parallel computing and GPU architecture. As a result, OCT has the potential to become a standard imaging modality in the near future [2,3].

Tomography is an imaging technology that uses numerous cross-sectional pictures to create 2D or 3D representations of the sample. Optical tomography is a type of tomography that uses photons to create images. Optical coherence tomography (OCT), Optical Diffraction Tomography (ODT), and Diffuse Optical Tomography (DOT) are the three primary forms of optical tomography [4]. OCT is one of the three that is particularly important for the following reasons:

• In OCT, the axial and lateral resolutions are decoupled or independent of one another.

• OCT provides millimetre-level depth resolution for in-vivo and ex-vivo whole-body imaging.

• OCT uses IR on near IR light for imaging, which has less scattering and has a higher penetration depth in biological tissues and is the only technology that delivers micrometre scale axial resolution for microscopic imaging structures.

• It is a non-invasive, label-free approach that can also be utilized for functional/multi-modal imaging, albeit exogenous contrast ants may be used if necessary

Low coherence sources like superluminescent diodes (SLD), wideband, or supercontinuum laser sources are used in OCT. This is due to the fact that the lateral resolution is inversely related to the light bandwidth [5]. A source with low spatial and temporal coherence is ideal for a high-resolution OCT device. However, there is typically an intrinsic trade-off between temporal and spatial coherence in most sources, as systems with low spatial coherence also have low temporal coherence. SLDs, which act in a similar way to laser diodes, are frequently used as sources in commercial systems. Because of their broad emission bandwidths and moderate temporal coherence, SLDs are a viable

choice for OCT sources. Combining two or more SLDs with different emission bandwidths can result in extremely high bandwidths and ultra-high-resolution imaging [6]. Broadband supercontinuum laser sources, on the other hand, are emerging as viable sources for OCT due to their massive emission bandwidths and better temporal coherence characteristic of laser sources.

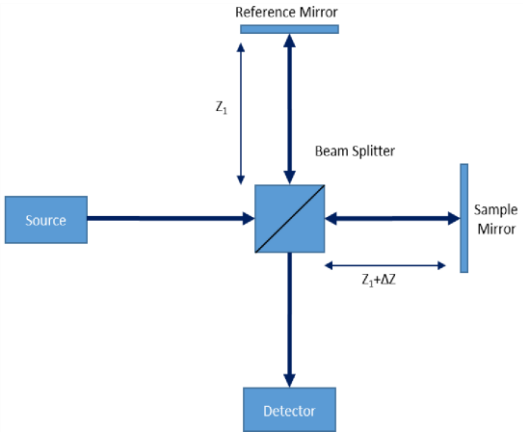

Figure 1. *Basic OCT set up using Michelson Interferometer*

Time Domain OCT (TD-OCT) and Fourier Domain OCT are the primary imaging modalities used in OCT (FD-OCT). The sample is placed in one of the arms of a balanced interferometer, and the interferogram is recorded with the help of a detector in TD-OCT. The refractive index variation in the depth profile of the sample is encoded in the interferogram, which will provide the variations in-depth, also known as an axial scan image or A-Scan image. A lateral scan or B -scan can be formed by raster scanning several A-scans along with the sample. Because each B-scan is a cross-sectional image, a volumetric image of the sample can be obtained by stacking B-scans.

On the other hand, FD-OCT records the spectrum using a dispersion element, commonly a grating. Later Fourier transform is applied on the spectrum to get the A-scan image. Hence, compared to TD-OCT, this gives higher scan rates and a significant SNR advantage to FD-OCT. OCT has a wide range of functional modalities. They get functional information by utilizing one or more of the sample's optical characteristics. Spectroscopic OCT, for example, employs spectral features such as wavelength-dependent absorption or scattering to acquire functional information from a sample, such as the concentration of a particular component [7].

Although OCT has a wide range of applications, it used to be an expensive optical setup, which was one of its main drawbacks and is the key reason why OCT is still not widely used in medical imaging. However, the cost of OCT systems is decreasing now as new technologies develop, such as fibre-based supercontinuum sources, fibre-based systems, integrated optical components, etc. Another issue is the OCT size of the OCT system. With the advent of small, fibre-based OCT devices [8], even this problem has an optimal solution. The development of integrated optical devices such as fibre mirrors, circulators, and other components is projected to reduce OCT system size further. OCT modules the size of a briefcase have previously been demonstrated, including a battery-operated source that makes the device portable [9].

Stomach cancer is the world's fifth most prevalent cancer and the third most significant cause of cancer-related death. Males are twice as likely as females to have it. Eastern Asia has the highest incidence rates of all geographic locations, and the bacterium Helicobacter Pilori is the primary etiological factor in nearly 90% of cases [10]. The Epstein-Barr virus is another pathogen linked to stomach cancer. This pathogen is present in the malignant cells of 80 per cent of stomach carcinomas with lymphoid stroma but not in the normal epithelial cells. However, its significance in carcinogenesis is unknown [11]. Other proven risk factors for stomach cancer include poor eating habits, heavy alcohol usage, persistent smoking, and a lack of fruit intake. Early detection of stomach cancer can dramatically enhance survival chances. Stomach cancers are divided into two types based on where they occur: (i) non-cardia gastric cancer, which affects the distal region of the stomach, and (ii) cancers of the gastric cardia [12].

Because most patients with early-stage stomach cancer are asymptomatic, diagnosis is typically delayed until the disease has progressed. Anorexia, dyspepsia, weight loss, and stomach pain are the most typical symptoms at the time of diagnosis. Dysphagia may be seen in patients with tumours at the gastro-oesophageal junction or in the proximal stomach. Endoscopy and biopsy are commonly used to diagnose stomach cancer. The chief staging modalities for locally advanced gastric cancer are endoscopic ultrasonography and chest and abdomen CT scans. Laparoscopy is performed to rule out the metastatic peritoneal disease with a limited volume. PET-CT and MRI aren't commonly used to diagnose and

stage stomach cancer. However, there is mounting evidence that PET-CT can help with staging by detecting affected lymph nodes and metastatic disease. On the other hand, these tests are not always accurate, especially in individuals with mucinous tumours, as they may underestimate the severity of the disease [13,14].

In this paper, we report using a Spectral Domain OCT system to detect malignancies in the Gastrointestinal tract. We demonstrate the application of OCT for the demarcation of tumours in stomach tissues and the identification of malignancies, and the diagnoses were later reaffirmed by comparing with results of gold standard histopathology

Experimental Methods:

Surgical tissue samples were taken from patients who had been diagnosed with a gastrointestinal tumour. The omentum was connected to the gastrectomy specimen, which measured 30x22x4cms. One end of the stomach was stapled (distal resected end), while the other was opened and everted. The specimen was promptly moved to a standard saline medium to avoid tissue breakdown. For imaging, the same was quickly kept under SD-OCT. B scan imaging was used to identify normal tissues and tumorous sections of the samples in various places. The sample was thoroughly inspected to determine the various stages of the tumour. The sites were then marked with India ink to be easily identified during histology. After the images are obtained, the specimen is put to a formaldehyde solution. Then the sample is sent for histopathology, and images are compared with OCT images.

Results:

OCT images were captured and processed to analyse different stages of tumours in the obtained sample. Figure 2 shows the sample and the processed OCT images.

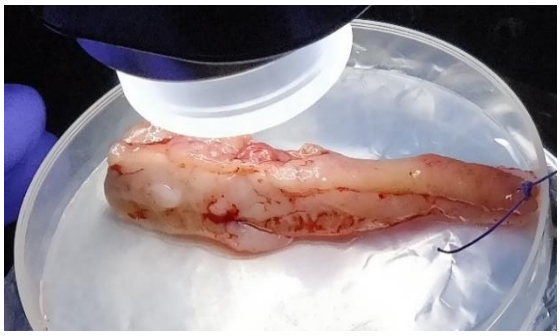

a.

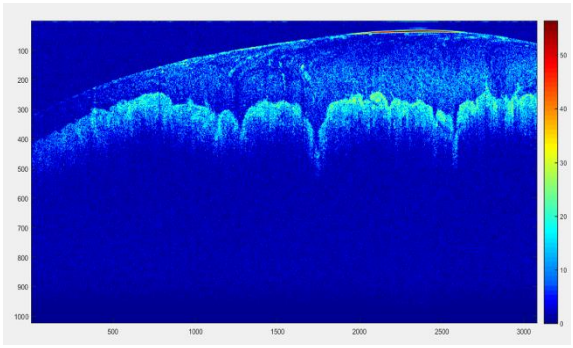

b.

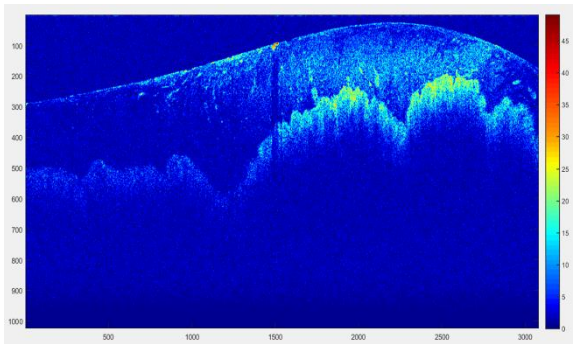

c.

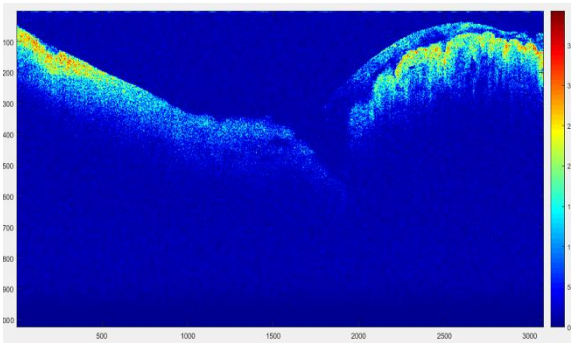

d.

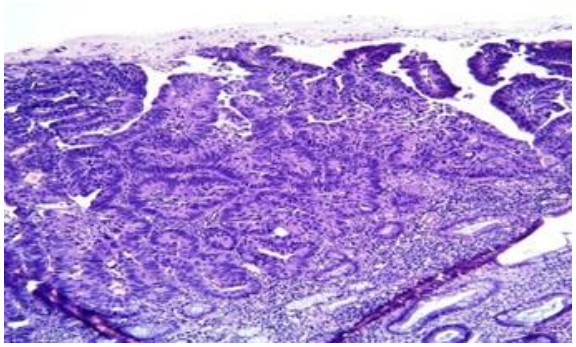

e.

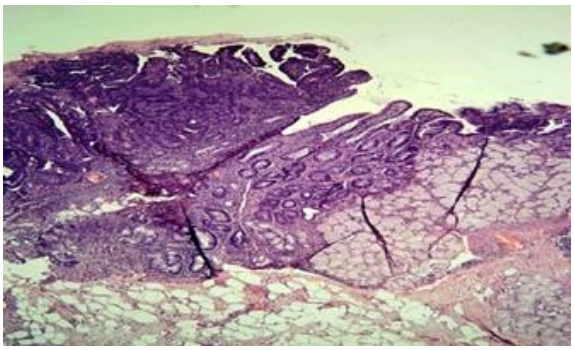

f.

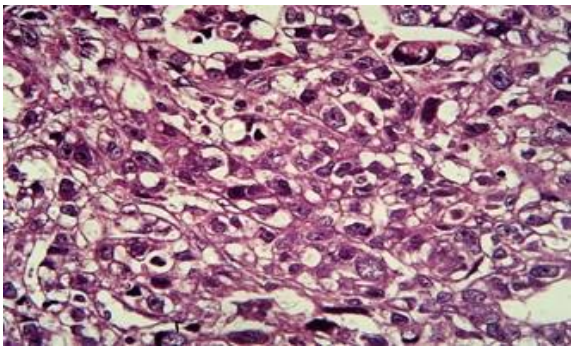

g.

Figure 2 *(a) Shows the sample (oesophagal tumour tissue) cross-section where OCT is performed (b) Normal tissue OCT image (c) OCT image of the tissue in transition stage (d) OCT image of a fully developed tumour (e) Histopathology result of normal tissue (f) histopathology result of marginal tissue (g) Histopathology shows infiltrating tumour to the muscularis mucosa*

Evident morphological differences between cancer and normal tissue could be observed. The presence of the gastric pits in the epithelium lining of the tissue indicates healthy mucosa. Neoplastic changes occur with the extinction of the gastric pits and entirely disappear in malignancy conditions. However, the morphological features observed in the cross-sectional image produced by the OCT system could not differentiate between dysplasia and cancer. After comparing the OCT images and histopathology results, we saw that the histopathology results confirm the OCT findings. The study reaffirms that the OCT can be used to detect gastrointestinal tumours in an early stage, as it can differentiate between normal, malignant, and marginally tumorous tissues. This can save a lot of time and effort as the OCT imaging can be done *in-vivo* compared to histopathology. Moreover, the system is real-time and can be used for quick imaging.

Conclusions:

The study reaffirms that the OCT can be used to detect gastrointestinal tumours in an early stage, as it can differentiate between normal, malignant, and marginally tumorous tissues. This can save a lot of time and effort as the OCT imaging can be done *in-vivo* compared to histopathology. Moreover, the system is real-time and can be used for quick imaging. The incorporation of artificial intelligence (AI) can further improve the diagnostic capability of OCT such that it can differentiate between dysplasia and cancer.

Reference:

[1] Fujimoto, James G., et al. "Optical biopsy and imaging using optical coherence tomography." *Nature medicine* 1.9 (1995): 970-972.

[2] Li, Xiqi, Guohua Shi, and Yudong Zhang. "High-speed optical coherence tomography signal processing on GPU." *Journal of Physics: Conference Series*. Vol. 277. No. 1. IOP Publishing, 2011.

[3] Jian, Yifan, Kevin Wong, and Marinko V. Sarunic. "Graphics processing unit accelerated optical coherence tomography processing at megahertz axial scan rate and high resolution video rate volumetric rendering." *Journal of biomedical optics* 18.2 (2013): 026002.

[4] Boas, David A., Constantinos Pitris, and Nimmi Ramanujam, eds. *Handbook of biomedical optics*. CRC press, 2016.

[5] Fujimoto, James G., et al. "Optical coherence tomography: an emerging technology for biomedical imaging and optical biopsy." *Neoplasia* 2.1-2 (2000): 9-25.

[6] Consortini, Anna. *Trends in Optics: Research, Developments, and Applications*. Academic Press, 1996.

[7] Kim, Jina, et al. "Functional optical coherence tomography: principles and progress." *Physics in Medicine & Biology* 60.10 (2015): R211.

[8] Schmitt, Joseph M. "Optical coherence tomography (OCT): a review." *IEEE Journal of selected topics in quantum electronics* 5.4 (1999): 1205-1215.

[9] Kim, Sanghoon, et al. "Design and implementation of a low-cost, portable OCT system." *Biomedical optics express* 9.3 (2018): 1232-1243.

[10] Bray, Freddie, et al. "Global cancer statistics 2018: GLOBOCAN estimates of incidence and mortality worldwide for 36 cancers in 185 countries (vol 68, pg 394, 2018)." *Ca-a Cancer Journal for Clinicians* 70.4 (2020): 313-313.

[11] Wu, Ming–Shiang, Chia–Tung Shun, Chung–Chun Wu, Tsuey–Ying Hsu, Ming–Tsan Lin, Ming–Chu Chang, Hsiu–Po Wang, and Jaw–Town Lin. "Epstein–Barr virus—associated gastric carcinomas: relation to H. pylori infection and genetic alterations." *Gastroenterology* 118, no. 6 (2000): 1031-1038.

[12] Layke, John C., and Peter P. Lopez. "Gastric cancer: diagnosis and treatment options." *American family physician* 69.5 (2004): 1133-1140.

[13] Altini, Corinna, Artor Niccoli Asabella, Alessandra Di Palo, Margherita Fanelli, Cristina Ferrari, Marco Moschetta, and Giuseppe Rubini. "18F-FDG PET/CT role in staging of gastric carcinomas: comparison with conventional contrast enhancement computed tomography." *Medicine* 94, no. 20 (2015).

[14] Waddell, T., M. Verheij, W. Allum, D. Cunningham, A. Cervantes, and D. Arnold. "Gastric cancer: ESMO–ESSO–ESTRO Clinical Practice Guidelines for diagnosis, treatment and follow-up." *Annals of Oncology* 24 (2013): vi57-vi63.

BIOPHOTONICS OF BODY FLUIDS FOR CLINICAL APPLICATIONS: MICRO-RAMAN STUDY OF BLOOD CELLS IN INTRAVENOUS FLUIDS

DOI 10.24412/cl-36896-2021-1-13-17

SANTHOSH CHIDANGIL, MITHUN N., REENA V. JOHN, SPHURTI S. ADIGAL, NIDHEESH V.R. AND JIJO LUKOSE

Centre of Excellence for Biophotonics
Department of Atomic and Molecular Physics,
Manipal Academy of Higher Education
Manipal, Karnataka, India-576104
Email:santhosh.cls@manipal.edu

Investigation of body fluids is of paramount importance since it carries a pool of biological markers, which can reflect the health status of humans. Technological advancements in the field of biophotonics offer highly sensitive, objective and rapid detection of abnormal health conditions from body fluid analysis. Raman spectroscopy has been widely regarded as reliable spectroscopic tool for the characterization of body fluids due to its minimal interference imposed by aqueous environment. Raman Investigation of blood cells under physiological condition is restricted due to Brownian motion of micron sized cells. In view of this, spectroscopic characterizations of live cells in intravenous fluids has been performed using a custom built Raman Tweezers, which involves the optical arresting of cells with the aid of tightly focused laser beam.

Introduction

Raman spectroscopy technique is considered as a widely accepted methodstechnique for studying biological samples [1]. The technique has been in use for various fields like molecular structure analysis, biochemical research, forensic science, disease diagnosis, chemical analysis etc. [2, 3]. Raman spectroscopy uses inelastic light scattering to provide enough details about the molecular makeup of materials, such as the specific functional groups found in biological and chemical analytes [4]. In Raman spectroscopy techniques the monochromatic light radiation is allowed to interact with the sample and the scattered light will detected by the spectrograph/spectrometer. The most of the light will be elastic scattered (Rayleigh scattering) and the small portion inelastic scattered (Raman scattering) [5]. The Raman signals (Stokes Raman scattered radiation) collected using an edge filter after removing the Rayleigh scattered radiation can be used as a "fingerprint" for the identification of the target molecular species.

Raman spectroscopic investigations of single live cells were possible with the aid of optical tweezers [6]. The Raman spectroscopic technique was combined with the Optical tweezers to form Laser tweezers Raman spectroscopy. The spectroscopic investigations of live cells were very difficult due to the Brownian motion of the cells from the liquid media. The hurdle was overcome by the invention of Optical tweezers technique by Arthur Ashkin [7, 8]. An optical tweezers technique consist of a tightly focused laser beam to arrest the moving cells for Raman measurements. Different research groups investigated the biochemical changes in Red Blood Cells (RBCs) as a function of temperature, the interaction of cells with various external agents (chemicals), laser irradiation, and so on [9-12].

Intravenous fluids (IV fluids) are liquids delivered straight into the veins of patients who are unable to meet their daily demands through food or drink. Water, salts, and sugar are all present in the intravenous fluids. There are different intravenous fluids in daily use under healthcare settings. Several groups are conducting research on intravenous fluid infusion and the after effects [13, 14]. Coburn H. Allen et al. conducted a study to compare the effects of normal saline and Plasmalyte-An intravenous fluid is a replacement in children suffering from moderate to severe dehydration due to acute gastroenteritis (AGE). From this study they have concluded that the plasmalyte-A infusion is more effective than normal saline infusion [15]. Scott A. Kirkley et al. conducted a comparative research based on Red Blood Cell washing with plasmalyte-A and normal saline. They found that RBCs held for 10 to 39 days and washed with plasmalyte-A had less hemolysis and a longer storage time than those stored in normal saline [16]. Neil Blumberg et.al conducted an experiment based on the impact of Normal saline and plasmalyte-A on sickle cell and normal RBCs [17]. The RBCs incubated (in-vitro) with normal saline was showing more hemolysis than Plasmalyte-A. They have also mentioned that the normal saline increases the rate of renal failure in critically ill patients. So the studies related to the impact of intravenous fluids on the single live RBCs have paramount importance. The microscopic images and quantitative phase images of the RBCs suspended in blood plasma and intravenous crystalloid fluids were also discussed in this current work.

Materials and methods

The samples were collected from the Blood Bank, Kasturba Medical College, Manipal with the permission of Institutional ethics committee. The fresh and healthy blood samples collected from the Blood bank was centrifuged for 5 minutes with 3000 rpm for obtaining packed RBCs. For the current study the packed RBCs were suspended in different intravenous crystalloid fluids (Normal saline 0.9%, Plasmalyte-A, Ringer lactate, Hypertonic saline 3%, Hypotonic saline

0.45%, Dextrose normal saline (DNS) and Dextrose 5%). The current experiment was carried out for studying the effect of intravenous crystalloid fluids on single live RBCs. Because blood plasma maintains physiological conditions to a large extent, RBCs suspended in blood plasma were used as a control. The large dilution of packed cells in the intravenous crystalloid fluids prevented multiple cell trapping (0.5 µl packed RBCs in 1 ml of crystalloid fluids).

The experiments were conducted using home-built Raman tweezers spectroscopy setup shown in Figure 1. The laser beam with the wavelength of 785 nm (Star bright diode laser, Torsana laser tech, Denmark) was used for both trapping as well as the excitation of the live RBCs suspended in intravenous crystalloid fluids. A 100X oil immersion microscope objective was employed to create a tightly focused laser beam for trapping a single living cell (Nikon, plan fluor, Japan). The back scattered signals from the sample were collected using the same 100X microscope objective, but the Rayleigh scattered signals were blocked using an Edge filter. The Raman signals were directed to the spectrometer (iHR320, Horiba Jobin Yvon) with liquid nitrogen cooled CCD (Symphony 1024 × 256-OPEN-1LS). All the spectra were recorded from different RBCs with 3 mW laser power for avoiding the photo-damage of the cells. The exposure time and accumulation number for each spectra were 60 seconds and 2 respectively.

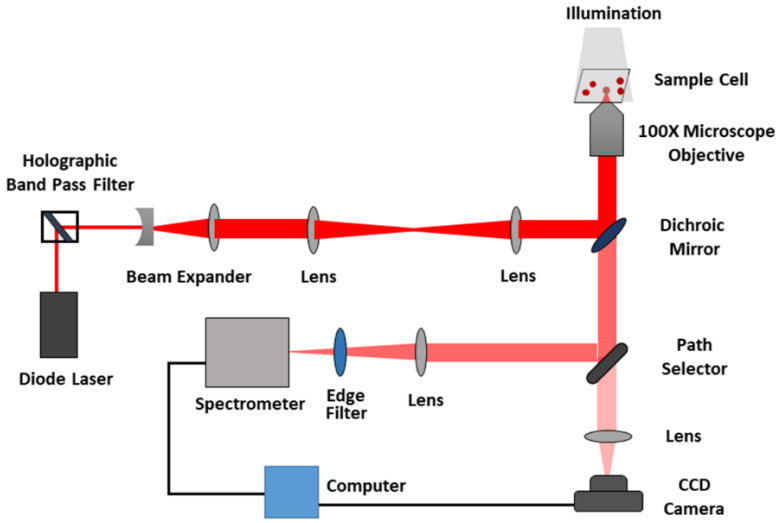

Figure 1. *The schematic diagram of the home-built Laser tweezers Raman spectroscopy setup.*

Results and discussion

The Raman spectra of single live RBCs suspended in different intravenous crystalloid fluids and blood plasma were shown in Figure 2. The RBCs suspended in blood plasma is considered as the control for the study. The arrows given in the particular peak positions indicating the intensity changes of the Raman bands. RBCs suspended in hypertonic saline, hypotonic saline, Dextrose 5%, and DNS showed notable Raman band intensity changes. The relative intensities of oxygenation marker peaks have visible changes. The Raman bands at 565 cm^{-1} (Fe-O_2 stretch region), 1222 cm^{-1} (Methine CH deformation region), 1561 cm^{-1} (Spin marker region) and 1636 cm^{-1} (spin marker region) have decreased intensity in all crystalloid fluids. The deoxygenation marker bands corresponding to 1209 cm^{-1} (Methine CH deformation region) and 1544 cm^{-1} (spin marker region) have higher intensity in all intravenous crystalloid fluids. Similarly the intensity of 1397 cm^{-1} (pyrrole deformation band) were decreased in all the crystalloid fluids mainly in hypotonic saline 0.45% and dextrose 5%. RBCs suspended in a hypotonic saline solution had a low overall spectral intensity. The decreased intensity of porphyrin breathing mode (752 cm^{-1}) indicate the hemoglobin depletion of RBCs in hypotonic saline 0.45%. The oxygenation marker band intensities of RBCs treated with Plasmalyte-A, Normal saline (0.9%) and Ringer lactate were also decreased.

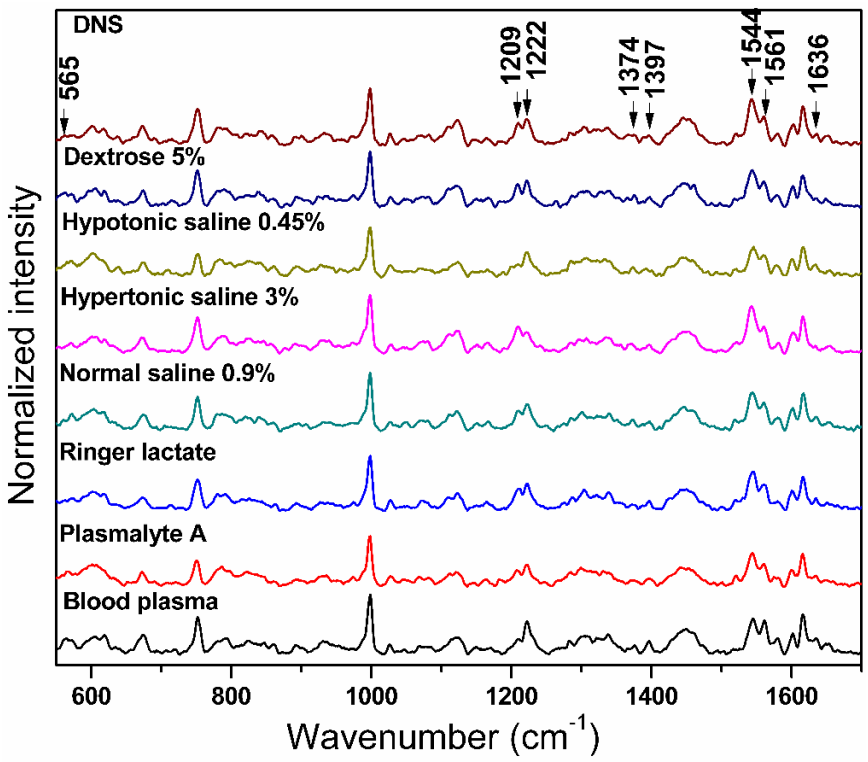

Figure 2. *The Raman spectra of single live RBCs treated with different intravenous crystalloid fluids.*

The microscopic images of RBCs treated with different intravenous crystalloid fluids were given in Figure 3. The images were captured using 100X oil immersion microscope objective. In blood plasma, the morphological changes of RBCs were not observed, which indicate that the blood plasma is acting as a buffer for the cells. The optically trapped RBC was shown in the red circle. Due to the higher flexibility of the RBC after trapping the cell was flipped and looks like a dumbbell shape, this shape change was observed in RBCs suspended in blood plasma, plasmalyte A, Ringer lactate and normal saline. The RBCs suspended in Plasmalyte-A was showing exactly similar morphological structure that of blood plasma. The RBCs were intact in plasmalyte-A. In the case of Ringer lactate and normal saline the morphology of some RBCs were started to change. The cells in normal saline was slowly changing into echinocyte stage, but the trapped RBC was showing exactly similar features as that of blood plasma. Thorn like projections were started to appear on the surface of some RBCs. The morphology of cells suspended in hypertonic saline was completely changed into echinocyte. The thorn like projections were easily visible on the cell surface. The RBCs became spherocytes in dextrose 5% and hypotonic saline 0.45%. The cells were bulged and the discoid shape of the cells were disturbed. In the case of spherocytes the optically trapped cells were not flipped, which shows that the deformation ability of the cells were reduced. These morphological changes will adversely effect the cytoskeleton structure of the RBCs and this may effect the deformability of the cells.

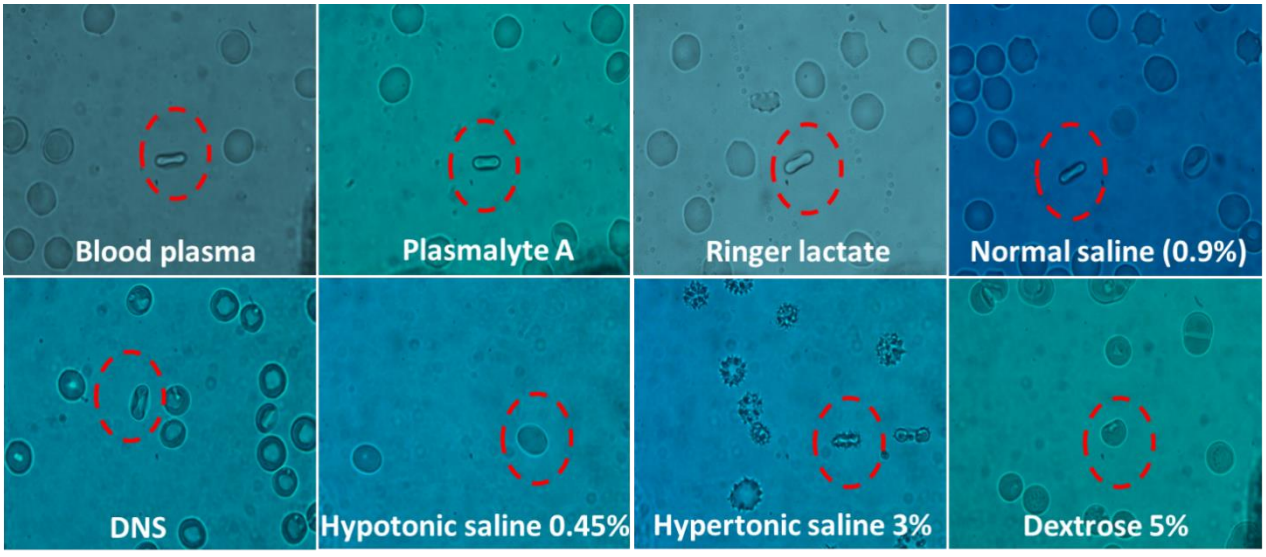

Figure 3. *The microscopic images of RBCs treated with blood plasma and different intravenous crystalloid fluids.*

The quantitative phase images of the RBCs suspended in different intravenous crystalloid fluids were captured using d'Bioimager (d' Optron) for studying the morphological variations of the cells. A microscope objective of 50X was used to magnify the pictures exhibited in Figure 4. Usually, the normal RBCs were discoid shape, the cells suspended in blood plasma also have a discoid shape and there is no morphological deformation of the cell. A shows almost similar morphological behavior to that of the cells in blood plasma, the cell membrane damage and other deformations were not seen in the image. The discoid shape of the cell was maintained in Plasmalyte-A. The RBCs suspended in normal saline show some projections or specular structure, indicating that the RBC is morphologically shifting to the echinocyte stage, which will result in a reduction in the cell's surface area and volume. The deformation ability of the cell also reduced in echinocyte. The specular structures formed on the membrane surface in presence of hypertonic saline are evident in Figure 4. Comparing to normal saline the echinocyte formation of RBC in hypertonic solution was faster, after suspending the cells in the solution within one or two seconds the discocyte will became echinocyte. The RBCs in Dextrose 5%, hypotonic saline and ringer lactate shows spherocyte formation. The center portion of the RBCs were bulged due to the effect of these intravenous fluids. The RBCs in Dextrose normal saline (DNS) was almost looks like stomatocytes.

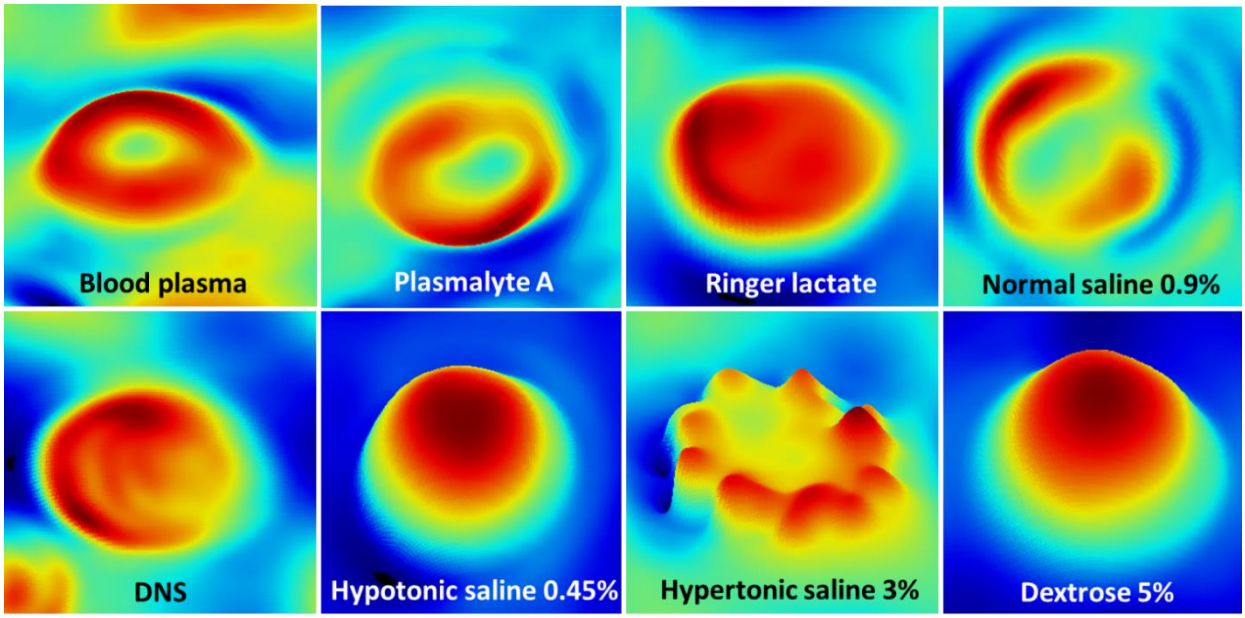

Figure 4. *The Quantitative phase images of RBCs treated with blood plasma and different intravenous crystalloid fluids.*

Conclusions

Micro-Raman combined with Optical Tweezers setup is a versatile tool to study the blood components e.g. RBCs, Platelets, WBCs etc and their interaction with external stressors. The effect of intravenous crystalloid fluids on single live RBCs were investigated using Raman tweezers spectroscopy technique. The deoxygenation tendency of the cells suspended in intravenous fluids were observed from the Raman bands. The hemoglobin depletion or denaturation was also evident from the Raman spectra of RBCs in certain intravenous crystalloid fluids. The morphological variations of the RBCs also evident from the microscopic images and quantitative phase images.

Acknowledgement:

Authors are thankful to DBT, Govt. of India for the Raman Tweezers setup and Mithun, Reena, Sphurt and Nidheesh are for their Dr. TMA Pai Ph.D. fellowships.

References

[1] A.M. Enejder, T.-W. Koo, J. Oh, M. Hunter, S. Sasic, M.S. Feld, G.L. Horowitz, Blood analysis by Raman spectroscopy, Optics letters, 27 (2002) 2004-2006.
[2] R.L. McCreery, Raman spectroscopy for chemical analysis, Measurement science and technology, 12 (2001) 653.
[3] S. Boyd, M.F. Bertino, S.J. Seashols, Raman spectroscopy of blood samples for forensic applications, Forensic science international, 208 (2011) 124-128.
[4] R.S. Das, Y. Agrawal, Raman spectroscopy: recent advancements, techniques and applications, Vibrational spectroscopy, 57 (2011) 163-176.
[5] R.R. Jones, D.C. Hooper, L. Zhang, D. Wolverson, V.K. Valev, Raman techniques: fundamentals and frontiers, Nanoscale research letters, 14 (2019) 1-34.

[6] A. Bankapur, E. Zachariah, S. Chidangil, M. Valiathan, D. Mathur, Raman tweezers spectroscopy of live, single red and white blood cells, PLoS one, 5 (2010) e10427.
[7] A. Ashkin, J.M. Dziedzic, J.E. Bjorkholm, S. Chu, Observation of a single-beam gradient force optical trap for dielectric particles, Optics Letters, 11 (1986) 288-290.
[8] A. Ashkin, J.M. Dziedzic, T. Yamane, Optical trapping and manipulation of single cells using infrared laser beams, Nature, 330 (1987) 769-771.
[9] S. Barkur, J. Lukose, S. Chidangil, Probing Nanoparticle–Cell Interaction Using Micro-Raman Spectroscopy: Silver and Gold Nanoparticle-Induced Stress Effects on Optically Trapped Live Red Blood Cells, ACS omega, 5 (2020) 1439-1447.
[10] J. Lukose, N. Mithun, G. Mohan, S. Shastry, S. Chidangil, Normal saline-induced deoxygenation of red blood cells probed by optical tweezers combined with the micro-Raman technique, RSC advances, 9 (2019) 7878-7884.
[11] J. Lukose, N. Mithun, M. Priyanka, G. Mohan, S. Shastry, S. Chidangil, Laser Raman tweezer spectroscopy to explore the bisphenol A-induced changes in human erythrocytes, RSC advances, 9 (2019) 15933-15940.
[12] R. Dasgupta, S. Ahlawat, R.S. Verma, A. Uppal, P.K. Gupta, Hemoglobin degradation in human erythrocytes with long-duration near-infrared laser exposure in Raman optical tweezers, Journal of biomedical optics, 15 (2010) 055009.
[13] D. Severs, E.J. Hoorn, M.B. Rookmaaker, A critical appraisal of intravenous fluids: from the physiological basis to clinical evidence, Nephrology Dialysis Transplantation, 30 (2015) 178-187.
[14] N. Karakala, K. Raghunathan, A.D. Shaw, Intravenous fluids in sepsis: what to use and what to avoid, Current opinion in critical care, 19 (2013) 537-543.
[15] C.H. Allen, R.D. Goldman, S. Bhatt, H.K. Simon, M.H. Gorelick, P.R. Spandorfer, D.M. Spiro, S.E. Mace, D.W. Johnson, E.A. Higginbotham, A randomized trial of Plasma-Lyte A and 0.9% sodium chloride in acute pediatric gastroenteritis, BMC pediatrics, 16 (2016) 1-9.
[16] S.A. Kirkley, K.F. Henrichs, A.P. Schmidt, M.A. Refaai, R.P. Phipps, S.L. Spinelli, D. Masel, J.M. Cholette, A. Pietropaoli, J.M. Heal, Decreased hemolysis of red cells washed with Plasma-Lyte as compared with 0.9% sodium chloride, American Society of Hematology Washington, DC, 2015.
[17] N. Blumberg, K. Henrichs, J. Cholette, A. Pietropaoli, S. Spinelli, S. Noronha, R. Phipps, M.A. Refaai, Sickle red blood cells are more susceptible to in vitro haemolysis when exposed to normal saline versus Plasma-Lyte A, Vox sanguinis, 114 (2019) 325-329.

STOKES VECTOR BASED POLARIZATION RESOLVED SECOND HARMONIC MICROSCOPY

DOI 10.24412/cl-36896-2021-1-18-20

NIRMAL MAZUMDER[1,*] AND FU-JEN KAO[2]

Department of Biophysics, Manipal School of Life Sciences, Manipal Academy of Higher Education, India
*nirmaluva@gmail.com

ABSTRACT

We developed a four-channel photon counting based Stokes polarimeter for spatial characterization of polarization properties of Second Harmonic (SH) light. In this way, the critical polarization parameters can be obtained concurrently without the need of repeated image acquisition. Various polarization parameters, including the degree of polarization (DOP), the degree of linear polarization (DOLP), and the degree of circular polarization (DOCP), are extracted from the reconstructed 2D Stokes vector based SH images in a pixel-by-pixel manner. The Stokes vector measurements are further extended by varying the polarization states of the incident light and recording the resulting Stokes parameters of the SH signal. In turn this allows the molecular structure and orientation of the samples including collagen fibers, skeletal muscle fiber, and starch granules. The combination of SHG microscopy and Stokes polarimeter hence makes a powerful tool to investigate the structural order of targeted specimens.

Keywords: Polarimetry, Second harmonic generation, nonlinear optics

INTRODUCTION

Second harmonic generation (SHG) microscopy is an effective analytical tool for detailed investigation of microscopic structure and orders of non-centrosymmetric molecules [1]. Stokes vector based SHG microscopy resolves the polarization states of the SH signal and allows the deduction of the molecular organization of collagen, skeletal muscle, starch etc [2-4]. The technique is also implemented to characterize the polarization properties of the SH signal during starch gelatinization. Starch in the form of grains is the major storage compound in plants and so is an important part of our food [5]. Scientists are keen to understand the origins in plants, and how changes to the plants' genes could affect the composition and properties of the starch in the grains [6]. The finest features in the starch granule structure are due to the molecular packing of amorphous amylose and crystalline amylopectin lamellae [7]. Also, the sample preparation for the high resolution microscopy provides a complete structural elucidation of starch in its native form. The optical microscopy provides non-invasively the detail of the microscopic structural information of starch [8]. A strong SH signal from semi-crystalline amylopectin chains which are assumed to lie in the amorphous lamellae (amylose) form radially distributed amorphous growth rings in starch [9, 10]. A Stokes vector based SHG microscopy scheme is distinct from several other previously demonstrated polarization resolved approaches in that it uses a large number of images rather than a single shot measurement [2,11-13]. The complete polarization states of the SH light of starch granules were characterized from SHG Stokes micrographs [2,3]. In order to optimize the processing operations and obtain the desired quality of starch-based foods, a thorough understanding of the starch-water interaction through the gelatinization process is required [14,15]. In pixel by pixel SH image analysis, it is found that at room temperature the structural distribution of double helical amylopectin is self-organized upon hydration within starch granules [12]. In this article, the thermal behavior of these structurally complex materials is investigated by Stokes vector based polarization resolved SHG imaging. In addition, the chemical interactions between different components are observed from the reconstructed 2D SHG images using various polarization parameters, such as the degree of polarization (DOP), the degree of linear polarization (DOLP) and the degree of circular polarization (DOCP) from the acquired Stokes parameters [2].

MATERIALS AND METHODS

The experimental arrangement for measuring the polarization properties of SH signal via SHG microscopy is described in detail in [2,3]. A modified inverted Olympus IX81 confocal microscope is used as our imaging setup. A femtosecond Ti: sapphire (Coherent Mira Optima 900-F) laser oscillator was used as the excitation light source. The center wavelength was set at 800 nm and had a full width at half maximum (FWHM) spectral width of 15 nm which gave transform limited pulses of ~ 100 fs, with average power ~550 mW and repetition rate~76 MHz. Our polarization microscope includes a polarization state generator (PSG), sample and polarization state analyzer (PSA). The various polarization states are generated using the PSG formed from a polarizer and a half wave plate. Samples were mounted upside-down on an XYZ stage and scanned with a laser scanning unit (Olympus, FV300). An objective lens (UPlanFLN 40X/N.A. 1.3, Olympus Co., Japan) is used for focusing the laser beam. The measured signals were analyzed by means of a polarization state analyzer (PSA), specifically, a four-channel Stokes-polarimeter [2]. The SH signal is collected in the forward direction using a 20X, 0.75 N.A. objective lens. A band pass filter of 400 ± 40 nm (Edmund Optics Inc., Barrington, New Jersey) was also inserted into the SHG emission path. Details regarding calibration and performance of our Stokes-polarimeter are given in [2-4]. The four-channel Stokes-polarimeter microscope is a variation in that we reconstructed the 2D intensity images as well as the corresponding Stokes vector images. Again, the different polarization parameters are reconstructed from the acquired TSCPC data pixel by pixel with a specialized homemade routine in MATLAB (MathWorks, R2009b, Natick, MA) [2]. We report on measurements and characterization of polarization properties of (SH) signals using a four-channel photon counting based Stokes polarimeter. In this way, the

critical polarization parameters can be obtained concurrently without the need of repeated image acquisition. The critical polarization parameters, including the degree of polarization (DOP), the degree of linear polarization (DOLP), and the degree of circular polarization (DOCP), are extracted from the reconstructed Stokes vector based SH images in a pixel-by-pixel manner [2].

RESULTS AND DISCUSSION

Stokes vector based SH microscopy was developed to investigate the molecular structure more precisely using polarization properties of SH. 2D Stokes vector images of collagen type-I are reconstructed to determine the image contrast and to examine molecular alignment in fiber [16]. It is evident that the horizontally polarized excitation beam is transformed into partially polarization light upon interaction with the collagen fibers. The spatial distribution of anisotropic and chiral properties from collagen type-I are differentiated using DOLP and DOCP parameters. The relative orientation of the optical axis of crystals with extraordinary and ordinary rays varies at different focal depth. Thus the chiral SHG response should depend on the variation in the contribution of chiral and achiral susceptibility elements [17]. This can, in turn reveal collagen-fiber orientation and structural order through SH detection. Therefore, the DOLP and DOCP values are complimentary; the region with higher/lower DOLP value shows lower/higher DOCP value. The measurements are further extended to angular dependence of Stokes parameters of the SH signal to characterize the molecular orientation more thoroughly [18]. The measurements are further extended by varying the polarization states of the incident light and recording the resulting Stokes parameters of the SH signal. In the previous study, it is demonstrated that due to type I phase matching and concentric shell like structure, starch granule acts as a polarization state analyzer [12]. Specifically, SH contrast depends on the polarization states of the excitation and reflects molecular arrangement accordingly. For example, starch granules are arranged in semi-crystalline shells, the amylopectin chains in the crystalline layers are strongly anisotropically ordered and thus yield strong SH [3, 12]. Right and left circularly polarized illumination is transformed into elliptically polarization, depending on the handedness and the absolute orientation of amylopectin molecules. The DOLP and DOCP distributions hence demonstrate the components of both linearly and circularly polarized light in the SH signal. The crystallized arrangement of collagen type-I and amylopectin seems to be an indispensable condition for efficient SH conversion. The optical nonlinearity in starch granules will facilitate further studies in food science and provide insights into bio-energy transformation dynamics.

CONCLUSION

In conclusion, this review has elucidated the uniqueness and the prospects of Stokes vector based polarization resolved SH imaging. Conventionally polarization microscopy usually characterized measured signals with a two-channel configuration. SH imaging, however, has the advantage of being highly sensitive to the structural order of targeted specimens. Generally, SH polarization analysis can be carried out with Jones calculus since SH is usually coherent and fully polarized. However, multiple or time-lapsed scans would be required if the phase relationship between the eigen-polarization vectors is to be uncovered. We have presented the basics and applications of linear and nonlinear polarization light microscopy techniques in details. The molecular orientation and retardance provides additional information on birefringent specimen with enhanced contrast. Nonetheless, deep imaging inside thick biological samples can distort the polarization linearity of the excitation laser beam before it reaches the focal volume. In SH anisotropy, birefringence of collagen may strongly affect the incident electric field. This effect is more pronounced in the forward geometry than the backward detection, which needs to be taken into account during image analysis. The integration of SH microscopy and Stokes polarimetry hence makes a powerful tool to investigate the complete polarization state of SH light as well as the structural order of collagen fiber, starch granules, skeletal muscle [2, 12, 18]. The analysis was therefore extended to include the orientation and degree of organization from type-I collagen by varying the incident laser polarization whilst detecting the resulting polarization state of SH light using the four-channel Stokes-polarimeter [19]. A full Mueller matrix formalism has long been shown a powerful method and applied under linear optics settings. PSA measures the polarization states of the signal beam. There is no need to control the incident beam polarization to a very specific state (such as being perfectly linearly or circularly polarized) on the samples. A specific polarization state, such as being “linearly horizontally polarized”, is usually referred to the coordinate of the observer, instead of the relative orientation (and thus interaction) between the incident beam and the samples. The important parameters to be extracted from the polarization measurements are the degree of polarization (DOP), the degree of linear polarization (DOLP), and the degree of circular polarization (DOCP) [2, 3, 12] Characterizing the polarization states of the outgoing signal beam and thus deducing these parameters will be sufficient to infer the status of and the SH response from the samples, which is the core idea of our method. The measured SH signals and the reconstructed Stokes images are originated from the focal plane within the sample, attributing to the optical nonlinearity. Importantly, it should be noted that in SH microscopy Type I phase matching is assumed, that is $h\nu_{\omega,\ \text{ordinary}} + h\nu_{\omega,\ \text{ordinary}} \rightarrow h\nu_{2\omega,\ \text{extraordinary}}$, for the SH signal, which also indicates the polarization states of the SHG would faithfully reflect those of the incident excitation beam.

ACKNOWLEDGEMENT

NM thank Department of Science and Technology (DST) [Project Number-SERB/MTR/2020/000058] and Indian Council of Medical Research (ICMR) [ICMR, ID No. 2020-3286], Government of India for financial support. NM also thank Manipal School of Life Sciences, Manipal Academy of Higher Education, Manipal for providing the infrastructure and facilities.

REFERENCES

[1] P. A. Franken, A. E. Hill, C. W. Peters, and G. Weinreich, Generation of optical harmonics, Phys. Rev. Letts. 7 (4) 118-120, 1961.

[7] N. Mazumder, J. Qiu, M. R. Foreman, C. M. Romero, C.W. Hu, H. R. Tsai, P. Török, and F. J. Kao, Polarization-resolved second harmonic generation microscopy with a four-channel Stokes-polarimeter, Opt. Express, 20 (13), 14090-14099, 2012.

[8] N. Mazumder, J. Qiu, M. R. Foreman, C. M. Romero, P. Török, and F.J. Kao, Stokes vector based polarization resolved second harmonic microscopy of starch granules, Biomed. Opt. Express, 4 (4), 538-547, 2013.

[9] N. Mazumder, G. Deka, W.W. Wu, A. Gogoi, G.Y. Zhuo, F.J. Kao, Polarization Resolved Second Harmonic Microscopy, Methods 128, 105-118, 2017.

[10] "Polysaccharides: Natural Fibers in Food and Nutrition," edited by Noureddine Benkeblia CRS press, Taylor and Francis Group, (2014).

[11] D. Le Corre, J. Bras, and A. Dufresne, Starch Nanoparticles: A Review, Biomacromolecules, 11, 1139–1153, 2010.

[12] A. Buléon, P. Colonna, V. Planchot, S. Ball, Starch granules: structure and biosynthesis, International Journal of Biological Macromolecules, 23 (2), 85–112, 1998.

[13] G. Mizutani, Y. Sonoda, H. Sano,M. Sakamoto, T. Takahashi, S. Ushioda, Detection of starch granules in a living plant by optical second harmonic microscopy, J. of Luminescence 87-89 824-826, 2000.

[14] G.Cox, N.Moreno, J.Feijó, Second-harmonic imaging of plant polysaccharides, J. Biomed.Opt.10 (2), 024013, 2005.

[15] R. Cisek, D. Tokarz, M. Steup, I. J. Tetlow, M. J. Emes, K. H. Hebelstrup, A. Blennow, and V. Barzda Second harmonic generation microscopy investigation of the crystalline ultrastructure of three barley starch lines affected by hydration, Biomed. Opt. Express, 6 (10), 3694-3700, 2015.

[16] A. D. Slepkov, A. Ridsdale, A. F. Pegoraro, D. J. Moffatt, and A. Stolow, Multimodal CARS microscopy of structured carbohydrate biopolymers, Biomed. Opt. Express 1(5), 1347–1357, 2010.

[17] N. Mazumder, L. Xiang, J. Qiu, F.J. Kao, Investigating starch gelatinization through Stokes vector resolved second harmonic generation microscopy, Scientific Reports 7, 45816, 2017.

[18] S. Psilodimitrakopoulos, I.A. Roldan, P.L. Alvarez, and D. Artigas, Estimating the helical pitch angle of amylopectin in starch using polarization second harmonic generation microscopy, J. Opt. 12(8), 084007, 2010.

[19] G. T. Oostergetel, E.F.J. van Bruggen, The crystalline domains in potato starch granules are arranged in a helical fashion, Carbohydr Polym, 21, 7-12, 1993.

[20] C. G. Biliaderis, T. J. Maurice, and J. R. Vose, Starch genatinization phenomena studied by differential scanning calorimetry, J. of Food Science, 45, 1669- 1674, 1980.

[21] N. Mazumder and F.J. Kao, Stokes-Polarimetry based Second Harmonic Generation Microscopy for Collagen and Skeletal Muscle Fiber Characterization, Lasers in Medical Science 36:1161–1167, 2021.

[22] K.M. Reiser, A.B. McCourt, D.R. Yankelevich, A. Knoesen, Structural origins of chiral second-order optical nonlinearity in collagen: amide I band, Biophys. J. 103(10) 2177–2186, 2012.

[23] N. Mazumder, C.W. Hu, J. Qiu, M. R. Foreman, C.M. Romero, P. Török , F.J. Kao, Revealing molecular structure and orientation with Stokes vector resolved second harmonic generation microscopy, Methods 66 (2) 237-245, 2014.

[24] G. Y. Zhuo, K U Spandana, K M Sindhoora, Y. V. Kistenev, F. J. Kao, V. V. Nikolaev, H. Zuhayri, N. A. Krivova, and N. Mazumder, Label-free Multimodal Nonlinear Optical Microscopy for Biomedical Applications, Journal of Applied Physics, 129, 21, 214901, 2021.

Multifunctional nano-photosensitizers for enhanced photodynamic therapy

DOI 10.24412/cl-36896-2021-1-21-21

BUHONG LI [1,*], LI LIN[1], XUEJIAO SONG[2] AND XIAOCHENG DONG[2]

[1] *Key Laboratory of OptoElectronic Science and Technology for Medicine of Ministry of Education, Fujian Normal University*
[2] *Key Laboratory of Flexible Electronics and Institute of Advanced Materials, Nanjing Technology University*

* *bhli@fjnu.edu.cn*

ABSTRACT

Photodynamic therapy (PDT) utilizes photosensitizers (PSs) together with irradiation light of specific wavelength interacting with oxygen to generate cytotoxic reactive oxygen species (ROS), and then the cell death could be induced directly by cell damage from apoptosis, necrocytosis and autophagy, or indirectly by vascular destruction, , as well as immune response activating cytotoxic T cell or antibody-dependent cellular cytotoxicity. Considering the critical role of ROS generation during PDT, multifunctional nano-PSs employing nanotechnology and nanoscience are being widely developed during the past two decades, which present not only photosensitizing properties but additionally accurate drug release abilities, efficient response to optical stimuli and hypoxia resistance. In addition, multifunctional nano-PSs have been developed to enhance PDT efficiency by improving the ROS yield. Moreover, nano-PSs with additive or synergistic therapies are significant for both current preclinical research and future clinical practice, given their capability of considerable higher therapeutic efficacy under safer systemic drug dosage. In this talk, multifunctional nano-PSs that allow precise drug delivery for efficient absorption by target cells are introduced. multifunctional Nano-PSs boosting sensitivity and conversion efficiency to PDT-activating stimuli are highlighted. multifunctional Nano-PSs developed to address the challenging hypoxia conditions during PDT of deep-sited tumors are summarized. Specifically, PSs capable of synergistic therapy and the recently emerging novel types that further enhance PDT efficacy are presented. Finally, future demands for ideal multifunctional nano-PSs, emphasizing clinical translation and application are discussed.

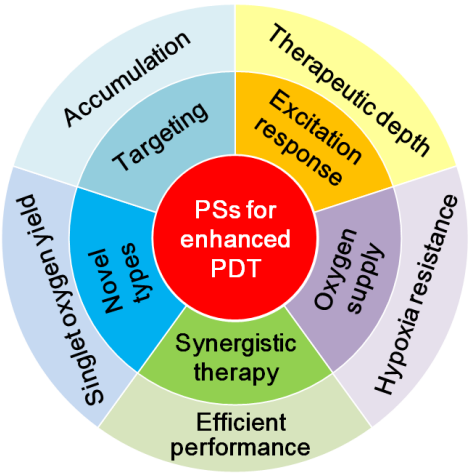

***Figure**: Multifunctional nano-PSs for enhanced PDT.*

REFERENCES

[1] X Yang, Q Yu, N Yang, L Xue, J Shao, B Li, J Shao, X Dong. Thieno[3,2-b]thiophene-DPP based near-infrared nanotheranostic agent for dual imaging-guided photothermal/photodynamic synergistic therapy. J. Mater. Chem. B. 2019, 7(15), 2454-2462.

[2] X Liao, Z Lin, Y Shen, H Lin, D Zhang, X Liu, B Li. Self-assembled metallo-supramolecular nanoflowers for NIR/acid-triggered multidrug release, long-term tumor retention and NIR-II fluorescence guided-phototherapy. Chem. Eng. J. 2020, 400: 125882.

[3] L Lin, X Song, X Dong, B Li. Nano-photosenitizers for enhanced photodynamic therapy, Photodiagn. Photodyn. Ther. 36:102597, 2021.

[4] J Zhu, A Jiao, Q Li, X Lv, X Wang, X Song, B Li, Y Zhang, X Dong. Mitochondrial Ca^{2+}-overloading by oxygen/glutathione depletion-boosted photodynamic therapy based on a CaCO3 nanoplatform for tumor synergistic therapy. Acta Biomater. 2021, 10.1016/j.actbio.2021.10.016.

[5] J Yin, X Wang, X Sun, H Dai, X Song, B Li, Y Zhang, P Chen, X Dong. Thrombin based photothermal-responsive nanoplatform for tumor-specific embolization therapy. Small, 2021:2105033.

TISSUE OPTICAL CLEARING WINDOWS FOR IN VIVO IMAGING

DOI 10.24412/cl-36896-2021-1-22-22

DAN ZHU[1,2]

[1] *Britton Chance Center for Biomedical Photonics, Wuhan National Laboratory for Optoelectronics, Huazhong University of Science and Technology, China*
[2] *MoE Key Laboratory for Biomedical Photonics, Huazhong University of Science and Technology, China*

dawnzh@mail.hust.edu.cn

ABSTRACT

Biomedical photonics is currently one of the fastest growing fields of life sciences since optical imaging techniques allow low-invasive *in vivo* structural and functional analysis of tissues with high resolution and contrast unattainable by any other method (1-2). However, the high scattering of turbid biological tissues limits the penetration of light, leading to strongly decreased imaging resolution and contrast as light propagates deeper into the tissue. For instance, observation of brain structure and neural activities is of great significance to understand not only normal brain physiology but also dysfunctions of vasculature and neural networks related to various brain diseases (3-4), while the skull above prevent *in vivo* optical brain imaging. Moreover, as the largest organ of the body, skin is an ideal target tissue for microvascular network and immune response monitoring, but its turbid nature severely limits the visualization by decreasing the imaging resolution as well as the imaging depth. Traditionally, to overcome the scattering of such barriers above the target tissue, surgery-based windows have to be performed. Fortunately, novel *in vivo* tissue optical clearing technique could reduce the scattering of tissue and make it transparent for higher optical imaging quality. This presentation will introduce the recently developed skin/skull optical clearing windows for imaging structure and function of cutaneous/cortical vascular and cells, as well as for manipulating cortical vasculature (5-8).

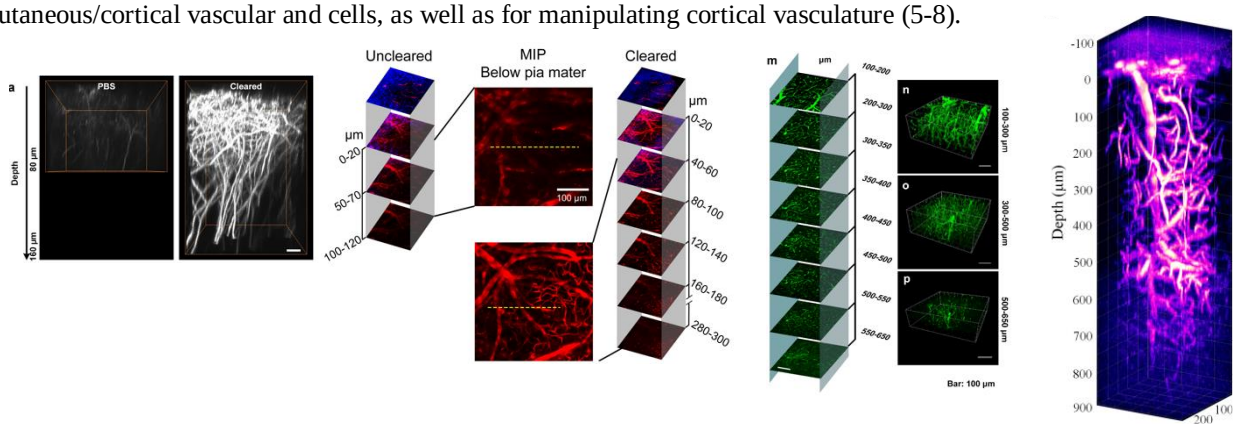

Figure: *Different optical clearing windows for improving cortical neuro/vascular imaging depth [4-8]*

REFERENCES

[1] N. Wagner et al., "Instantaneous isotropic volumetric imaging of fast biological processes," Nat Methods 16(6), 497 (2019).

[2] R. Prevedel et al., "Fast volumetric calcium imaging across multiple cortical layers using sculpted light," Nat Methods 13(12), 1021-1028 (2016).

[3] P. McGonigle, "Animal models of CNS disorders," Biochem. Pharmacol. 87(1), 140-149 (2014).

[4] M. Wiesmann et al., "A specific dietary intervention to restore brain structure and function after ischemic stroke," Theranostics 7(2), 493-512 (2017).

[5] Y. J. Zhao et al., "Skull optical clearing window for in vivo imaging of the mouse cortex at synaptic resolution," Light-Sci Appl 7(2), 17153 (2018).

[6] C. Zhang et al., "Age differences in photodynamic therapy-mediated opening of the blood-brain barrier through the optical clearing skull window in mice," Laser Surg Med 51(7), 625-633 (2019).

[7] D. Li, et al., Visible-near infrared-II skull optical clearing window for in vivo cortical vasculature imaging and targeted manipulation, Journal of Biophotonics, e202000142, 2020

[8] Y. Chen, Coherent Raman Scattering Unravelling Mechanisms Underlying Skull Optical Clearing for Through-Skull Brain Imaging, Analytical Chemistry, 91, 9371-9375, 2019

MUELLER MATRIX MICROSCOPY AND POLARIZATION DIGITAL PATHOLOGY

DOI 10.24412/cl-36896-2021-1-23-23

HUI MA [1,2]

[1] *Shenzhen International Graduate School, Tsinghua University, Shenzhen 518055, China;*
[2] *Department of Physics, Tsinghua University, Beijing 100084, China.*

mahui@tsinghua.edu.cn

ABSTRACT

In digital pathology, stained histopathology slides are digitized by scanners to generate digitized whole-slide images (WSI). Then image processing and classification based on either imageomics or artificial intelligence (AI) approaches are used for tasks such as object detection and segmentation, as well as predicting disease diagnosis and prognosis of treatment response on the basis of patterns in the images. It has been known that Mueller matrices encode rich information on the microstructural features of complex samples, such as histopathology features of tissues. WSI by a Mueller matrix microscope is expected to reveal more abundant information in both the polarization and image features for medical doctors making more objective decision in clinical diagnosis. In this talk, we present a brief summary on our continuous efforts to realized polarization digital pathology. We have developed Mueller matrix microscopes by adding polarization optics in the existing optical path of commercial upright transmission optical microscope, and used them for taking Mueller matrix WSI of both stained and unstained pathological slides from adjacent sections of the same tissues. Diagnosis by medical doctors based on high resolution color images of the stained slides are used as gold standard for supervised learning to extract the corresponding polarization features. Although the results are still preliminary, we have proved that taking into account both the polarization and image features results in significant improvements in the performance of digital pathology.

DEEP IMAGING AND FOCUSING WITHIN HIGHLY SCATTERING MEDIUM BASED ON REFLECTION MATRIX MEASUREMENT

DOI 10.24412/cl-36896-2021-1-24-25

JING CAO[1], LING FU [1,2] AND QIAN LIU [1]

[1]*Key Laboratory of Biomedical Engineering, School of Biomedical Engineering, Hainan University, Hainan, China*
[2]*Wuhan National Laboratory for Optoelectronics, Huazhong University of Science and Technology, Wuhan, China*

caoj@hainanu.edu.cn

ABSTRACT

Over the past decade, modern advanced optical imaging technologies change people's ways of understanding the world in many aspects, including clinical application, industrial measurement, and fundamental research [1-3]. For all-optical imaging methods, there always exists a trade-off between high resolution and deep penetration depth [4]. Among them, a group of imaging methods, which collect ballistic or single scattering photons [5,6]. They commonly provide high-resolution imaging power but the imaging depth limit to a superficial layer. For those methods that are deep imaging availably, they generally rely on diffuse photons [7]. But the imaging resolution is degraded a lot. The fundamental limitation of this phenomenon is the multiple scattering of light. The primary cause is the anisotropy of biological tissues and the impact of photons on the micro-particles. To solve this problem, pioneers' have done significant work in improving society. Reflection matrix measurement and decomposition of the time-reversal method have shown their abilities to tell the single scattering photons from the multiple scattering [8,9]. By shaping the wavefront of light, scattering events become controllable so that light is focused even transmits through a highly scattering medium [10].

Here, we present our work for the following two purposes--- deep imaging and focusing. In the aspect of deep imaging purpose, we combine optical heterodyne detection and lock-in amplitude to detect those weak signals drowned in the background noise [11]. After reconstructing the reflection matrix that describes the light propagation process in the sample, and applying a singular value decomposition of the matrix. We succeed in imaging through a sample with 15.2 times scattering means free path (SMFP) without compromising to resolution decline. It is a significant improvement in imaging depth when compared to confocal microscopy ~ 2-3 SMFP or optical coherence tomography ~ 6-7 SMFP.

In the aspect of focusing light deep within media purposes, we have done two types of work. The first work is a high-speed wavefront determination for millisecond beam focusing through a scattering medium. For a very long time, one of the major challenges to apply wavefront shaping methods in practical applications is the required long optimization time. In this work, we propose an in-&-out light field analysis method to calculator the matched wavefront. The advantage of this technology is that the speed of the whole beam focusing process is ~113ms [12]. When compared to the conventional iterative feedback wavefront of transmission matrix measurement methods, it has shortened the time consumption for 2~3 orders. We believe this work shows the potential to enable the translation of the wavefront shaping method to increase image depth in a highly scattering medium such as biological tissues. The second work is to focus the beam inside the scattering medium without any guide-star assistant. Firstly, we applied time-reversal operation to the reflection matrix to filter out those multiple scattering photons that arrived at the target position. Then, by shaping the incident light according to the optimal wavefronts, the above-mentioned multiple scattering photons would travel in the "open channels" this time. Light travel in the open channel will experience zero-energy loss and the shortest flight of time towards the target. After optimal, the intensity of light distribution, at the imaging depth of 9.6 times scattering mean free path, becomes focusing again. At the same time, the energy has also been improved by one order.

In conclusion, we have combined decomposition of time-reversal operation, reflection matrix measurement, and wavefront shaping to imaging and focusing ultra-deep inside the complex medium. Based on the above research, we plan to apply this technology to a broader range of fields in the coming work. Such as brain science research, the skull layer is considered a typical highly scattering layer. We want to provide a new in-vivo, noninvasive, and high-resolution optical imaging method to imaging the nerve and blood vessels beneath mice skulls. In the field of fundamental research, we show the potential of this method in studying the light propagation process, separating single from multiple scattering photons, and the ability to control photons' travel path within the scattering medium.

REFERENCES

[9] K. Si, R. Fiolka, and M. Cui, Fluorescence imaging beyond the ballistic regime by ultrasound pulse guided digital phase conjugation, Nat. Photonics 6(10), 657–661, 2012.

[10] Jochen Aulbach, Bergin Gjonaj, Patrick M. Johnson, Allard P. Mosk, and Ad Lagendijk, Control of Light Transmission through Opaque Scattering Media in Space and Time, Phys. Rev. Lett. 106, 2011.

[11] T. Čižmár, M. Mazilu, and K. Dholakia, In situ wavefront correction and its application to micromanipulation, Nat. Photonics 4(6), 388–394, 2010.

[12] Ntziachristos, V. Going deeper than microscopy: the optical imaging frontier in biology. Nat Methods 7, 603–614, 2010.

[13] D. Huang, E. A. Swanson, C. P. Lin, J. S. Schuman, W. G. Stinson, W. Chang, M. R. Hee, T. Flotte, K. Gregory, C. A. Puliafito, J. G. Fujimoto, Optical coherence tomography. Science 254, 1178–1181, 1991.

[14] P. Theer, M. T. Hasan, W. Denk, Two-photon imaging to a depth of 1000 mm in living brains by use of a Ti: Al2O3 regenerative amplifier. Opt. Lett. 28, 1022–1024, 2003.

[15] T. Durduran, R. Choe, W. B. Baker, A. G. Yodh, Diffuse optics for tissue monitoring and tomography. Rep. Prog. Phys. 73, 076701, 2010.

[16] A. Badon, D. Li, G. Lerosey, A. Boccara, M. Fink, and A. Aubry, Smart optical coherence tomography for ultra-deep imaging through highly scattering media, Sci. Adv. 2(11), e1600370 (2016).

[17] Ntziachristos, V. Going deeper than microscopy: the optical imaging frontier in biology. Nat Methods 7, 603–614, 2010.

[18] I. M. Vellekoop and A. P. Mosk, Focusing coherent light through opaque strongly scattering media, Opt. Lett. 32, 2309-2311, 2007.

[19] Qiang Yang, Jing Cao, Yusi Miao, Jiang Zhu, and Zhongping Chen, Extended imaging depth of en-face optical coherence tomography based on fast measurement of a reflection matrix by wide-field heterodyne detection, Opt. Lett. 45, 828-831, 2020.

[20] Jing Cao, Qiang Yang, Yusi Miao, Yan Li, Pinghe Wang, and Zhongping Chen, High-speed wavefront determination method based on single in-and-out electric field analysis to focus light through highly scattering medium, APL Photonics 6, 036107, 2021

IMAGE-BASED HIGH-THROUGHPUT PHENOTYPING OF AGRI-PHOTONICS

DOI 10.24412/cl-36896-2021-1-26-29

DAN WU[1], LINGBO LIU[1], LEJUN YU[1, 3], WANNENG YANG[2] AND QIAN LIU[3]

[1] *Britton Chance Center for Biomedical Photonics, Wuhan National Laboratory for Optoelectronics, and Key Laboratory of Ministry of Education for Biomedical Photonics, Department of Biomedical Engineering, Huazhong University of Science and Technology, People's Republic of China*

[2] *National Key Laboratory of Crop Genetic Improvement, National Center of Plant Gene Research, Huazhong Agricultural University, People's Republic of China*

[3] *School of biomedical engineering, Hainan University, People's Republic of China*

qliu@hainanu.edu.cn.

ABSTRACT

In the past decade, the development of phenotypic detection was greatly promoted by advanced photonics-based technologies. A variety of imaging techniques, including visible light imaging, hyperspectral imaging, structured light, X-ray computed tomography, have been applied in the case of rice, maize, rape, cotton and grapevine. Phenotypic data were extracted from crop images using specialized algorithm, which generally adopted classical image processing and machine learning methods. Traditional phenotyping that depends largely on manual measuring were tend to be replaced by automatic, non-destructive image-based phenotyping, bringing the functional analysis of crop genome into a high-throughput stage.

Keywords: high-throughput phenotyping, imaging techniques, image processing, machine learning.

1. Common photonics-based techniques in phenotypic detection

The evaluation of crop phenotypic traits is the foundation of functional genomics and crop breeding. The high-throughput phenotyping refers to extracting multi-dimensional crop phenotypic information on high-throughput phenotyping platforms which is usually the combination of a range of devices for automatic image acquisition and specialized algorithms for traits extraction [1-3].

Commonly adopted imaging techniques in our works included visible light imaging, hyperspectral imaging, structured light and X-ray computed tomography. The visible light imaging is low-cost and adaptable in indoor and outdoor environments. Line-scan RGB imaging were used to measure maize ear traits [4]. 2D RGB images were used to evaluate shoot biomass, leaf area, and yield-related traits of the rice plants [5, 6]. 3D RGB imaging techniques, including stereo vision, shape from silhouette and structure from motion, were used to generate the 3D models of rape [7], rice [8] and grapevine [9], respectively, which allowed more comprehensive understandings of the plant morphological structures in 3D level. Besides, visible cameras can be mounted on unmanned aerial vehicle (UAV) for field-scale monitoring [10]. The hyperspectral imaging, integrating spectroscopic and imaging techniques and producing data that contains both spatial and spectral dimensions, were employed to explore genetic variation in rice by performing genome-wide association study of hyperspectral indices and traditional agronomic traits in different rice accessions [11]. Since plant pigments varies in spectral reflectance, the hyperspectral imaging was also used for non-destructive prediction of rice chlorophyll content [12]. The structured light is a 3D imaging technique with high resolution and accuracy, it was applied to measure leaf area, leaf perimeter, leaf angle, leaf rolling degree and leaf yellow ratio of cotton plants during seedling stage [13]. Distinguishing from above mentioned kinds, the X-ray based imaging techniques, including X-ray digital radiography and X-ray computed tomography that are able to detect inner structures of crops from cellular to organ scale, were used to quantify wheat tiller morphological traits [14], rice grain traits [15], rice panicle traits [16] and lodging resistance-related traits of the rice plants [17]. The application of these imaging techniques in our work were shown in Fig. a. The photonic imaging system equipped in a dark chamber generally contains an electromechanical controller to move the plants, an imaging device connected to a computer for automatic image acquisition and several light sources to ensure suitable illumination.

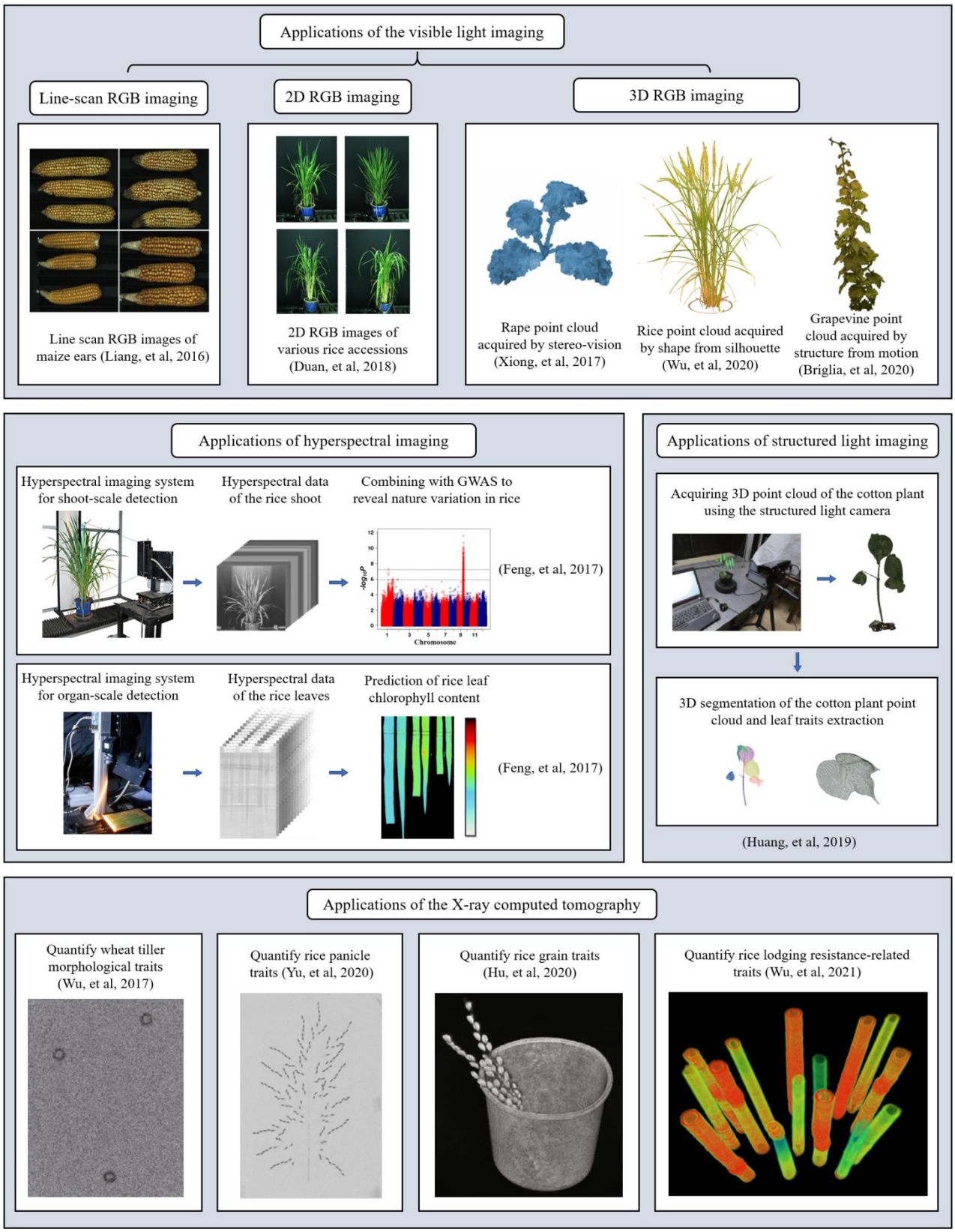

Figure: *(a) The application of various photonics imaging techniques in high-throughput crop phenotyping*

2. Methodologies for phenotypic traits extraction from crop images

The phenotypic traits extraction from crop images is a core procedure of image-based phenotyping. Part of this could be achieved by a variety of classical image processing algorithms such as thresholding, connected component analysis, morphological operations including dilation and erosion, skeleton extraction and so on. While some complex issues - for instance - segmenting target objects from background with similar colours and detection tasks when there are frequent

overlaps of target objects, were quite intractable with classical image processing algorithms. Fortunately, these could be well addressed using deep learning methods (Fig. b). The Panicle-Seg software was established on the basis of a convolutional neural network and superpixel optimization for segmentation of rice panicles in field [18]. The faster region-based convolutional neural network (Faster R-CNN) was applied to evaluate spikelet numbers in panicle images [16]. Besides, the Culms-SegNet, which was based on SegNet - a deep fully convolutional neural network for semantic pixel-wise segmentation, was built for extraction of rice lodging resistance-related traits from computed tomography rice stem slices [17]. Manual measuring of phenotypic traits were performed to evaluate the prediction accuracies of the high-throughput phenotypic systems, in which the squares of the correlation coefficients, the mean absolute percentage error and the root mean square error were generally adopted. The specialized algorithms for traits extractions were basically developed with the OpenCV library and accelerated by CUDA. Furthermore, the PCL library which provides powerful supports for point cloud processing, were applied to calculate complex 3D phenotypic traits.

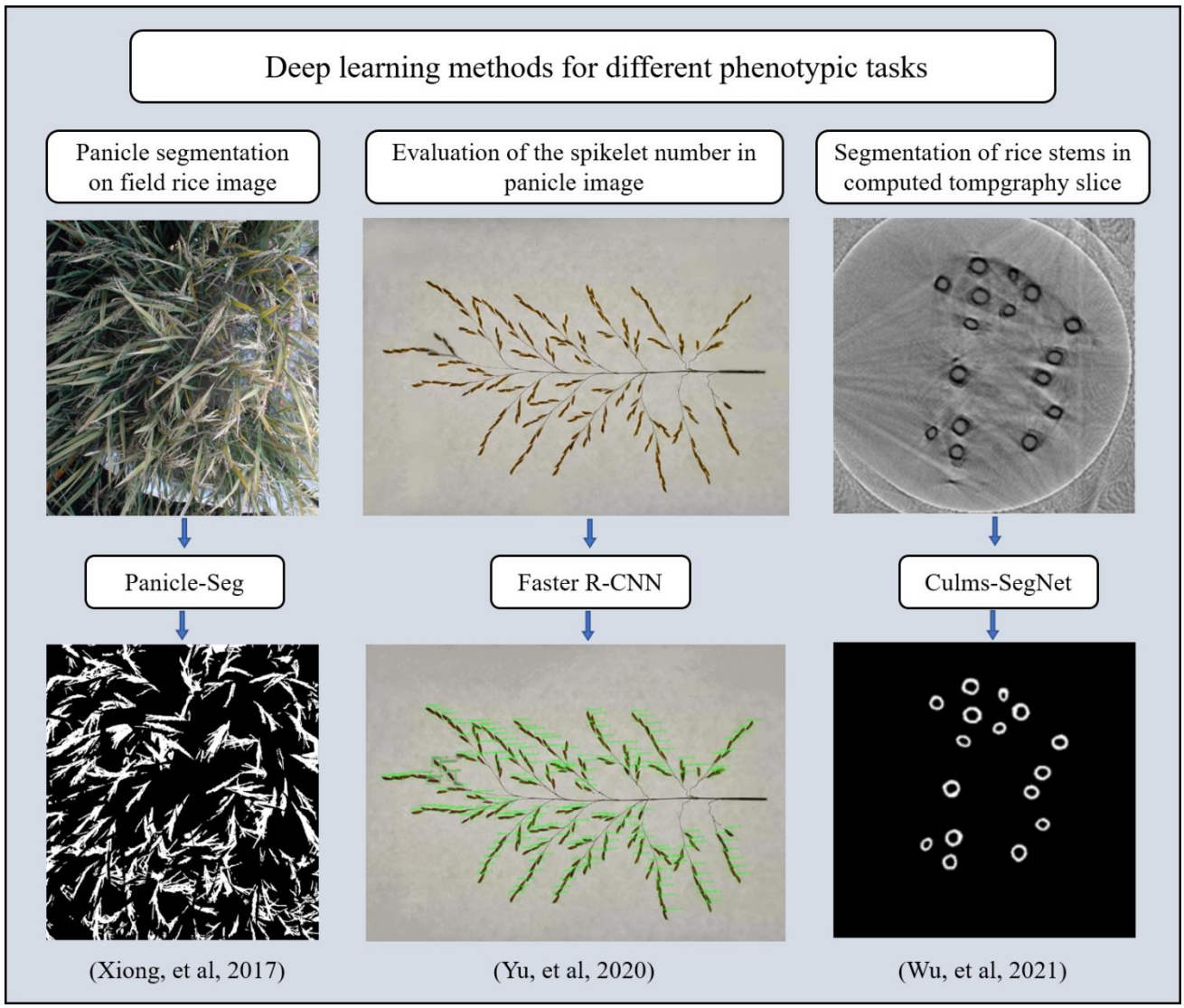

Figure: *(b) Deep learning methods for different phenotypic tasks.*

CONCLUSIONS

The image-based phenotyping provided high-efficient and objective methods for quantification of multi-dimensional crop agronomic traits. This paper introduced the advanced photonics imaging techniques and the classical and the state-of-the-art image processing techniques that have been applied in our previous phenotypic works. We expect these high-throughput phenotypic methods benefit more genetics and crop breeders.

REFERENCES

[1] Yang W, Duan L, Chen G, et al. Plant phenomics and high-throughput phenotyping: Accelerating rice functional genomics using multidisciplinary technologies. Current opinion in plant biology. 2013;16.

[2] Yang W, Feng H, Zhang X, et al. Crop Phenomics and High-Throughput Phenotyping: Past Decades, Current Challenges, and Future Perspectives. Molecular Plant. 2020;13(2):187-214.

[3] Song P, Wang J, Guo X, et al. High-throughput phenotyping: Breaking through the bottleneck in future crop breeding. The Crop Journal. 2021;9.

[4] Liang X, Wang K, Huang C, et al. A high-throughput maize kernel traits scorer based on line-scan imaging. Measurement. 2016;90:453-60.

[5] Yang W, Guo Z, Huang C, et al. Combining high-throughput phenotyping and genome-wide association studies to reveal natural genetic variation in rice. Nature communications. 2014;5:5087.

[6] Duan L, Han J, Guo Z, et al. Novel Digital Features Discriminate Between Drought Resistant and Drought Sensitive Rice Under Controlled and Field Conditions. Frontiers in plant science. 2018;9:492.

[7] Xiong X, Yu L, Yang W, et al. A high-throughput stereo-imaging system for quantifying rape leaf traits during the seedling stage. Plant methods. 2017;13:7.

[8] Wu D, Ye J, Wang K, et al. Three-dimension reconstruction method based on silhouette for pot rice. Journal of Agricultural Science and Technology. 2020;22:9.

[9] Briglia N, Williams K, Wu D, et al. Image-Based Assessment of Drought Response in Grapevines. Frontiers in plant science. 2020;11:595.

[10] Zhang J, Zhao B, Yang C, et al. Rapeseed Stand Count Estimation at Leaf Development Stages With UAV Imagery and Convolutional Neural Networks. Frontiers in plant science. 2020;11.

[11] Feng H, Guo Z, Yang W, et al. An integrated hyperspectral imaging and genome-wide association analysis platform provides spectral and genetic insights into the natural variation in rice. Scientific Reports. 2017;7.

[12] Feng H, Chen G, Xiong L, et al. Accurate Digitization of the Chlorophyll Distribution of Individual Rice Leaves Using Hyperspectral Imaging and an Integrated Image Analysis Pipeline. Frontiers in plant science. 2017;8.

[13] Huang C, Li Y, Luo S, et al. Cotton seedling leaf traits extraction method from 3d point cloud based on structured light imaging. Transactions of the Chinese Society for Agricultural Machinery. 2019;50:8.

[14] Wu D, Yang W, Niu Z, et al. Non-destructive detection of wheat tiller morphological traits based on X-ray CT technology. Transactions of the Chinese Society of Agricultural Engineering. 2017;33:14.

[15] Hu W, Zhang C, Jiang Y, et al. Nondestructive 3D Image Analysis Pipeline to Extract Rice Grain Traits Using X-Ray Computed Tomography. Plant Phenomics. 2020;2020:1-12.

[16] Yu L, Shi J, Huang C, et al. An integrated rice panicle phenotyping method based on X-ray and RGB scanning and deep learning. The Crop Journal. 2020;9.

[17] Wu D, Wu D, Feng H, et al. A deep learning-integrated micro-CT image analysis pipeline for quantifying rice lodging resistance-related traits. Plant Communications. 2021;2:100165.

[18] Xiong X, Duan L, Liu L, et al. Panicle-SEG: A robust image segmentation method for rice panicles in the field based on deep learning and superpixel optimization. Plant methods. 2017;13:104.

VISUALIZING BRAIN-WIDE NETWORKS AT SINGLE-NEURON RESOLUTION WITH MICRO-OPTICAL SECTIONING TOMOGRAPHY

DOI 10.24412/cl-36896-2021-1-30-30

QINGMING LUO [1,2,3]

[1] *School of Biomedical Engineering, Hainan University, 58 Renmin Ave., Haikou 570228, China*
[2] *HUST-Suzhou Institute for Brainsmatics, JITRI Institute for Brainsmatics, Suzhou 215123, China*
[3] *Britton Chance Center for Biomedical Photonics, Wuhan National Laboratory for Optoelectronics, MoE Key Laboratory for Biomedical Photonics, School of Engineering Sciences, Huazhong University of Science and Technology, Wuhan 430074, China*

qluo@hainanu.edu.cn

ABSTRACT

The brain is the most complex and significant organ, but little is known regarding to the mechanisms of its function, which is related to brain anatomy. Conventional anatomical methods based on brain slices fail to reconstruct the neural projection in axial direction at single-cell resolution. To solve the problem, my lab has spent more than ten years developing Brain-wide Positioning System (BPS), a novel solution combining microscopic optical imaging and physical sectioning to obtain the tomographic information of a whole brain with sub-micron voxel resolution. BPS includes several generations such as Micro-Optical Sectioning Tomography (MOST) and several types of fluorescence MOST (fMOST). In this talk, I will introduce the principles of BPS and demonstrate how to locate and visualize the labelled neurons and neuronal networks in the whole brain. The pipeline includes whole-brain sample preparation, whole-brain optical imaging, and massive brain image processing and analyzation. BPS may play a crucial role and usher in a new era of Brainsmatics. Brainsmatics refers to the integrated, systematic approaches of measuring, analyzing, managing, and displaying brain spatial data, including but not limited to the concepts of digital mapping and visualization of the brain neuronal/vascular networks, brain atlas, brain connectome and projectome, brainnetome, neuroinformatics, and neuroimaging. Brainsmatics will provide comprehensive and systematic information to understand the brain, defeat the brain disease, and develop the brain-inspired intelligence.

METHODOLOGY OF MICROCIRCULATORY-TISSUE SYSTEMS MULTIMODAL OPTICAL DIAGNOSTICS

DOI 10.24412/cl-36896-2021-1-31-31

ANDREY DUNAEV[1]

[1]*Research and Development Center of Biomedical Photonics, Orel State University, Russia*

dunaev@bmecenter.ru

Violations of the microcirculatory-tissue systems (MTS) of the human body play a key role in the pathogenesis of various diseases complications, for example, rheumatological and endocrinological ones. Moreover, microcirculatory dysfunction plays a key role in the pathogenesis of gastrointestinal diseases, as well as ischemic organ damage in some acute abdominal surgical diseases. A modern trend in the development of optical non-invasive diagnostics (OND) is a multimodal approach combining several optical (less often – additional non-optical) methods in one diagnostic technology. This allows one to obtain highly efficient diagnostic tools for rheumatology, endocrinology, surgery, oncology, neurology, and other areas of medicine requiring determining the parameters of tissue perfusion-metabolic status. In order to ensure wider implementation of OND technologies into clinical practice, it is necessary to improve the multimodal approach methodology in the development of new methods and technical means for assessing the functional state of MTS in various fields of medicine. It is also necessary to resolve physical and technical issues, including substantiating medical and technical requirements for improving OND devices, carefully working out the issues of monitoring the technical condition to check their performance, identify hidden defects and failures, and compare the results obtained on various devices.

The aim of this work is to improve the quality of optical diagnostics of human body MTS and ensure the conditions for its widespread introduction into clinical practice through scientific substantiation and development of a general methodology of multimodal OND.

To solve the research problems, a systematic approach was used to develop algorithm for the synthesis of multimodal OND for assessing the functional state of MTS in various diseases. According to the developed scheme of interrelations between the main parameters and states of the MTS in various diseases, depending on research purposes, it is proposed to jointly apply the appropriate methods of OND. According to the biotechnical approach, a generalized biotechnical system (BTS) of multimodal optical diagnostics was synthesized to assess the functional state of the MTS of the human body. In addition to the decision rule, the developed BTS consists of hardware and software, including 4 main blocks: direct impact on the object, including, in addition on the biological tissue itself, test objects (optical phantoms); registration and processing of data. According to the proposed approach, the use of the decision rule (classifier) allows one to provide a diagnostic result to the doctor in the form of the presence/absence of microcirculatory-tissue disorders, as well as to determine the causes of the identified disorders and, thereby, brings the OND technology closer to the level of standard diagnostic methods.

Based on the BTS of multimodal OND a methods for assessing angiospastic and microcirculatory disorders in rheumatic diseases, and a method for assessing microcirculatory-metabolic disorders in MTS of lower limbs in diabetes mellitus were developed. Also in this work, algorithms were developed for assessing the state of the MTS of the human body under various conditions, such as sports and physiological stresses, during physiotherapeutic treatment and minimally invasive surgical procedures. The developed methods are based on the combined application of several widely used methods of OND, such as laser Doppler flowmetry (LDF), tissue reflectance oximetry, diffuse reflectance spectroscopy, fluorescence spectroscopy (FS) etc. It is important to emphasize that in these cases the results of multimodal diagnostics are not just a set of registered biomedical parameters, which are difficult to interpret by doctors due to both their complexity and high variability, but the information about the presence/absence of specific disorders in the MTS with the possibility of analyzing their causes.

In addition to the considering of the general issues of multimodal OND devices constructing, the substantiation of specialized medical and technical requirements was carried out. It allowed one to take into account the effect of blood circulation in biological tissue and pressure of the optical probe on the measurement results. To improve the metrological and technical support of multimodal OND, it is also necessary to develop new approaches and devices for monitoring their technical condition. Improved test objects (optical phantoms) for the most common optical methods in medical practice (LDF and FS) have been proposed, since they are the basic ones in modern multimodal OND.

The developed methodology of multimodal OND can be used to build medical decision support systems for the widest areas of medicine. The results of the work can be extended to other areas of medicine, for example, to improve optical biopsy methods in minimally invasive surgery, rheumatology, endocrinology, otolaryngology, dermatology, neurology, etc. The introduction of multimodal diagnostics into wearable devices (fitness bracelets, smartwatches) for long-term *in vivo* monitoring (daily or during sleep, tracking of circadian biorhythms; during treatment in a hospital or at home) also has great diagnostic potential.

The study was supported by the Russian Science Foundation under the project №21-15-00325.

MULTI-MODE COOPERATIVE PRECISION THERAPY OF TUMOR BASED ON PHOTOTHERAPY

DOI 10.24412/cl-36896-2021-1-32-32

SIWEN LI1*, YUEQING GU

State Key Laboratory of Natural Medicines, Jiangsu Key Laboratory of Drug Screening, Department of Biomedical Engineering, School of Engineering, China Pharmaceutical University, China.

lsw@cpu.edu.cn

ABSTRACT

Cancer remains one of the deadliest diseases and causes millions of deaths every year. Nowadays, chemotherapy and radiotherapy and surgery are the major clinical treatments, all of which frequently cause adverse effects and pose a risk of recurrence. In contrast, phototherapy, a rising platform with specific spatiotemporal selectivity and minimal invasiveness, has become an emerging solution for cancer therapy. Phototherapy, including photodynamic therapy and photothermal therapy, relies on the conversion of light energy into chemical and thermal energy by phototherapeutic moieties to kill tumors, and the in vivo biological effects induced can be combined with other therapeutic modalities to achieve synergistic treatment. In the meantime, the development of nanomedicine has ushered new frontiers in cancer therapy, holding great promise for improving the therapeutic index and reducing side effects. We always focused on the construction of a multi-functional nano-drug delivery system for phototherapy combined with other treatments for multimodal synergistic therapy of tumors. Centering on the above concept, we utilized targeted cascade delivery [1], tumor oxygenation enhanced photodynamic therapy [2], photothermal therapy combined with immunotherapy and other strategies which through liposomes, micelles, biofilm fusion liposomes, biological vesicles to make each treatment cooperative and enhance cancer treatment. In vitro and in vivo experiments have shown that these tactics may provide a promising and pragmatic platform for clinical applications.

REFERENCES

[1] Ma Y, Zhang J, Rui Y, Rolle J, Xu T, Qian Z, Gu Y, Li S. Depletion of glioma stem cells by synergistic inhibition of mTOR and c-Myc with a biological camouflaged cascade brain-targeting nanosystem. Biomaterials.268:120564. 2021.

[2] Xu T, Ma Y, Yuan Q, Hu H, Hu X, Qian Z, Rolle JK, Gu Y, Li S. Enhanced Ferroptosis by Oxygen-Boosted Phototherapy Based on a 2-in-1 Nanoplatform of Ferrous Hemoglobin for Tumor Synergistic Therapy. ACS Nano.14(3):3414-3425. 2020.

ADAPTIVE OPTICAL BESSEL BEAM TWO-PHOTON FLUORESENCE MICROSCOPY FOR VOLUMETRIC IMAGING OF SYNAPES IN DEEP CORTEX

DOI 10.24412/cl-36896-2021-1-33-34

WEI CHEN[1], RYAN NATAN[1], YUHAN YANG[1] AND NA JI[1]
[1]*Department of physics, UC Berkeley, USA*
wei.chen.cal@berkeley.edu

ABSTRACT

Deciphering the information processing within neuronal circuities demands a technique that is capable to record multitude neuronal inputs at synaptic resolution and the dynamic of neuron ensembles across a large brain volume. In favor of its non-diffractive propagation in space, Bessel beam has been demonstrated in two-photon microscopy as an approach to improve the volumetric imaging speed via an axially elongated focus [1, 2]. However, the impacts of phase turbulence, such as aberrations presented in the imaging system and biological samples, are usually overlooked and less studied for Bessel beam. In this study, we have shown that aberrated Bessel beam reduces the two-photon excitation efficiency and degrades the signal-to-noise ratio (SNR) especially for small neuronal structures in deep cortical layers.

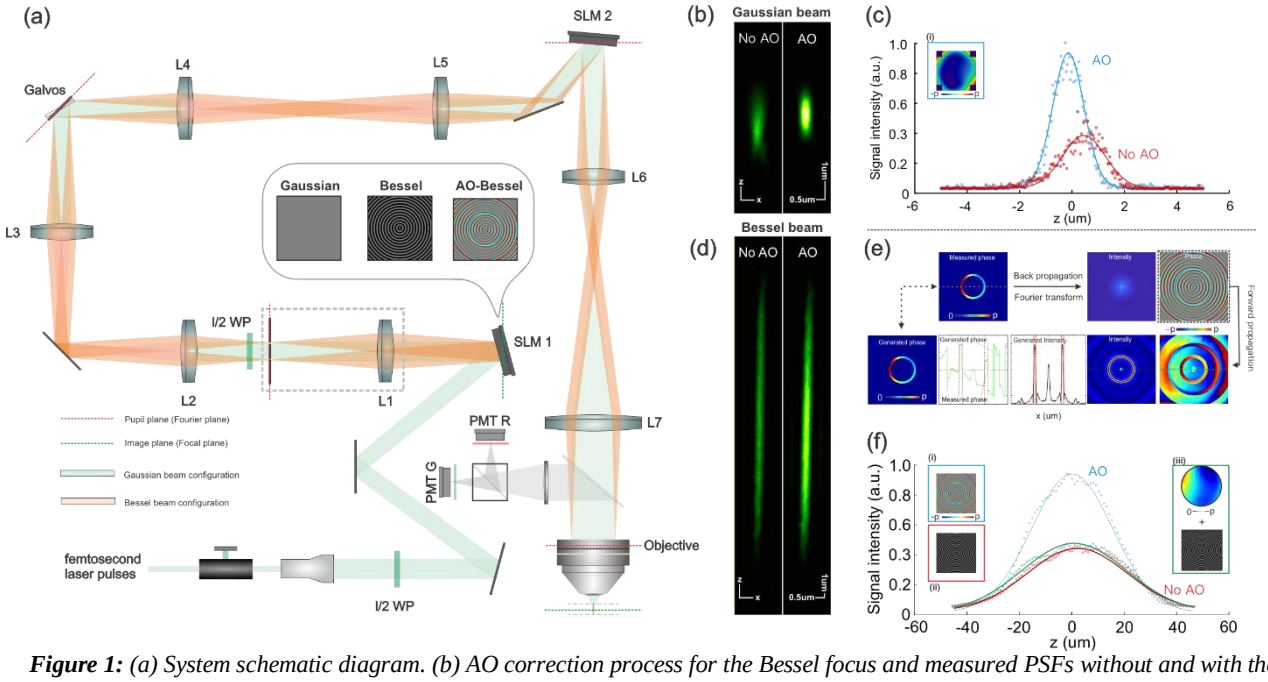

Figure 1: *(a) System schematic diagram. (b) AO correction process for the Bessel focus and measured PSFs without and with the system AO correction.*

In order to correct the aberrations for Bessel beam, we developed an adaptive optical (AO) Bessel beam multiphoton microscopy, which was enabled by two spatial light modulators conjugated to the image plane (SLM1) and the pupil plane (SLM2) respectively (Fig. 1a). System and sample induced aberrations were first probed by the Gaussian beam at the pupil plane based on the pupil-segmentation methods [3]. The wavefront correction pattern was then confirmed by imaging a 0.1um fluorescence bead and yielded about threefold signal improvement for Gaussian beam (Figs. 1b, c). Given a small interactive area between the SLM2 and the Bessel beam profile at the pupil plane, the wavefront correction pattern was computationally propagated to the image plane (SLM1) to construct the aberration-corrected Bessel beam for a greater correction efficiency (Fig. 1e). Imaging of a 0.1um bead by aberration-corrected Bessel beam (blue curve in Fig. 1f) showed about twofold signal improvement (Figs. 1d, 1f) and a dramatic higher correction efficiency compared to the AO correction directly applied at the pupil plane (green curve in Fig. 1f).

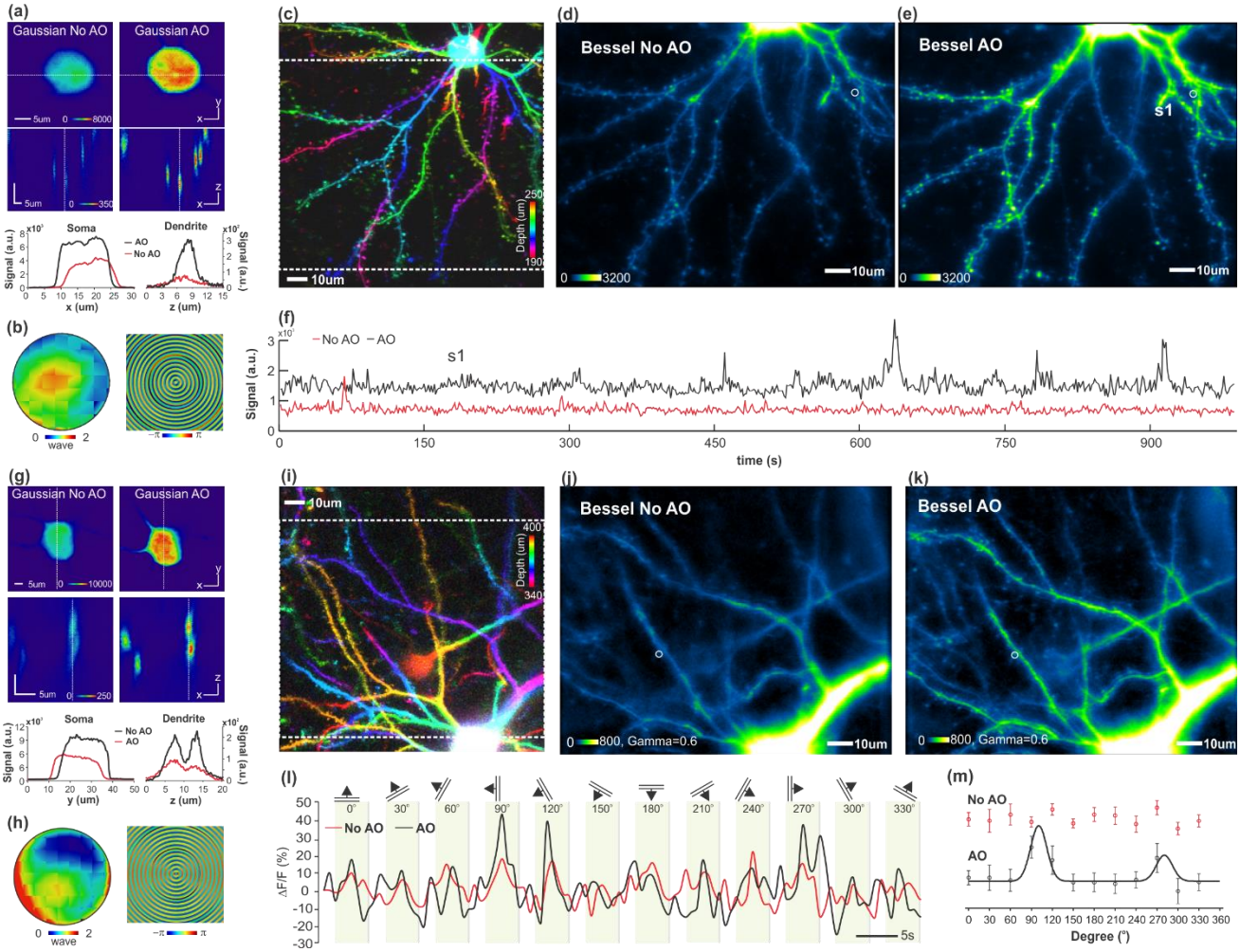

Figure 2: *In vivo volumetric imaging of synaptic activity in the deep cortical layers with AO corrected Bessel two-photon fluorescence microscopy.*

By sparsely expressing GCaMP6s in layer 2/3 (200um below pial) and GCaMP7s in layer 4/5 (400um below pial) in the mice primary visual cortex, we were able to measure the sample induced aberration using the bright soma body as a guide star. The wavefront correction not only improved the signal and resolution for Gaussian imaging (Figs. 2a, 2g), but also enhanced the contrasts and resolvability of small structures (e.g., spines) for Bessel imaging (Figs. 2d, 2e, 2j, 2k). With AO-corrected Bessel beam, more photons were effectively delivered to the desired region of interest. Therefore, more Ca^{2+} transients can be detected for spines (Fig. 2f) and the orientation selectivity of dendritic spines could be determined with more confidence owe to the improved signal-to-noise ratio (Figs. 2l, 2m).

REFERENCES

[1] Lu, R., et al., Video-rate volumetric functional imaging of the brain at synaptic resolution. Nature Neuroscience, 20: p. 620, 2017.

[2] Botcherby, E., R. Juškaitis, and T. Wilson, Scanning two photon fluorescence microscopy with extended depth of field. Optics communications, 268(2): p. 253-260, 2006.

[3] Ji, N., D.E. Milkie, and E. Betzig, Adaptive optics via pupil segmentation for high-resolution imaging in biological tissues. Nat Methods, 7(2): p. 141-7, 2010.

IN VIVO FLOW CYTOMETRY REVEALS A CIRCADIAN RHYTHM OF CIRCULATING TUMOR CELLS

DOI 10.24412/cl-36896-2021-1-35-35

XI ZHU[1], YUANZHEN SUO[1] AND XUNBIN WEI[1,2]

[1] *School of Biomedical Engineering, Shanghai Jiao Tong University, Shanghai 200030, China*
[2] *Biomedical Engineering Department, Peking University, Beijing, 100081, China*

xwei@bjmu.edu.cn

ABSTRACT

Circulating tumor cells (CTCs) is an established biomarker of cancer metastasis. The circulation dynamics of CTCs are important for understanding the mechanisms underlying tumor cell dissemination. Although studies have revealed that the circadian rhythm may disrupt the growth of tumors, it is generally unclear whether the circadian rhythm controls the release of CTCs. In clinical examinations, the current in vitro methods for detecting CTCs in blood samples are based on a fundamental assumption that CTC counts in the peripheral blood do not change significantly over time, which is being challenged by recent studies. Since it is not practical to draw blood from patients repeatedly, a feasible strategy to investigate the circadian rhythm of CTCs is to monitor them by in vivo detection methods. Fluorescence in vivo flflow cytometry (IVFC) is a powerful optical technique that is able to detect flfluorescent circulating cells directly in living animals in a noninvasive manner over a long period of time. In this study, we applied fluorescence IVFC to monitor CTCs noninvasively in an orthotopic mouse model of human prostate cancer. We observed that CTCs exhibited stochastic bursts over cancer progression. The probability of the bursting activity was higher at early stages than at late stages. We longitudinally monitored CTCs over a 24-h period, and our results revealed striking daily oscillations in CTC counts that peaked at the onset of the night (active phase for rodents), suggesting that the release of CTCs might be regulated by the circadian rhythm.

SYNERGISTIC THERAPEUTIC STRATEGIES FOR CANCER TREATMENT

DOI 10.24412/cl-36896-2021-1-36-37

FEIFAN ZHOU
Key Laboratory of Biomedical Engineering of Hainan Province, School of Biomedical Engineering, Hainan University, China
zhouff@hainanu.edu.cn

ABSTRACT

Cancer is one of the major causes of death, with high incidence and mortality in the world, and is expected to continue increasing in the following 20 years. The survival time of patients with localized tumor is significantly prolonged, while that of patients with distant metastases is still short. As an example, the five-year relative survival for patients with melanoma, the most aggressive form of skin cancer, decreased from 99 to less than 30% when the tumors progressed from localized to metastatic tumors [1]. Monotherapy is difficult to achieve complete cure in malignant tumors, even causing drug resistance and severe side effects. Developing collaborative strategies of different treatments for both primary tumors clearance and distant metastases elimination is urgently required.

Immunotherapy has brought a bright future of cancer therapy that can stimulate host immune system to destroy cancer cells. The discovery of immune checkpoint inhibitors marks a major breakthrough in cancer immunotherapy, including cytotoxic T lymphocyte associated antigen-4 (CTLA-4) and programmed cell death-1 (PD-1), which have been awarded the Nobel Prize in 2018 [2, 3]. Ipilimumab, a CTLA-4 antibody, has been approved by U.S. Food and Drug Administration for the treatment of patients with advanced melanoma [4]. The mechanism of action of ipilimumab in patients with melanoma is indirect, acting through T cell mediated antitumor immune responses. Therefore, a large number of cytotoxicity T cells were required to enhance the therapeutic effect of immunotherapy.

Phototherapy was supposed to a promising cancer therapy due to its effectiveness in producing *in situ* whole tumor cell vaccine and destroying primary tumors with non-invasiveness [5]. The effective conversion from light energy to heat is necessary for phototherapy, which can be achieved by introducing appropriate photoagents. Primary tumors were ablated after the specific near infrared light (NIR) irradiation to generate prophagocytic signals, such as tumor-associated antigens, damage-associated molecular patterns and proinflammatory cytokines, which subsequently were recognized by dendritic cells (DCs). This process is considered as immunogenic cell death, which potentiated the activation and infiltration of DCs to trigger robust cytotoxicity T cells response [6]. Thus, photo-immunotherapy may provide an excellent solution to inhibit both primary tumors and distant metastases [7]. Herein, in order to verify the therapeutic outcomes and support the synergistic hypothesis of combination between phototherapy and immunotherapy, we present one case of stage IV melanoma treated with laser irradiation and ipilimumab [8] (Figure 1).

The patient had primary tumor and several epidermal metastases in head and neck, as well as metastatic tumor in the lungs (AJCC stage IV M1b), repeated attempts at surgical resection and high-dose radiation therapy had failed. On physical examination, a primary melanoma site and surgical scars were observed near the vertex of the bald scalp. There was also a 5- or 6-cm ‘drinking straw’-like chord of metastatic deposits in his head and neck that probably represented a series of small nodular and diffuse lymphatic infiltrates. From the chest PET image, several metastatic nodules in the lungs were observed.

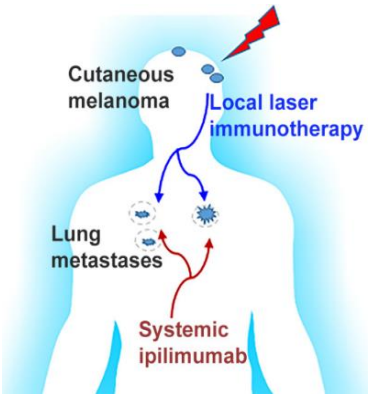

Figure 1. *Schematic of treatment using phototherapy and ipilimumab on a stage IV melanoma patient.*

The patient was treated with non-invasive NIR laser irradiation (805 nm, 1 W/cm^2, 10 min) and topical imiquimod as the immunoadjuvant (5% cream, 250 mg per dose, twice daily) on the site of cutaneous melanoma. After three months, all cutaneous melanoma in head and neck had been completely cleared. However, the pulmonary metastases remained no shrinking. To further improve the therapeutic effects, three months after the first phototherapy, an initial course of ipilimumab (3 mg/kg) was started, for a total of four infusions, one every three weeks. Another three months later, immediately after the ipilimumab treatment cycle, compared to the treatment before (Figure 2A), a repeat chest CT image showed that two small nodules in right lobe were disappearing (Figure 2B). Nine months after ipilimumab treatment the larger nodule had completely resolved (Figure 2C-D).

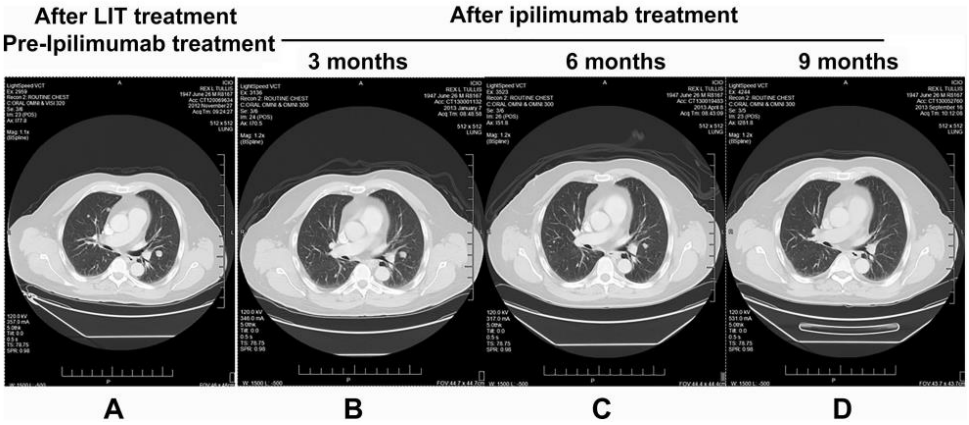

Figure 2. *CT images of the patient taken three months apart showing the same level in the thorax.*

In summary, the combination of phototherapy and ipilimumab was determined could achieve completely clearance of both primary and metastatic tumors in one patient with stage IV melanoma. All melanoma nodules on the head and neck were inhibited after phototherapy. However, there were no changes in pulmonary metastases. After the implementation of ipilimumab, all the pulmonary metastases were decreased and finally disappeared. Clinical response of this patient supports the hypothesis that phototherapy increases the number and quality of T cells in the tumor microenvironment, making the treatment more effective in combination with the CTLA-4 inhibitor. We look forward to extending these observations to a greater number of patients to prove this hypothesis.

REFERENCES

[1] R. L. Siegel, K. D. Miller, H. E. Fuchs, A. Jemal, Cancer statistics, 2021, CA Cancer J. Clin. 7–33, 2021.
[2] M. F. Krummel, J. P. Allison, CD28 and CTLA-4 have opposing effects on the response of T cells to stimulation, J. Exp. Med. 459–465, 1995.
[3] Y. Ishida, Y. Agata, K. Shibahara, T. Honjo, Induced expression of PD-1, a novel member of the immunoglobulin gene superfamily, upon programmed cell death, EMBO J. 3887–3895, 1992.
[4] V. K. Sondak, K. S. Smalley, R. Kudchadkar, S. Grippon, P. Kirkpatrick, Ipilimumab, Nat. Rev. Drug Discov. 411–412, 2011.
[5] F. Zhou, X. Li, M. F. Naylor, et al, InCVAX - A novel strategy for treatment of late-stage, metastatic cancers through photoimmunotherapy induced tumor-specific immunity, Cancer Lett. 169-177, 2015.
[6] J. Zhou, G. Wang, Y. Chen, H. Wang, Y. Hua, Z. Cai, Immunogenic cell death in cancer therapy: present and emerging inducers, J. Cell Mol. Med. 4854–4865, 2019.
[7] M. Wang, J. Rao, M. Wang, et al, Cancer photo-immunotherapy: from bench to bedside, Theranostics, 2218–2231, 2021.
[8] M. F. Naylor, F. Zhou, B. V. Geister, R. E. Nordquist, X. Li, W. R. Chen, Treatment of advanced melanoma with laser immunotherapy and ipilimumab, J. Biophotonics, 618–622, 2017.

LASER INDUCED FLUORESCENCE (LIF) SPECTROSCOPIC INVESTIGATION OF CERVIX TISSUE FOR THE DETECTION OF CHRONIC CERVICITIS

DOI 10.24412/cl-36896-2021-1-38-38

AJAYA KUMAR BARIK[1], SANOOP PAVITHRAN M[1], JIJO LUKOSE[1], REKHA UPADHYA[2], MURALIDHAR V PAI[2], AJEETKUMAR PATIL[1], ASEEFHALI BANKAPUR[1] AND SANTHOSH CHIDANGIL[1]

[1]Department of Atomic and Molecular Physics, Manipal Academy of Higher Education, Manipal

[2]Department of Obstetrics & Gynaecology, Kasturba Medical College, Manipal, Manipal Academy of Higher Education, Manipal.

Email: ajaykumarbarik@gmail.com

ABSTRACT

Cervical cancer is one of the leading cause of cancer mortalities. The detection of any abnormality like chronic cervicitis (CC), low grade intraepithelial lesion (LGSIL) and high grade intraepithelial lesion (HGSIL) may prevent further progression diseases. Optical techniques are explored for the early detection and diagnosis for diseases in which laser induced fluorescence (LIF) is one of the simple methods for the detection of various types of cancers. This technique is capable of discriminating normal and abnormal tissue sample without the necessity of exogenous fluorophores. In the present work, LIF studies have been performed using cervix tissues obtained from volunteers who have undergone hysterectomy. The tissue fluorescence was acquired by exciting the sample with 325 nm He-Cd laser through a fiber optic probe. The fluorescence spectra show two distinct peaks due to collagen and NADH around 390 nm and 440nm respectively. The fluorescence intensity of collagen and NADH is different for normal and chronic cervicitis tissue. As the disease progresses, the NADH intensity increases and the collagen intensity decreases. The device has proven to be a reliable technique for the early detection, in vivo screening and surgical demarcation.

REFERENCES

[1] Jemal, Ahmedin, Taylor Murray, Elizabeth Ward, Alicia Samuels, Ram C. Tiwari, Asma Ghafoor, Eric J. Feuer, and Michael J. Thun. "Cancer statistics, 2005." *CA: a cancer journal for clinicians* 55, no. 1 (2005): 10-30.

[2] Rodero, Ademir Barianni, Landulfo Silveira Jr, David Augusto Rodero, Roberto Racanicchi, and Marcos Tadeu T. Pacheco. "Fluorescence spectroscopy for diagnostic differentiation in uteri's cervix biopsies with cervical/vaginal atypical cytology." *Journal of fluorescence* 18, no. 5 (2008): 979-985.

[3] Chidananda, Siddappa M., Kapaettu Satyamoorthy, Lavanya Rai, Attibele P. Manjunath, and Vasudevan B. Kartha. "Optical diagnosis of cervical cancer by fluorescence spectroscopy technique." *International journal of cancer* 119, no. 1 (2006): 139-145.

BIOPHOTONICS OF BODY FLUIDS FOR CLINICAL APPLICATIONS

DOI 10.24412/cl-36896-2021-1-39-39

SANTHOSH CHIDANGIL, MITHUN N., REENA V. JOHN, SPHURTI S ADIGAL, NIDHEESH V.R. AND JIJO LUKOSE

Centre of Excellence for Biophotonics
Department of Atomic and Molecular Physics,
Manipal Academy of Higher Education
Manipal, Karnataka, India-576104
Email:santhosh.cls@manipal.edu

ABSTRACT

Investigation of body fluids is of paramount importance since it carries a pool of biological markers, which can reflect the health status of humans. Technological advancements in the field of biophotonics offer highly sensitive, objective and rapid detection of abnormal health conditions from body fluid analysis. Raman spectroscopy has been widely regarded as reliable spectroscopic tool for the characterization of body fluids due to its minimal interference imposed by aqueous environment. Raman Investigation of blood cells under physiological condition is restricted due to Brownian motion of micron sized cells. In view of this, spectroscopic characterizations of live cells under various stress agents and health abnormalities has been performed using a custom built Raman Tweezers, which involves the optical arresting of cells with the aid of tightly focused laser beam. Besides Raman Tweezers spectroscopy, High-performance liquid chromatography-Laser Induced Fluorescence (HPLC-LIF) technique have been also explored for the protein profiling of body fluids such as blood serum, saliva and tears collected from healthy and abnormal subjects. The ultra-sensitive HPLC–LIF system developed in our lab have been effective in carrying out screening, early detection, and staging for various cancers. Research and development is progressing well for the analysis exhaled breath for the detection of volatile organic compound as markers for various diseases including COVID-19 infection. An overview of these research activities will be discussed during the workshop.

OPTO-THERMO-ACOUSTIC STUDIES FOR CANCER DIAGNOSIS

DOI 10.24412/cl-36896-2021-1-40-42

UTTAM M. PAL and HARDIK J. PANDYA
Department of Electronic Systems Engineering, Indian Institute of Science, Bangalore.
hjpandya@iisc.ac.in

ABSTRACT
Breast cancer is one of the leading reasons for mortality for women accounting for around 6.9% of breast cancer-related deaths worldwide in 2020. If the patient undergoing X-Ray mammography and sonography are suspicious, they are recommended for histopathology tests to confirm a breast cancer diagnosis. Histopathology is considered a gold standard; however, it requires a skilled clinician and is time-consuming [1]. A multimodal system that can characterize the bulk optical, thermal and acoustic properties of the tissue is designed and developed. The measurements were carried out on ex-vivo breast biopsy tissues from N = 44 patients, and it was observed that the reduced scattering coefficient (μ'_s) and acoustic attenuation (α) of the malignant tissue were more than the normal tissues. In contrast, an opposite trend was ascertained for the thermal conductivity. Exceptional statistical significance was found when the combined μ'_s, thermal conductivity (k), and α measurements were considered [2-6].

METHOD
The combined optical, thermal, and acoustic measurements were performed on a set of N = 6 subjects with invasive ductal carcinoma and adjacent normal breast biopsy tissues from each subject. The tissues were extracted during the breast lumpectomy surgery and stored in 10% formalin-fixed solution, as shown in Fig. 1a. Patients' consent was obtained through the institutional ethics committee of Assam Medical College (AM/EC/1333) and the Indian Institute of Science (14012020) to perform this study. These tissues were sliced into uniform cylindrical blocks as shown in Fig. 1b and measured using the upgrade Hybrid Spectral-IRDx system, which includes the optical, thermal, and acoustic measurements as shown in Fig. 1c.

RESULTS & DISCUSSION
The mean values of μ'_s for cancer and normal tissue were 13.32 1/cm and 8.70 1/cm respectively at 850 nm, 11.12 1/cm and 5.64 1/cm at 940 nm, and 7.42 1/cm and 6.39 1/cm at 1060 nm as shown in Fig. 2a. The mean absorption coefficient (μ_a) for normal tissues was more (1.60 1/cm, 2.66 1/cm, and 3.17 1/cm) than the cancerous tissues (1.08 1/cm, 1.12 1/cm, and 2.52 1/cm) while operating at 850 nm, 940 nm, and 1060 nm, respectively. The mean α for cancerous tissue was reported to be more (20.14 dB/cm) than the normal tissue (8.79 dB/cm), as shown in Fig. 2b. The bulk averaged thermal conductivity (k) for cancerous tissue was evaluated to be lower (0.035 W/m/K) compared to normal tissue (0.052 W/m/K), as shown in Fig. 2c. While the average specific heat capacity (Cp) for normal tissue and cancerous was 3594 J/Kg/K and 3611 J/Kg/K, respectively, as shown in Fig. 2d.

The individual statistical analysis was performed by Mann-Whitney U test while the combined statistical analysis with Fisher's combined probability test. The normal and cancerous tissue differentiated based on only μ'_s when the LED was operated at 850 nm and 940 nm was statistically significant (p = 4.53 e-2, 2.04 e-2) while operating at 1060 nm was statistically insignificant (p = 4.71 e-1). While considering only α was found to be statistically significant (p = 5.07 e-3). Considering only k was statistically significant (p = 5.07 e-3); however, Cp was statistically insignificant (p = 3.78 e-1).

While combining the outcomes from μ'_s and k, the outcomes are statistically significant (p = 4.15 e-4). When combining the outcomes from μ'_s and α, the results are also considerably statistically significant (p = 4.15 e-4). The statistical

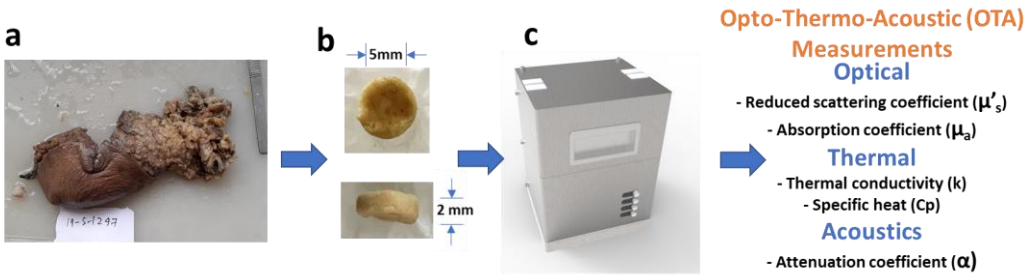

Figure 1: Schematic of the clinical workflow of breast cancer diagnosis: *(a) The excised breast tissue, b) Preparation of uniform samples with 2 mm thickness and 5 mm diameter are prepared using the punch biopsy, (c) Opto-Thermo-Acoustic (OTA) Hybrid Spectral-IRDx system*

significance improves when the thermal and acoustic results are combined (p = 2.97 e-4). However, the most statistical

significance is observed when the μ'_s, k, and α are combined (p = 2.60e-5). The complete statistical analysis is tabulated in Table 1.

It can be observed from the results that the statistical significance to demarcate the cancerous tissue from normal tissues can be notably improved by involving optical measurements with thermal and acoustic modalities. These bulk tissue properties can be used as biomarkers to physiologically characterize the cancerous and normal tissues, aiding the pathologist in making an assertive diagnosis.

Table 1: Individual and combined statistical analysis of optical, thermal, and acoustic modalities

Modality	Parameters	C & N
Optical	μ'_s (850 nm)	4.53 e-2 (*)
	μ'_s (940 nm)	2.04 e-2 (*)
	μ'_s (1060 nm)	4.71 e-1 (ns)
Acoustic	α	5.07 e-3 (**)
Thermal	k	5.07 e-3 (**)
	C_p	3.78 e-1 (ns)
Combined Optical-Thermal	μ'_s (850 nm and 940 nm), and k	4.15 e-4 (***)
Combined Optical-Acoustics	μ'_s (850 nm and 940 nm), and α	4.15 e-4 (***)
Combined Thermal-Acoustics	k and α	2.97 e-4 (***)
Combined Opto-Thermal-Acoustic	μ'_s (850 nm and 940 nm), k, and α	2.60 e-5 (****)

C = Cancerous tissue, N = normal tissues

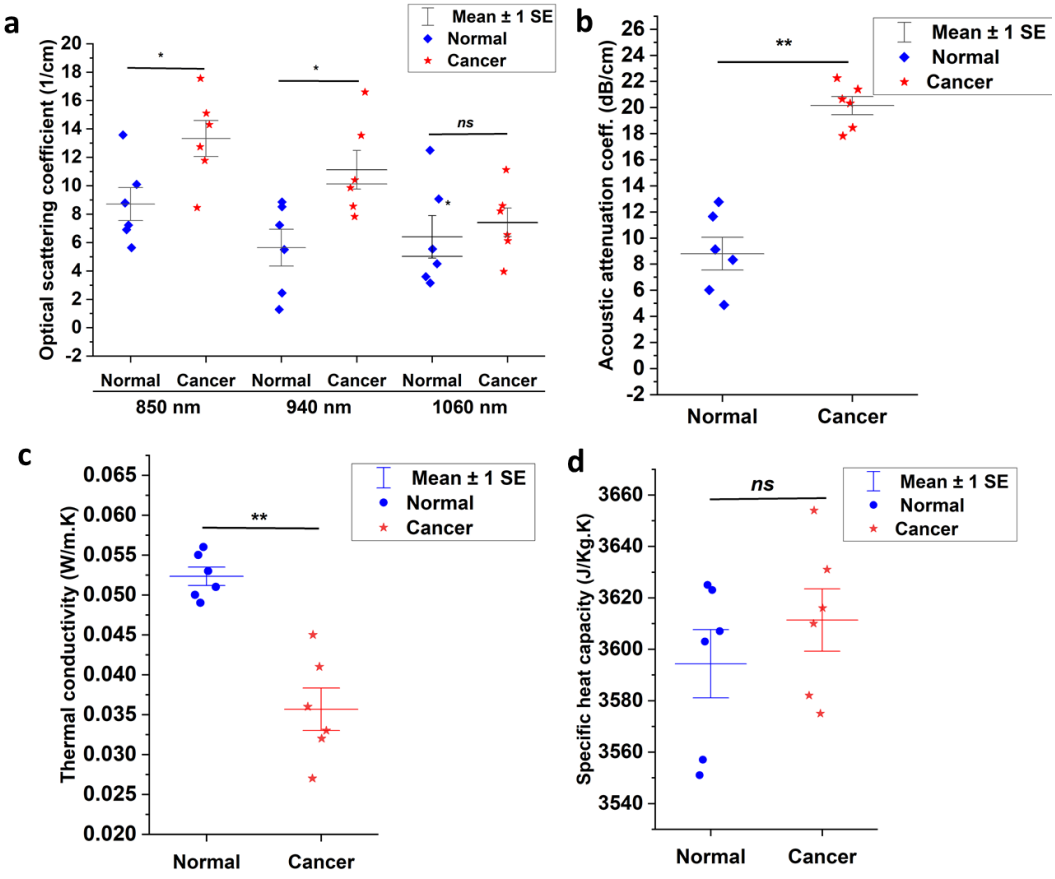

Figure 2: *Combined optical, acoustic, and thermal results: (a) Reduced scattering coefficient ($\mu`_s$) measured at 850 nm, 940 nm, and 1060 nm, (b) Acoustic attenuation, (c) Averaged thermal conductivity (k), and (d) Averaged specific heat capacity (Cp) for N = 6 subjects.*

CONCLUSION

The combined measurements were statistically significant to differentiate the cancerous tissues from the normal tissues. The upgraded Hybrid-Spectral-IRDx system can be used inside the operating room for rapid breast cancer diagnosis. Once the system's performance is measured using a large cohort of breast cancer patients, the opto-thermo-acoustic modalities can aid and support the histopathology test for an improved cancer diagnosis.

REFERENCES

[1] Uttam M. Pal, Mansi Saxena, G. K. Anil Vishnu, Darshan Parsana, B. S. R. Sarvani, Manoj Varma, Mahesh Jayachandra, Vishnu Kurpad, Deb Baruah, Gayatri Gogoi, Jayant S. Vaidya & Hardik J. Pandya (2020) Optical spectroscopy-based imaging techniques for the diagnosis of breast cancer: A novel approach, Applied Spectroscopy Reviews, 55:8, 778-804, 2020.

[2] Uttam M. Pal, Anil Vishnu GK, Manoj Varma, Jayant S. Vaidya, Hardik J. Pandya, Thermo-Optic Measurements and their Inter-Dependencies for Breast Cancer Diagnosis, J. Biophotonics, 14 (8), 2021.

[3] Uttam M. Pal, Ashika Nayak, Tejaswi Medisetti, Gayatri Gogoi, Himanshu Shekhar, M.S.N. Prasad, Jayant S. Vaidya, Hardik J. Pandya, Hybrid Spectral-IRDx: Near-IR and Ultrasound Attenuation System for Differentiating Breast Cancer from Normal Tissue, IEEE Trans Biomed Eng., 2021.

[4] Uttam M. Pal, Arif Mohd Kamal, Ashika Nayak, Tejaswi Medisetti, Hardik J. Pandya, "Towards an Opto-Thermo-Acoustic (OTA) based Diagnostic Tool to Delineate Normal from Cancerous Tissue for Cancer Margin Assessment", in European Conferences on Biomedical Optics 2021 (ECBO), OSA Technical Digest, paper ETu4A.4, 2021.

[5] Uttam M. Pal, Anil Vishnu GK, Saeed Rila, Saahil Shroff, Gokul A M, Deb Baruah, Jayant S. Vaidya, Gayatri Gogoi, and Hardik J. Pandya, "Towards a Portable Platform Integrated with Multispectral Noncontact Probes for Delineating Normal and Breast Cancer Tissue Based on Near-Infrared Spectroscopy" in IEEE Transactions on Biomedical Circuits and Systems, vol. 14, no. 4, pp. 879-888, 2020.

[6] Arif Mohd. Kamal, Uttam M. Pal, Ashika Nayak*, Tejaswi Medisetti*s, Arjun B.S., Gayatri Gogoi, Jayant S. Vaidya, Hardik J. Pandya, "Towards Development of LED-based Time-Domain Near-IR Spectroscopy System for Delineating Breast Cancer from Normal Tissue", IEEE Sensors Journal, vol. 21, no. 16, pp. 17758-17765, 2021.

UVA LED ANTIVIRAL ACTION ON CORONAVIRUS

DOI 10.24412/cl-36896-2021-1-43-43

I. N. ZAVESTOVSKAYA [1], V. A. GUSCHIN [2], L. I. RUSSU [2], E. A. CHESHEV [1], A. L. KOROMYSLOV [1], I. M. TUPITSYN [1], A. A. FRONYA [1,3] , AND M. S. GRIGORYEVA [1, 3]

[1] *Lebedev Physical Institute, Russian Academy of Sciences, Moscow, 119991 Russia*

[2] *National Research Center for Epidemiology and Microbiology named after Honorary Academician N.F. Gamaleya, Moscow, 123098 Russia*

[3] *National Research Nuclear University MEPhI (Moscow Engineering Physics Institute), Moscow, 115409 Russia*

fronyaaa@lebedev.ru

In the presented work, the experimental investigation of coronavirus inactivation was carried out, stand based on laser diodes for further applications as an antiviral device was tested. In experiments laser diodes from the UVA spectral range (385 and 395 nm) were used.

Recently, research on the effects of UV radiation has intensified and focused on SARS-Cov-2 (COVID-19) and its equivalent pathogens. One of the areas of research is the development of safe for humans means for treating contact surfaces in order to reduce the number or complete inactivate of pathogenic microorganisms in the environment and on surfaces. UV irradiation is an environmentally friendly method of destruction bacteria, viruses and fungi without the use of harmful chemicals or heat.

Over the past decade, groups of scientists from different countries have demonstrated a number of pathogenic agent's inactivation effectiveness under the influence of ultraviolet and visible radiation in various wavelength ranges - from 220 to 480 nm [1,2]. The SARS-CoV-2 virus is very contagious, it already has numerous mutations, and its transmission occurs by airborne droplets through water and surface [3].

In presented work, for the experiments commercially available LEDs with different wavelengths in the UVA ranges of 385 and 395 nm and a divergence of 70 degrees were used. Experimental studies of the ultraviolet radiation UVA effect on the infectious properties of β-coronavirus have been carried out. Bovine coronavirus has been selected for research as a prototype of the pathogen agent COVID-19 (SARS-CoV-2) [4].

The initial viral titer before irradiation was 10^5 $TCID_{50}$/ml. The LED aperture was located at a distance of 4 cm from the surface of the virus-containing fluid. The irradiation dose was determined as the product of the measured power density on the surface of the virus-containing fluid in the cell tablet and the exposure time. The difference in virus titers in the control (without irradiation) and irradiated groups, expressed in logarithms - Δ log $TCID_{50}$ ml, was presented as a criterion for the antiviral efficiency of UV radiation. In virological studies, it is considered a satisfactory antiviral effect of the drug at Δlg $TCID_{50}$/ml $\geq$ 2.0.

UV irradiation at 385 nm and 395 nm is an effective antiviral means. It was found that the threshold value of the radiation dose, which provides a decrease in the titer of the virus by 2 orders of magnitude, depends on the irradiation scheme, and depends on the divergence of the LED. In the presented experiments, the maximum values for reducing the virus titer were achieved for the UVA 385 nm LED - by 4 orders of magnitude at a dose of 157 J/cm^2 [5].

The reported study was funded by RFBR according to the research project № 20-04-60292.

REFERENCES

[1] 1. L. Horton, et al. Photochem. Photobiol. Sci. (2020) Vol.19, No.10, pp. 1262–1270;

[2] 2. M G Strakhovskaya, et al. Laser Phys. Lett. (2020) Vol. 17, No.9, 093001;

[3] 3. N. van Doremalen, et al., J. Med. 382 (2020) 1564–1567, G. Kampf, et al. J Hosp Infect 104 (2020) 246–251;

[4] 4. N. Yoshizawa, et al. Viruses (2020) Vol.12, No.12, p. 1372;

[5] 5. I. N. Zavestovskaya, et al. Bulletin of the Lebedev Physics Institute Vol. 48, No. 7, 2021, p. 195-202.

INCORPORATING CHAOS THROUGH A BUNIMOVICH INSPIRED STADIUM DESIGN FOR UV-C DISINFECTION CHAMBER

DOI 10.24412/cl-36896-2021-1-44-45

SWATI MISHRA[1], DEVENDRA SINGH[2], HARSHAWARDHAN WANARE[2,3]
[1]Department of Biological Sciences & Bioengineering, Indian Institute of Technology, Kanpur, India-208016
[2]Centre for Engineering in Lasers & Photonics and [3]Department of Physics, Indian Institute of Technology, Kanpur, India- 208016
hwanare@iitk.ac.in

ABSTRACT

UV-C radiation has been used extensively in disinfection chambers to neutralize a variety of microorganisms. The UV-C radiation is used to steralize air, water, food and a variety of tools in medical as well as food industry. The microorganisms like *Clostridium* spores and *Klebsiella pneumoniae* commonly found on frequently touched surfaces in healthcare settings that were not killed by the standard disinfecting procedure are removed by 254 nm UV-C wavelength [1]. Paramount in the above applications is that the UV-C radiation must efficiently reach every nook and cranny of the chamber evenly, which is extremely challenging to ensure in most disinfection chamber designs [2,3]. In actual practice, this is not guaranteed and the radiation dosage available may be differ widely at different spatial locations within the chamber, even leading to dark regions wherein radiation levels could be negligible. The light intensity distribution depends on the light source's placement, the chamber's design that supports reflections from the walls and the nature and location of the object placement. The presence of "dark spots" severely compromises complete sterilization. In order to address this issue, we propose a stadium design chamber with specific shape parameters that results in chaotic dynamics of the radiation leading to uniform UV-C radiation distribution. We demonstrate the use of chaotic Buminovich stadium design to ensure space-fillig characteristics of the underlysing chaotic UV-C field distribution. This leads to a complete elimination of the "dark spots" within the chamber. We show other advantages of such a UV-C which ensures a more evenly distributed UV-C light intensity distribution in the proposed stadium chamber in comparison to the commonly used cuboidal box. This chaotic field distribution mechanism has been adapted in the photovoltaic cells to maximize the trapped sun rays' trajectories for enhanced absorption within the active medium [4]. This effect has also been used in a microcavity laser wherein cavity modes' interaction with the lasing medium caused due to deformation of the two-dimensional cavity shape that led to chaotic dynamics simultaneously resulted in a single-mode lasing [5]. It should be noted that the parameters chosen for the Bunimovich stadium lie well within the completely chaotic regime as presented by *Lopac et al.*, i.e. there is a complete absence of islands of stability that involve regular periodic orbits [6]. The presence of such islands of stability would imply that light cannot escape these regions and in other words, the light from the surrounding region gets delimited from these regions leading to the formation of "dark spots". Hence, one needs to choose the parameters of the Bunimovich stadium that correspond to the completely chaotic regine. The other important aspect is that of dimensionality, the Bunimovich stadium is a two-dimensional system, yet we simply extend the third dimension and arrange the UV -C source lamp parallel to this third dimension that provides the depth to the enclosure for undertaking radiation disinfection and individual planes themselves would support the chaotic dynamics.

The 2-D Bunimovich stadium is characterized by two shape parameters in the x-y plane of the central rectangle where 2δ is its horizontal width and 2γ is its vertical height, the radius of the curved region is $1-\delta$. We provided an extra depth to the chamber along the z-direction, the experiments involved a sealed stadium shaped chamber made of metallic aluminium sheets with a rectangular front door opening as shown in Figure 1. The UV-C light sources are the Philips TUV PL-S lamp placed along the four edges of the chamber parallel to the depth. A Lutron UVC- 254 UV light meter probe placed inside the chamber measures the intensity, whereas the controller unit is placed outside which displays the readings in mW/cm^2.

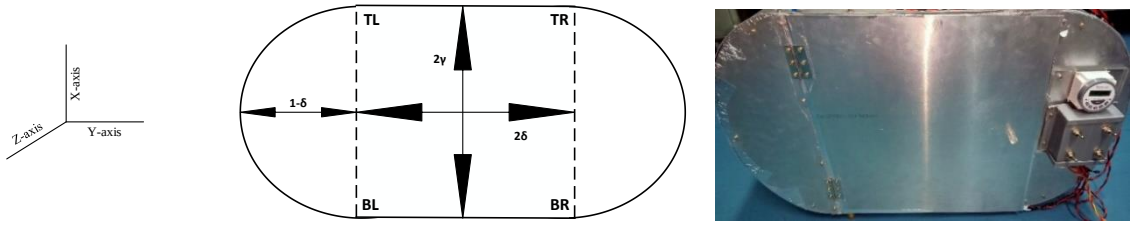

Figure 1. *Design of the UV chamber. TL: Top Left; TR: Top Right; BL: Bottom Left; BR: Bottom Right is the location of the UV-C light source placed parallel to the z- axis.*

The UV-C probe is kept at the center of the rectangular stage (about 6 inches from the chamber floor) inside the UV chamber facing upwards in the x-direction and tilted at various angles using a goniometer. The range of the angles was [-70,+70] degrees about both the z- and y- direction. The measurements are made in two different scenarios, namely when the chamber is empty with only the UV-C probe placed on the stage, and the second when a stack of papers cover about two-third of the stage with the probe in both sections. The second measurement protocol is to test out the effect of

shadow regions that invariably results from keeping multiple object within the chamber. Its computational simulations was performed in COMSOL 5.6 Ray Optics Module.
Figure 2 demonstrates that the stadium design significantly aids in uniform distribution of the radiation due to the chaotic scattering of the light trajectories. Note that the geometery leads to an exponential separation (related to the Lyapunov exponent that characterizes Chaos) of the light rays after multiple reflections that were nearly identical to being with. The space filling nature of the light field also arises due to the same underlying chaotic dynamics. This central advantage is lost in the conventional cuboidal or circular geometry chambers. Our experimental results are validated by quantifying the the standard deviation of the UV-C intensity in stadium ($std._{stadium}$) and cuboidal chambers ($std._{cuboidal}$) which reveals a more uniform light intensity distribution in the proposed stadium chamber in comparison to more the commonly used cuboidal counterpart, shown in the yellow panel in Fig. 2.

Incorporation of a simple design variation offers tremendous benefits by invoking chaotic dynamics and we believe this strategy is quite powerful and can easily be adapted in multifarious applications requiring unform radiation distribution.

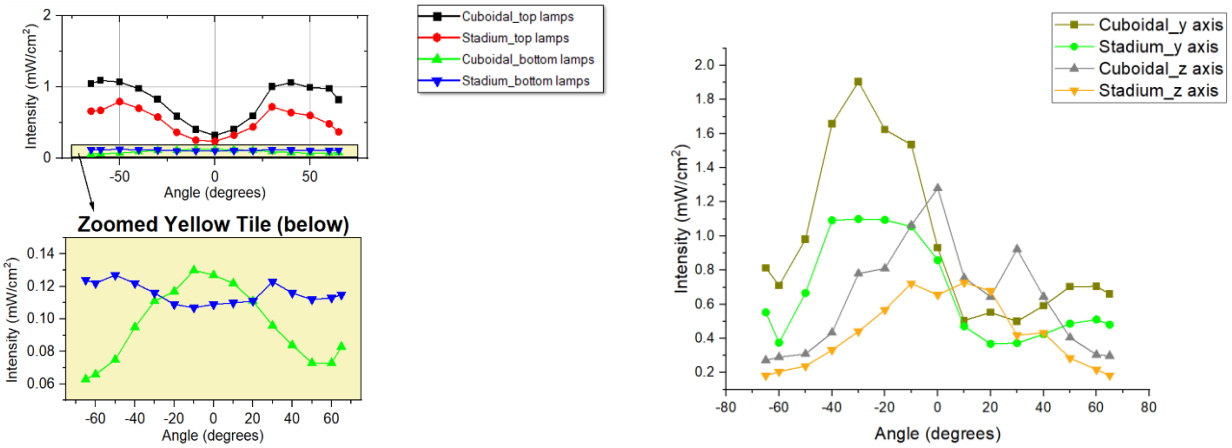

Figure 2. *Experimental results showing comparison of the light intensity distribution to the angle at which the probe is tilted (left) contains only probe in z- direction in cuboidal and stadium chambers when the top lamps are switched on [$std._{stadium}$ = 0.174; $std._{cuboidal}$ = 0.265] and when the bottom lamps are on [$std._{stadium}$ = 0.006; $std._{cuboidal}$ = 0.022] (right) contains both the stack of papers and the UV-C probe when all the four lamps are switched on in y-axis [$std._{stadium}$ = 0.283; $std._{cuboidal}$ = 0.460] and z-axis [$std._{stadium}$ = 0.198; $std._{cuboidal}$ = 0.307]*

REFERENCES

[1] Kowalski, W. J., Bahnfleth, W. P., & Hernandez, M. T. (2009). A genomic model for predicting the ultraviolet susceptibility of viruses. IUVA News, 11(2), 15–28.

[2] Garciá De Abajo, F. J., Hernández, R. J., Kaminer, I., Meyerhans, A., Rosell-Llompart, J., & Sanchez-Elsner, T. (2020, July 28). Back to Normal: An Old Physics Route to Reduce SARS-CoV-2 Transmission in Indoor Spaces. ACS Nano. American Chemical Society. https://doi.org/10.1021/acsnano.0c04596

[3] Atci, F., Cetin, Y. E., Avci, M., & Aydin, O. (2020). Evaluation of in-duct UV-C lamp array on air disinfection: A numerical analysis. Science and Technology for the Built Environment, 27(1), 98–108. https://doi.org/10.1080/23744731.2020.1776549

[4] Seim, E., Kohler, A., Lukacs, R., Brandsrud, M. A., Marstein, E. S., Olsen, E., & Blümel, R. (2019). Chaos: A new mechanism for enhancing the optical generation rate in optically thin solar cells. Chaos, 29(9). https://doi.org/10.1063/1.5111042

[5] Harayama, T., Sunada, S., & Shinohara, S. (2017). Universal single-mode lasing in fully chaotic two-dimensional microcavity lasers under continuous-wave operation with large pumping power [Invited]. Photonics Research, 5(6), B39. https://doi.org/10.1364/prj.5.000b39

[6] Lopac, V., Mrkonjić, I., Pavin, N., & Radić, D. (2006). Chaotic dynamics of the elliptical stadium billiard in the full parameter space. Physica D: Nonlinear Phenomena, 217(1), 88–101. https://doi.org/10.1016/j.physd.2006.03.0

GAP-ENHANCED RAMAN TAGS FOR ANALYTICAL AND IMAGING APPLICATIONS

DOI 10.24412/cl-36896-2021-1-46-48

BORIS KHLEBTSOV[1], ANDREY BUROV[1], DANIIL BRATASHOV[2], NIKOLAI KHLEBTSOV[1,2]

[1] *Institute of biochemistry and physiology of plants and microorganisms RAS, 410049 Saratov, Russia*

[2] *Saratov State University, 410012 Saratov, Russia*

Khlebtsov_b@ibppm.ru

ABSTRACT

Gap-enhanced Raman tags (GERTs) are new emerging probes of the surface-enhanced Raman scattering (SERS) spectroscopy that have found promising analytical and bioimaging applications. Because of the internal localization of Raman reporter molecules, they are protected from unwanted external environments and particle aggregation and demonstrate superior SERS responses due to strongly enhanced electromagnetic fields in the gaps between metal core-shell structures. We discuss recent progress in the synthesis, design of optical properties, and biomedical applications of novel spherically symmetrical and anisotropic GERTs. Particular attention is paid to the use of nanoparticles as labels for immunoassays and for Raman bioimaging of cancer cells and tissues.

Plasmonic enhancement of local electromagnetic (EM) fields by metal nanostructures is the key physical process behind the surface-enhanced Raman spectroscopy (SERS). Raman spectra provide unique information about molecular vibration modes, thus ensuring analytical means for the detection of molecules and their local environment in condensed phases.

There are several ways to enhance the local EM fields through the EM coupling of excited modes, including the formation of a small nanogap between plasmonic particles or between particles and tips or flat metal surfaces. Although such nanostructures can be fabricated through modern controllable technologies with predicted geometrical parameters, the SERS response may suffer from possible unwanted interference effects of surrounding media. From this point of view, the nanostructures with Raman molecules (RMs) embedded into internal nanogaps seem very promising for biomedical applications. SERS core/shell tags with inner nanogaps (also called gap-enhanced Raman tags – GERTs [1]) have attracted considerable attention because of several advantage features: (1) RMs are protected from desorption and environmental conditions; (2) they are subjected to a uniform and strongly enhanced EM field in the gap; (3) GERT probes can be multiplexed by incorporating different RMs into two-layered or multilayered GERTs.

Our talk include our recent data on the synthesis and plasmonic properties of GERTs, and biomedical and theranostic topics such as analytical sensing, *in vivo* and *in vitro* bioimaging, and intra-operation diagnostic of cancer tumor margins.

The widely used Raman reporters for GERTs are thiolated aromatic molecules that possess a number of promising modalities. Because of the high chemical affinity of the thiol group to the metal surface, thiolated molecules can easily be conjugated to a wide range of NPs by simple mixing. Synthesis of such GERTs starts with the synthesis of CTAC stabilized spherical Au particles as cores, followed by conjugation with a monolayer of 1,4-BDT (Fig. 1B) and growth of Au shell on the cores by mixing Au salt ($HAuCl_4$) with a capping agent (CTAC) and ascorbic acid as a mild reducing agent. The HRTEM images of resulted particles reveal a sub-nm gap between core and shell indicating the successful trapping of the Raman reporters between the core and shell. Note that 1,4-BDT embedded GERTs demonstrated the SERS response one order of magnitude higher compared other particles with surface adsorbed 1,4-BDT molecules. We have also demonstrated that not only 1,4-BDT, but also other thiolated aromatic molecules, such as 4-aminothiophenol (4-ATP) and 4-methylthiophenol (4-MTP), can be used to synthesize core/shell particles with embedded Raman reporters and distinct gaps [2, 3].

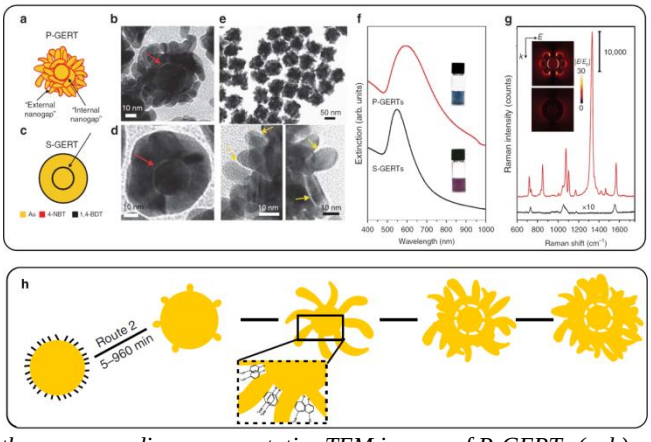

Figure 1 *Schematic structures and the corresponding representative TEM images of P-GERTs (a, b) and S-GERTs (c, d); Red and yellow arrows indicate the internal and external nanogaps, respectively. The panels (f) and (g) represent sample photos and extinction spectra, FDTD simulations and SERS spectra. The bottom panel (h) illustrates the synthetic scheme of P-GERTs.*

GERTs with spherical symmetry and smooth outer shell demonstrate typically high but not extraordinary EFs. To increase the SERS performance of gap-enhanced tags, several attempts have been made to modify the outer shell morphology in a star-like [4] or irregular roughness manners [5]. Still, there is an urgent need in strong increasing the GERT efficiency down to single-particle level. Recently, we fabricated a new version of GERTs with spherical core, hollow gap, and a branched petal-like shell structures (for brevity, such particles were called P-GERTs; Fig. 3) [6]. Because of the generation of strong EM hot spots in both the internal gap and petal-like structures, the fundamental EF was as high as 5×10^9, thus enabling single-particle detection. Remarkably, the synthetic protocols of both conventional GERTs (S-GERTs) and P-GERTs are very similar and differ mainly in using 1,4-BDT and 4-NBT as spacers.

The quantitative determination of bioactive molecules, including proteins, nucleic acids, aptamers and small molecules, are the common goals in biodetection assays. In the SERS tag based biodetection procedures, a sandwich assay is widely adopted as the analyte is "sandwiched" between two targeting sites: typically, the targeting site (such as antibodies or complementary nucleic acids) are first immobilized onto the substrates; the target biomarkers are then captured by them; afterward, the biofunctionalized GERTs are attached through the recognition of biomarkers onto the substrate, contributing a distinct signal for quantitative analysis. GERTs are advantageous as optical labels in the biodetection assay owing to their super-high sensitivity (down to a single-NP level) and specificity, leading to an improved limit of detection (LOD) compared to common SERS tags.

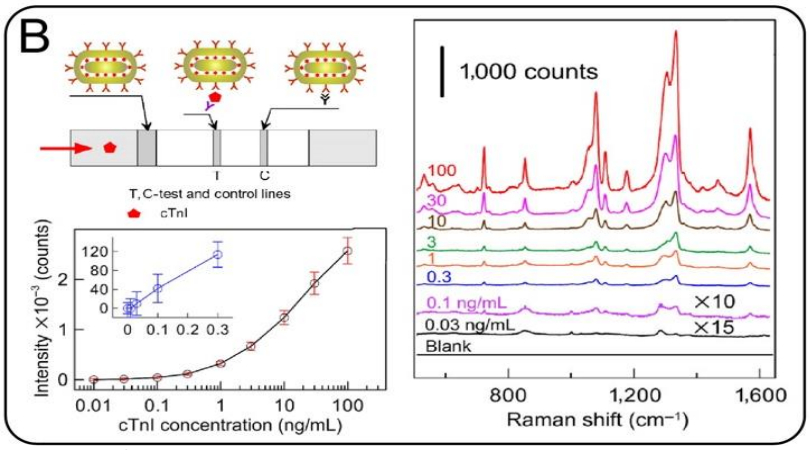

Figure 2 *The GERT-based LFIA for cTnI, the average SERS spectra in the test zones and the standard curve of different cTnI concentrations*

More importantly, the embedded Raman reporters can be considered as the internal standard for the calibration of Raman signal fluctuations induced by different measurement conditions and local states of the NPs, such as aggregation. This can greatly overcome the reproducibility issue in common quantitative SERS-based biodetection [7]. Recently, we have reported the successful application of GERTs-based lateral flow immunoassay (LFIA), either using anisotropic rod-like GERTs (Fig. 2) [8] or using bimetallic double-shell structured GERTs [**Error! Bookmark not defined.**]. The sensitivity of the former has highly surpassed that of colorimetric LFIA, with a LOD for cardiac troponin I (cTnI) to be 0.1 ng/mL, close to the diagnostic criteria for blood serum in the case of heart infarction. The latter has reached a LOD of 0.025 mIU human chorionic gonadotropin (HCG), which is three orders of magnitude better than the commercial strips.

Despite major advances in targeted drug and radiation therapies, surgery is still the most preferred and effective treatment for localized tumors. Precision cancer surgery guided by intraoperative optical imaging is of broad interest in engineering and medicine.

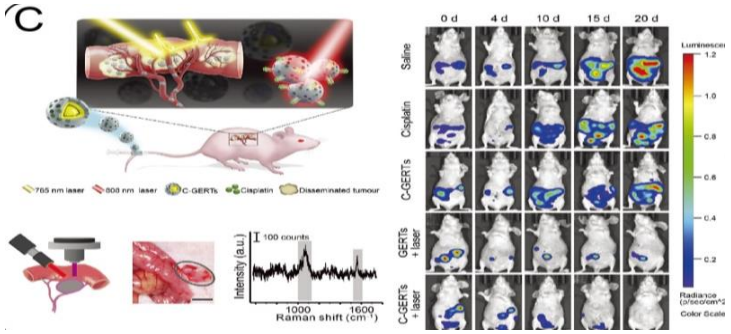

Figure 3 *The SERS-guided detection and chemo-photothermal therapy of abdominal disseminated microtumors in mice using GERTs loaded with cisplatin.*

Over the past decade, many efforts have been made to optimize the performances of SERS-guided surgery from three strategies: developing superior SERS tags, achieving higher specificity in delivery, improving the speed by optimizing Raman system and imaging methodologies. When it comes to a more complete tumor resection of the primary tumor, draining lymph nodes and metastatic sites, a superior SERS is required to be of high brightness, good targeting capability and specificity [9]. From this point, GERTs can be the promising probes. We have reported on GERT-guided surgery and

cancer therapy. The 1,4-BDT embedded GERTs developed by us appeared to have a detection limit in liquid of 20 fM with the laser energy of 10^5 W/cm^2 and an integration time of 1.86 s [10].

The high brightness makes it possible for the real-time intraoperative sensitive detection and treatment of the residual prostate tumors [10] as well as the diagnostics of disseminated ovarian cancers (Fig. 3). These tags can specifically identify and eliminate the tumor margin and micro satellite metastases, making it possible to have a complete tumor resection. Furthermore, by loading the chemotherapy drug cisplatin within the mesoporous silica layer of GERTs, the Raman-guided chemo-photothermal synergistic therapy can be achieved to kill tumor cells in a precise way (Fig. 3). These investigations unveil the attractiveness of GERTs as a robust platform for the intraoperative diagnosis and eradication of microtumors, which would push Raman technologies forward to deep theranostic and related biomedical applications.

We acknowledge the financial support from the Russian Scientific Foundation (project no. 18-14-00016)

REFERENCES

[1] Y. Zhang, Y .Qiu, L. Lin, H. Gu, Z. Xiao, J.Ye, Ultraphotostable mesoporous silica-coated gap-enhanced Raman tags (GERTs) for high-speed bioimaging, ACS Appl Mater Interfaces. 3995–4005, 2017.

[2] L. Lin, H. Gu, J.Ye, Plasmonic multi-shell nanomatryoshka particles as highly tunable SERS probes with built-in tags, Chem Commun. 17740–17743, 2015.

[3] B. Khlebtsov, V. Khanadeev, N. Khlebtsov, Surface-enhanced Raman scattering inside Au@Ag core/shell nanorods, Nano Res. 2303–2318, 2016.

[4] D. Jana, Z. Gorunmez, J. He, I. Bruzas, T. Beck, L. Sagle, Surface enhanced Raman spectroscopy of a Au@Au core−shell structure containing a spiky shell, J Phys Chem C. 20814–20821, 2016.

[5] J.H. Lee, J.W. Oh, S.H. Nam, Y.S. Cha, G.H. Kim, W.K. Rhim, Synthesis, optical properties, and multiplexed Raman bio-imaging of surface roughness-controlled nanobridged nanogap particles, Small. 4726–4734, 2016.

[6] Y. Zhang, Y. Gu, J. He, B.D. Thackray, J. Ye, Ultrabright gap-enhanced Raman tags for high-speed bioimaging, Nat Commun. 3905, 2019.

[7] X. Jiang, Z. Tan, L. Lin, J. He, C. He, B.D. Thackray, Surface-enhanced Raman nanoprobes with embedded standards for quantitative cholesterol detection, Small Methods. 1800182, 2018.

[8] B.N. Khlebsov, D.N. Bratashov, N.A. Byzova, B.B. Dzantiev, N.G. Khlebtsov, SERS-based lateral flow immunoassay of troponin I using gap-enhanced Raman tags, Nano Res. 413–420, 2019.

[9] C. Jiang, Y. Wang, W. Song, L. Lu, Delineating the tumor margin with intraoperative surface-enhanced Raman spectroscopy, Anal Bioanal Chem. 3993–4006, 2019.

[10] Y. Qiu, Y. Zhang, M. Li, G. Chen, C. Fan, K. Cui, Intraoperative Detection and Eradication of Residual Microtumors with Gap-Enhanced Raman Tags, ACS Nano.7974–7985, 2018.

[11] Y. Zhang, Z. Liu, B.D. Thackray, Z. Bao, X. Yin, F. Shi, Intraoperative Raman-guided chemo-photothermal synergistic therapy of advanced disseminated ovarian cancers, Small. e1801022, 2018.

AGENT-BASED MODELLING OF THE FIRST AND THE SECOND WAVES OF COVID-19 SPREADING IN RUSSIAN FEDERATION REGIONS

DOI 10.24412/cl-36896-2021-1-49-52

MIKHAIL KIRILLIN[1], EKATERINA SERGEEVA[1], ALEKSANDR KHILOV[1], VALERIYA PEREKATOVA[1], DARIA KURAKINA[1], ILYA FIKS[1], NIKOLAY SAPERKIN[2], MING TANG[3], AND ELBERT MACAU[4]

[1] Institute of Applied Physics RAS, Nizhny Novgorod, Russia,
[2] Privolzhsky Research Medical University, Nizhny Novgorod, Russia
[3]School of Physics and Electronic Science, East China Normal University, Shanghai, China
[43]Instituto de Ciências e Tecnologia, Universidade Federal de São Paulo, São Paulo, Brasil

mkirillin@yandex.ru

ABSTRACT

The COVID-19 pandemics remains one of the largest worldwide challenges. Necessity of effective systemic aids for the minimization of losses leads to the requirement of adequate models allowing to predict the impact of different factors on the spread of disease. Traditionally employed simulation approaches are based on derivatives of a SIR model, which major drawback is not accounting for random factors. Agent-based simulation models provide a suitable solution with the possibility to accurately account for such factors as age structure of population, features of isolation and self-isolation strategies and testing strategies, presence of super-spreaders etc. In this paper we report on the results of modelling the first and the second waves of COVID-19 spreading in regions of Russian Federation. The simulations approach employs an agent-based model with a general pool with the inclusion of a model of the population testing strategy. The model accounts for key epidemiologic characteristics, such as population age distribution, spreading rate, isolation factors etc. It is demonstrated that the daily case curves for different regions are reproduced well with the same spreading rate parameter, while the initial number of infected agents, testing and isolation strategies, which serve as other tuning parameters of the model, are region-dependent.

INTRODUCTION

Prediction of further development of disease outbreaks for the purpose of timely introduction of preventive measures require reliable tools for pandemic spread simulations. Several classes of models are traditionally employed for the prognosis of the spread of infections.

Regression models allow to obtain rapid estimations of the diseases spread [1,2]. They include non-adaptive models, which ignore local perturbations of epidemical characteristics and are not suitable for short-term prognosis, and adaptive models, which are predominantly applied for short-term prognosis only. Short-term prognosis can be made with the application of autoregressive moving average models [3], while autoregressive integrated moving average model allows both for short-term and long-term prognosis [4]. Dynamic Bayesian networks [5], neural networks and other machine learning based methods are applicable for short-term prognosis only. Feedforward neural networks and backpropagation algorithm provide with prognosis of infections spread [6].

Long-term prognosis is traditionally made with the application of dynamic systems based on differential equations, which are the class of compartmental models. SIR model, firstly introduced by Kermack and McKendrick [7], is based on the division of the population into three groups — susceptible (*S*), infected (*I*), recovered (*R*) — and the description of their interaction with non-linear differential equations. Further development of compartmental models includes the accounting for bigger number of groups, such as exposed (*E*), hospitalized (*H*), critical (*C*), dead (*D*), and those at the quarantine (*Q*) or isolation (*J*). SEIR model has been applied for simulation of COVID-19 spread [8-11] and the estimation of the efficacy of governmental measures during early COVID-19 spread [12]. The major drawback of compartmental models is the fact that they do not account for random factors and individual characteristics of population members.

For both short-term and long-term prognosis, it is reasonable to employ individually-oriented models, which include so-called agent-based models. Agent-based model consists of the description of every member of population (agent) by a set of characteristics with the determination of rules of interactions between the agents. Agent-based models showed their efficiency in the description of the propagation of infections, such as Ebola [13] and flu [14], in the population of different sizes. They were also applied for the modeling of COVID-19 development and regress in different cities such as Helsinki [15], New York [16], Singapore [17]. Some agent-based models are based on previously developed models for the prediction of flu pandemics, for example, NotreDame-FRED model [18], model of Ferguson's research group from Imperial College London [19] and model for simulation of the COVID-19 pandemic in Australia [20]. A number of studies utilized agent-based models for assessing the impacts of universal face mask wearing [21], digital contact tracing [22-24] and social distancing [24-26] as well as analyzing various intervention scenarios [16,19,24,27-31]. Some agent-

based models are developed for modeling COVID-19 transmission in small communities such as a university [32], a supermarket [33] and a small town [34].

The aim of this paper is the development of an agent-based model capable of simulating and predicting the progress of the COVID-19 outbreak in different regions of the Russian Federation. Another important problem to be resolved in this study is the determination of the key model parameters that provide the agreement of the simulated dynamics and actual statistics on daily new infection cases and deaths associated with COVID-19.

AGENT-BASED COVID-19 SPREADING MODEL

A general pool model, in which all the individuals (agents) may interact with each other, was employed for the fit of official statistics of COVID-19 spread. Every agent is described with a number of binary states, which values are scenario-dependent and governed by the Monte Carlo simulations: susceptible, infected, contagious, with disease manifestations, critical, recovered. The simulations feature day-scale time resolution. The model accounts for the population age structure based on the information on different disease progression in different age groups. Typical lengths of disease manifestation, progression, critical, and symptomless periods are introduced in accordance with the available data. Any agent with status "critical" may die on any day of critical period with given death probability p_d.

The average number of individuals R, to which an infected agent may transmit the infection within one week in the case of no restriction measures applied, is considered as the main model parameter (spreading rate) directly related to infection transmission coefficient. Given that the probabilities to be infected from different agents are independent, the contamination probability P for a given agent interacting with the general pool in a particular day is calculated as $P = \frac{RN_i}{7N_t}$, where N_i is the number of infected individuals in the general pool in the current day and N_t is the total number of agents in the considered population. The N_t number is chosen for simulations in accordance with the population of the simulated region.

The developed simulation model accounts for the efficiency of the following restrictive measures with the employment of a so-called self-isolation index, firstly introduced by Yandex (Russia) during the first wave of COVID-19 outbreak, which represents a cumulative parameter reflecting population activity based on both traffic information and activities in different internet services. The self-isolation index varies in the range between 0 and 5, and it is assumed during the simulations that its value is proportional to the percentage of agents that obey the restrictive rules and do not interact with the general pool in the current day.

The introduced rules of testing are an important part of the model, since the real data for the comparison to the results of numerical simulation are daily statistics on number of newly revealed cases and deaths. In the model, the number of daily tests for each region is either taken from official statistics or determined from the daily number of cases for the entire Russian Federation in proportion to the region population. The tunable parameter is a number of tested agents, which were in contact with an agent with positive COVID-19 test.

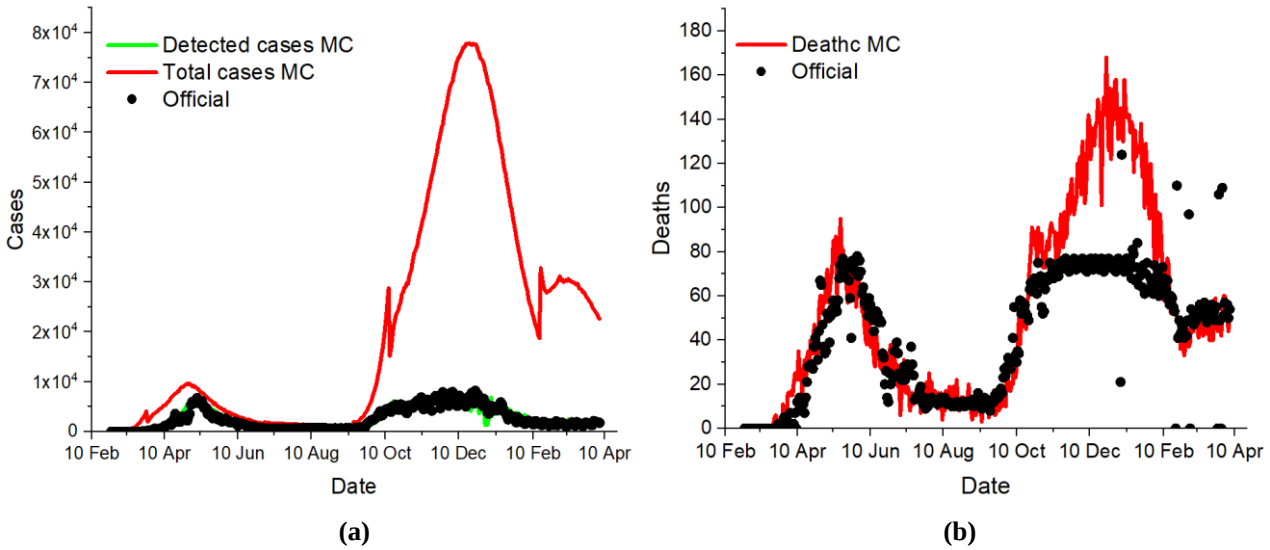

Fig. 1. Comparison of simulated scenarios and real statistical data for daily numbers of newly revealed COVID-19 (a) and lethal COVID-19 associated (b) cases in Moscow within the period of 23 March 2020 – 07 April 2021.

RESULTS

Figure 1 demonstrates the results of simulations of the epidemic progress in Moscow (N_t = 11.4 ·10^6) derived from modelling. The spreading rate value were extracted from the simulations of the first wave performed in our previous study [35].

To provide a best-fit scenario, we manipulated with other parameters of the model, namely, the number of initial infected agents, percentage of deaths among agents in the critical state p_d, and testing strategies. Each scenario was constructed by averaging five scenarios that are the closest to the real statistical data over a total of 10 realizations with the same parameters. In Fig. 1a solid green lines demonstrate calculated dynamics of daily detected cases and red solid lines demonstrate dynamics of total COVID-19 cases, while black dots indicate official statistics data, which were fitted with data for detected cases in simulations. The results indicate a larger percentage if hidden cases in the case of the second wave in comparison with the first one. The deaths statistics demonstrate hidden cases resulting in exceeding the number of daily cases in official statistics by the simulations results. This could be explained by COVID-induces deaths cases which were attributed to other causes in official statistics. The simulations were also performed for Nizhny Novgorod region and Novosibirsk region demonstrating similar dynamics. They demonstrate the prediction abilities of the model for regions with relatively small number of confirmed COVID-19 daily cases and single deaths.

CONCLUSION

In this paper we presented an agent-based model of COVID-19 epidemic spread with the employment of Monte Carlo simulation principles. The model is able to account for the age-dependent disease development, restrictive measures as well as testing system. It was validated on the statistical data for daily new cases and deaths which were reported during 1st and 2nd waves of COVID-19 pandemics from two representative regions of Russia, the Moscow city and Nizhny Novgorod region. The results of simulations show the possibilities of developed model for the prediction of disease spread with the application of restrictive measurements and different testing strategies.

ACKNOWLEDGEMENTS

The study is supported by RFBR (project no. 20-51-80004), CNPq (project no. 441016/2020-0), and NSFC (project no. 82161148012).

REFERENCES

1. H.S. Burkom, S.P. Murphy, and G. Shmueli, "Automated time series forecasting for biosurveillance," *Statistics in medicine*, **26**(22), pp. 4202-4218, 2007.
2. J.C. Brillman et al., "Modeling emergency department visit patterns for infectious disease complaints: results and application to disease surveillance," *BMC medical informatics and decision making*, **5**(1), p. 4, 2005.
3. D. Lai, "Monitoring the SARS epidemic in China: a time series analysis," *Journal of Data Science*, **3**(3), pp. 279-293, 2005.
4. J. Diaz-Hierro et al., "Evaluation of time-series models for forecasting demand for emergency health care services," *Emergencias*, **24**(3), pp. 181-188, 2012.
5. S. Unkel et al., "Statistical methods for the prospective detection of infectious disease outbreaks: a review," *Journal of the Royal Statistical Society: Series A (Statistics in Society)*, **175**(1), pp. 49-82, 2012.
6. R. Kiang et al., "Meteorological, environmental remote sensing and neural network analysis of the epidemiology of malaria transmission in Thailand," *Geospatial health*, **1**(1), pp. 71-84, 2006.
7. W.O. Kermack, and A.G. McKendrick, "A contribution to the mathematical theory of epidemics," *Proceedings of the royal society of London. Series A, Containing papers of a mathematical and physical character*, **115**(772), pp. 700-721, 1927.
8. Z. Zhao et al., "Prediction of the COVID-19 spread in African countries and implications for prevention and controls: A case study in South Africa, Egypt, Algeria, Nigeria, Senegal and Kenya," *Science of the Total Environment*, **729**, p. 138959, 2020.
9. N. Ghaffarzadegan, and H. Rahmandad, "Simulation-based estimation of the early spread of COVID-19 in Iran: actual versus confirmed cases," *System Dynamics Review*, **36**(1), pp. 101-129, 2020.
10. S. Annas et al., "Stability analysis and numerical simulation of SEIR model for pandemic COVID-19 spread in Indonesia," *Chaos, Solitons & Fractals*, **139**, p. 110072.
11. L. López, and X. Rodo, "A modified SEIR model to predict the COVID-19 outbreak in Spain and Italy: simulating control scenarios and multi-scale epidemics," *medRxiv*:20045005, 2020.
12. Y. Fang, Y. Nie, and M. Penny, "Transmission dynamics of the COVID-19 outbreak and effectiveness of government interventions: A data-driven analysis," *Journal of medical virology*, **92**(6), pp. 645-659, 2020.
13. S. Siettos et al., "Modeling the 2014 Ebola virus epidemic–agent-based simulations, temporal analysis and future predictions for Liberia and Sierra-Leone," *PLoS currents*, **7**, 2015.
14. H. Arduin et al., "An agent-based model simulation of influenza interactions at the host level: insight into the influenza-related burden of pneumococcal infections," *BMC infectious diseases*, **17**(1), p. 382, 2017.

15. J.T. Tuomisto et al., “An agent-based epidemic model REINA for COVID-19 to identify destructive policies,” *medRxiv*:20047498, 2020.
16. N. Hoertel, et al., “Facing the COVID-19 epidemic in NYC: a stochastic agent-based model of various intervention strategies,” *medRxiv*: 2020.04.23.20076885, 2020.
17. J.R. Koo, et. al., “Interventions to mitigate early spread of SARS-CoV-2 in Singapore: A modelling study,” *The Lancet Infectious Diseases* 20(6), 2020.
18. *Retrieved from* https://github.com/confunguido/covid19_ND_forecasting
19. N. M. Ferguson, et al, Impact of non-pharmaceutical interventions (NPIs) to reduce COVID-19 mortality and healthcare demand, *available at https://doi.org/10.25561/77482, Report of the Imperial College London, UK.*
20. S.L. Chang, et. al., “Modelling transmission and control of the COVID-19 pandemic in Australia,” *Nature Communications* 11, 5710, 2020.
21. D. Kai, et. al., “Universal masking is urgent in the COVID-19 pandemic: SEIR and agent based models, empirical validation, policy recommendations,” *arXiv*:2004.13553, 2020.
22. J. A. M. López, et. al., “Anatomy of digital contact tracing: Role of age, transmission setting, adoption, and case detection,” *Science Advances*, 7(15), 2021.
23. M.S. Shamil, et. al., “An Agent-Based Modeling of COVID-19: Validation, Analysis, and Recommendations,” *Cognitive Computation*, 19:1-12, 2021.
24. A. Aleta, et. al., “Modeling the impact of social distancing, testing, contact tracing and household quarantine on second-wave scenarios of the COVID-19 epidemic,” *medRxiv*: 2020.05.06.20092841, 2020.
25. P. Silva, et. al., “COVID-ABS: An agent-based model of COVID-19 epidemic to simulate health and economic effects of social distancing interventions,” *Chaos Solitons Fractals*, 139:110088, 2020.
26. P. Keskinocak, et. al., “The impact of social distancing on COVID19 spread: State of Georgia case study,” *PLoS One*, 15(10), e0239798, 2020.
27. B. Goldenbogen, et.al., “Geospatial precision simulations of community confined human interactions during SARS-CoV-2 transmission reveals bimodal intervention outcomes,” *medRxiv*:2020.05.03.20089235, 2020
28.R. Hinch, et. al., “OpenABM-Covid19 - an agent-based model for non-pharmaceutical interventions against COVID-19 including contact tracing,” *PLoS Computational Biology*, 17(7):e1009146, 2021.
29. A. Staffini A, et. al., “An Agent-Based Model of the Local Spread of SARS-CoV-2: Modeling Study,” *JMIR Med Inform*, 9(4):e24192, 2021.
30. D.L. Chao, et. al.,“Modeling layered non-pharmaceutical interventions against SARS-CoV-2 in the United States with Corvid,” *MedRxiv* , 2020.04.08.20058487, 2020.
31. E. Cuevas, “An agent-based model to evaluate the COVID-19 transmission risks in facilities,” *Computers in Biology and Medicine*, 121: 103827, 2020.
32. P. T. Gressman and J. R. Peck, “Simulating COVID-19 in a university environment,” *Mathematical Biosciences*, 328, 108436, 2020.
33. F. Ying and N. O’Clery,“Modelling COVID-19 transmission in supermarkets using an agent-based model,” *PLoS One*, 16(4): e0249821, 2021.
34. A. Truszkowska et. al., “High-Resolution Agent-Based Modeling of COVID-19 Spreading in a Small Town,” *Advanced Theory and Simulations.*, 4(3):2000277, 2021.
35. M. Kirillin, E. Sergeeva, A. Khilov, D. Kurakina, and N. Saperkin “Monte Carlo simulation of the COVID-19 spread in early and peak stages in different regions of the Russian Federation using an agent-based modelling”, *Chinese-Russian Workshop on Biophotonics and Biomedical Optics-2020 Book of Abstracts,* 71-74 (2021).

IN VIVO CLINICAL RAMAN SPECTROSCOPY: NON-INVASIVE APPLICATIONS IN CANCERS

DOI 10.24412/cl-36896-2021-1-53-56

DR. C. MURALI KRISHNA
Advanced Centre for Treatment Research and Education in Cancer, Tata Memorial Centre, India
*mchilakapati@actrec.gov.in, pittu1043@gmail.com

ABSTRACT

Conventionally, diseases are diagnosed by clinical examination followed by relevant biochemical/microbiological/pathological examinations. Such approaches, rely on symptoms, are considered to diagnose an existing disease, and could be a late diagnosis which often leads to poor prognosis. Therefore early stage diagnosis can provide better prognosis. Since morphological changes could be rather late signs, diagnostics should be sensitive to biochemical changes, thus can pave early diagnosis. This is particularly applicable to diseases like cancers which are multi-step process and usually pass through multiple stages, i.e., hyperplasia/metaplasia, dysplasia, carcinoma in situ, and eventually to invasive cancers. During this process several biomolecules (tumour markers/biomarkers) are expressed which can be exploited to diagnose the pathological conditions. Though tumour markers are also been employed for diagnosis, it is been limited by paucity of reliable markers, hence proteomics/genomics based methods are also explored to get holistic information. Such global biochemical information also can be obtained using Raman spectroscopy, an analytical chemistry tool. Raman spectroscopy, named after its discoverer Sir C.V. Raman is a better tool as it provides 'molecular fingerprint' of a sample and less interference due to water spectrum. Raman scattered photon is generated when incident photon cause change in the vibrational state of a molecule. Since this frequency shift is unique to specific molecular vibration of the molecule, either by direct comparison of the spectra of known and unknown materials recorded consecutively or by comparison of the spectrum of the unknown compound with catalogues of reference spectra, identification of 'chemical moieties' provides 'molecular fingerprint' of the sample. Hence Raman spectroscopy is been pursued as potential alternatives/adjuncts due to attributes, in addition to sensitivity to biochemical composition, such as- less time consuming, no external labelling or sample processing, more objective, and most importantly feasible in vivo/in situ on line diagnosis. Objective disease diagnosis by Raman spectral molecular signatures of tissue or body fluids is achieved using multivariate analysis. The aim of multivariate analysis is to train models that distinguish seemingly similar patterns in pathological conditions. Multivariate analysis can be unsupervised where no prior information is given and the method tries to establish relationships or trends in classification de novo. In the absence of preliminary information, non-supervised methods provide a first-hand estimate about the nature of data. Supervised learning methods are used to predict the association of new variables to one of the pre-existing groups.

Cancer is one of the leading causes of death and high mortality rate, mainly due to late detection and recurrences, ascribed to limitations of conventional diagnostic methodologies, which involve invasive procedures and are prone to subjective errors. Screening and early detection are thus main stay for the overall management of cancer and to improve prognosis. The routine cancer diagnosis involves a clinical examination followed by biopsy. The biopsied sample is subjected to histopathology, the gold standard. This procedure is shown to be prone to subjective errors, time consuming and depends on visible morphological alterations which are late signs of an existing disease. In this context extensive studies have been carried out on applications of Raman spectroscopy in cancer theranostics, i.e., diagnostic/screening and therapeutic monitoring. The present paper would provide an update of our explorations in theranostic applications. The non-invasive (in vivo - on subjects) approaches included screening/diagnosis, recurrence prediction, and disease-free survival, in oral and cervical cancers.

Before undertaking in vivo studies, it is prerequisite to demonstrate efficacy in ex vivo biopsied specimen. Hence studies were carried out on several cancers such as, oral, uterine, cervix, breast, stomach, colon and ovarian cancers [1-16]. The ex vivo studies could distinctly stratify the inflammatory, premalignant, and malignant oral tissues [1], normal and malignant oral and cervix tissues [2,3,6], and normal, malignant and 2-fractions after radiotherapy formalin-fixed cervix tissues [5]. Multiparametric approach unambiguously classified normal and malignant cervix tissue with 99.5% sensitivity and specificity [7]. Studies further demonstrated the feasibility of stratifying radiotherapy responders, partial responders and non-responders [8,9]. Rubina et al [10] showed utility of fibre-optic Raman probe for early prediction of CCRT response in locally advanced cervical cancers. The study also showed distinct stratification of normal tissue from pre- and post-treatment biopsies. Kumar et al. [11] analysed 69 breast tissue samples, of which 61 were unambiguously diagnosed as 29 normal, 15 benign, and 17 malignant while the remaining 8 samples were diagnosed as pathological. Chowdary et al. [13] has shown classification of normal, benign and malignant breast tissues and reported excess of lipids in malignant tissues and excess of proteins in benign tissues. Studies were subsequently extended to stomach, colon and ovarian cancers, and showed distinct classification between normal and malignant stomach mucosal tissues with 93% and 84% sensitivity and specificity [14], normal and malignant colon tissues with 95% sensitivity and specificity [15] and normal and malignant ovarian tissues with 95% sensitivity and specificity [16].

On obtaining robust demonstration of classification of ex vivo tissues in single as well as multiple cancer scenario [17], extensive non-invasive in vivo studies on oral and cervical cancer subjects have been taken up, as to be described in succeeding sections.

***Oral cancers*:** Cancers of the oral cavity predominantly occur with a higher frequency in South Central Asian countries and Melanesia. According to Globocan 2020, oral cancer has the highest mortality rate among Indian men [18]. Early diagnosis / detection of the precancerous lesions of oral cancer would aid in improving patient prognosis. In this context, Singh et al. [19-21] showed stratification of premalignant, malignant and healthy controls with and without tobacco habits, in clinically implementable spectral acquisition time (5 sec) The same group later showed correlation between spectral and biochemical markers i.e., higher intensity of lipids in normal and proteins in tumor tissues by carrying out Raman and biochemical evaluations[22]. Singh et al. [23] conducted a clinical trial on 84 oral cancer subjects including, healthy, habitué, tobacco habitué with pre-cancerous lesions, contralateral, and subjects with cancerous lesions. The study stratified the healthy, habitué, premalignant and malignant conditions and also reported MAC / CFE in contralateral normal mucosa. Identification of these early events in oral carcinogenesis demonstrated the feasibility of Raman spectroscopy in detection of recurrence and thereby improving disease free survival [24-26]. The findings are also suggestive of the potential of Raman spectroscopy as an early detection tool.

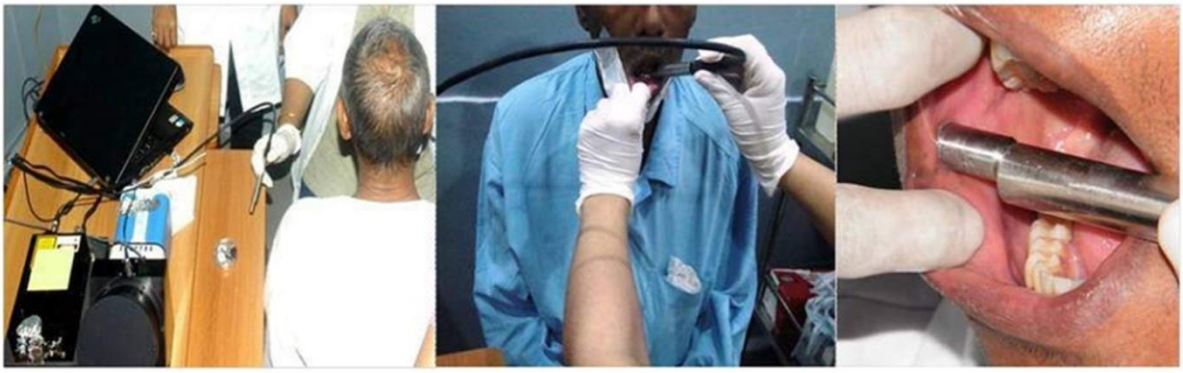

Figure 1 Fiberoptic in vivo clinical Raman spectroscope for oral cancer applications

***Cervical cancers*:** Cervical cancer is the fourth most commonly diagnosed cancer with high mortality rate in 36 countries. An in vivo Raman Spectroscopy clinical trial conducted on 93 subjects of cervical cancers showed 97% classification efficiency in stratification of normal and tumour tissues [27]. Due to the biochemical similarity between vagina and ecto-cervix, the study explored the feasibility of vagina as an internal control. Similar spectral features were observed in normal cervix and vaginal controls of healthy and tumour subjects [27]. Furthermore, a comparative study of Diffuse Reflectance Spectroscopy (DRS) and Raman Spectroscopy for detection of cervical cancer [28]. 20 cervical tumours and 6 normal cervix subjects were recruited in the study and the spectra were recorded from 67 tumour, 22 normal cervix and 57 normal vagina sites. The sensitivity and specificity of Raman spectroscopy was slightly higher than that of DRS [28].

Figure 2: Fiberoptic in vivo clinical Raman spectroscope for cervical cancers

Raman Spectroscopy has shown to detect and discriminate tumor stages across different cancers, such as brain, breast, colon, bladder and gynecological cancer [29]. Molckovsky et al. [30], demonstrated utility of RS in differentiating normal, hyperplastic and adenomatous polyps in colorectal cancer with high diagnostic accuracy. Kendall et al. [31] on comparing histopathology and Raman classification results for differentiating pathological subtypes in esophageal cancer observed 73% - 100% sensitivity and 90% - 100% specificity. Teh et al. [32] explored near-infrared (NIR) Raman spectroscopy for detecting malignant changes in gastric cancer and reported specific spectral differences in signals related to amide III and amide I proteins, CH_3CH_2 twisting of proteins/nucleic acids, and C=C stretching mode of phospholipids. Further, Bergholt et al. [33] evaluated clinical utility of image guided - Raman endoscopy and showed diagnostic sensitivity of 94.6% and specificity of 94.6% while discriminating normal tissue and gastric neoplasia. The

study also reported reduction of collagen content, increased nucleic acid to lipid ratio and increased nucleic acid/cytoplasmic ratio in cancer tissues.

To summarize, the non-invasive in vivo clinical applications of Raman Spectroscopy in oral and cervical cancers demonstrate the potential of the technique in early diagnosis, identification of MAC/ CFE and prediction of recurrence and disease free survival. However, clinical translation of Raman Spectroscopy poses certain challenges, such as, need for transportability of data collected across different platforms which is being pursued [34].

REFERENCES

[1] Malini R, Venkatakrishna K, Kurien J, M. Pai K, Rao L, Kartha VB, Krishna CM. Discrimination of normal, inflammatory, premalignant, and malignant oral tissue: a Raman spectroscopy study. Biopolymers: Original Research on Biomolecules. 2006;81(3):179-93.

[2] Kartha VB, Jyothi Lakshmi R, Mahato KK, Murali Krishna C, Santhosh C, Venkata Krishna K. Raman spectroscopy in clinical investigations. Indian Journal of Physics. 2003;77:113-23.

[3] Venkatakrishna K, Kurien J, Pai KM, Valiathan M, Kumar NN, Murali Krishna C, Ullas G, Kartha VB. Optical pathology of oral tissue: a Raman spectroscopy diagnostic method. Current science. 2001;80(5):665-9.

[4] Chilakapati MK, Sockalingum GD, Vidyasagar MS, Manfait M, Fernanades DJ, Vadhiraja BM, Maheedhar K. An overview on applications of optical spectroscopy in cervical cancers. Journal of Cancer Research and Therapeutics. 2008;4(1):26.

[5] Krishna CM, Sockalingum GD, Vadhiraja BM, Maheedhar K, Rao AC, Rao L, Venteo L, Pluot M, Fernandes DJ, Vidyasagar MS, Kartha VB. Vibrational spectroscopy studies of formalin-fixed cervix tissues. Biopolymers: Original Research on Biomolecules. 2007;85(3):214-21.

[6] Maheedhar K, Vadhiraja BM, Pralahad K, Vidyasagar MS, Fernandes DJ, Kartha VB, Muralikrishna C. Evaluation and validation of Raman spectroscopic diagnostic methodology of cervix cancers by blind studies. International Journal of Radiation Oncology, Biology, Physics. 2007;69(3):S400.

[7] Krishna CM, Prathima NB, Malini R, Vadhiraja BM, Bhatt RA, Fernandes DJ, Kushtagi P, Vidyasagar MS, Kartha VB. Raman spectroscopy studies for diagnosis of cancers in human uterine cervix. Vibrational Spectroscopy. 2006;41(1):136-41.

[8] Vidyasagar MS, Maheedhar K, Vadhiraja BM, Fernandes DJ, Kartha VB, Muralikrishna C. Raman spectroscopy of tissues collected at different fractions of radiation therapy: Response assessment to radiotherapy in cervix cancers. International Journal of Radiation Oncology, Biology, Physics. 2007;69(3):S388-9.

[9] Vidyasagar MS, Maheedhar K, Vadhiraja BM, Fernendes DJ, Kartha VB, Krishna CM. Prediction of radiotherapy response in cervix cancer by Raman spectroscopy: a pilot study. Biopolymers: Original Research on Biomolecules. 2008;89(6):530-7.

[10] Rubina S, Vidyasagar MS, Murali Krishna C. Raman spectroscopic study on prediction of treatment response in cervical cancers. Journal of Innovative Optical Health Sciences. 2013;6(02):1350014.

[11] Kalyan Kumar K, Chowdary MV, Mathew S, Rao L, Murali Krishna C, Kurien J. Raman spectroscopic diagnosis of breast cancers: evaluation of models. Journal of Raman Spectroscopy: An International Journal for Original Work in all Aspects of Raman Spectroscopy, Including Higher Order Processes, and also Brillouin and Rayleigh Scattering. 2008;39(9):1276-82.

[12] Krishna CM, Kurien J, Mathew S, Rao L, Maheedhar K, Kumar KK, Chowdary MV. Raman spectroscopy of breast tissues. Expert review of molecular diagnostics. 2008;8(2):149-66.

[13] Chowdary MV, Kumar KK, Kurien J, Mathew S, Krishna CM. Discrimination of normal, benign, and malignant breast tissues by Raman spectroscopy. Biopolymers: Original Research on Biomolecules. 2006;83(5):556-69.

[14] Kumar KK, Anand A, Chowdary MV, Kurien J, Krishna CM, Mathew S. Discrimination of normal and malignant stomach mucosal tissues by Raman spectroscopy: a pilot study. Vibrational Spectroscopy. 2007;44(2):382-7.

[15] Chowdary MV, Kumar KK, Thakur K, Anand A, Kurien J, Krishna CM, Mathew S. Discrimination of normal and malignant mucosal tissues of the colon by Raman spectroscopy. Photomedicine and Laser Surgery. 2007;25(4):269-74.

[16] Maheedhar K, Bhat RA, Malini R, Prathima NB, Keerthi P, Kushtagi P, Krishna CM. Diagnosis of ovarian cancer by Raman spectroscopy: a pilot study. Photomedicine and Laser Surgery. 2008;26(2):83-90.

[17] Ghanate AD, Kothiwale S, Singh SP, Krishna CM, Bertrand D. Comparative evaluation of spectroscopic models using different multivariate statistical tools in a multicancer scenario. Journal of Biomedical Optics. 2011;16(2):025003.

[18] Sung H, Ferlay J, Siegel RL, Laversanne M, Soerjomataram I, Jemal A, Bray F. Global cancer statistics 2020: GLOBOCAN estimates of incidence and mortality worldwide for 36 cancers in 185 countries. CA: a cancer journal for clinicians. 2021;71(3):209-49.

[19] Singh SP, Deshmukh A, Chaturvedi P, Krishna CM. In vivo Raman spectroscopic identification of premalignant lesions in oral buccal mucosa. Journal of biomedical optics. 2012;17(10):105002.

[20] Singh SP, Deshmukh A, Chaturvedi P, Krishna CM. Raman spectroscopy in head and neck cancers: toward oncological applications. Journal of cancer research and therapeutics. 2012;8(6):126.

[21] Singh SP, Deshmukh A, Chaturvedi P, Krishna CM. In vivo Raman spectroscopy for oral cancers diagnosis. InBiomedical Vibrational Spectroscopy V: Advances in Research and Industry 2012 (Vol. 8219, p. 82190K). International Society for Optics and Photonics.
[22] Singh SP, Krishna CM. Raman spectroscopic studies of oral cancers: correlation of spectral and biochemical markers. Analytical Methods. 2014;6(21):8613-20.
[23] Singh SP, Sahu A, Deshmukh A, Chaturvedi P, Krishna CM. In vivo Raman spectroscopy of oral buccal mucosa: a study on malignancy associated changes (MAC)/cancer field effects (CFE). Analyst. 2013;138(14):4175-82.
[24] Bhattacharjee A, Hole A, Malik A, Sahu A, Singh SP, Deshmukh A, Nair S, Chaturvedi P, Krishna CM. Risk prediction by Raman spectroscopy for disease-free survival in oral cancers. Lasers in Medical Science. 2021;4:1-0.
[25] Malik A, Sahu A, Singh SP, Deshmukh A, Chaturvedi P, Nair D, Nair S, Murali Krishna C. In vivo Raman spectroscopy–assisted early identification of potential second primary/recurrences in oral cancers: an exploratory study. Head & neck. 2017;39(11):2216-23.
[26] Krishna CM, Sahu A. Water Concentration Analysis of the Surgical Margin. Cancer research. 2017;77(11):3121-2.
[27] Shaikh RS, Dora TK, Chopra S, Maheshwari A, Kedar DK, Bharat R, Krishna CM. In vivo Raman spectroscopy of human uterine cervix: exploring the utility of vagina as an internal control. Journal of Biomedical Optics. 2014;19(8):087001.
[28] Shaikh R, Prabitha VG, Dora TK, Chopra S, Maheshwari A, Deodhar K, Rekhi B, Sukumar N, Krishna CM, Subhash N. A comparative evaluation of diffuse reflectance and Raman spectroscopy in the detection of cervical cancer. Journal of biophotonics. 2017;10(2):242-52.
[29] Mahadevan-Jansen A, Richards-Kortum R. Raman spectroscopy for cancer detection: a review. In Proceedings of the 19th Annual International Conference of the IEEE Engineering in Medicine and Biology Society.'Magnificent Milestones and Emerging Opportunities in Medical Engineering' 1997 (Vol. 6, pp. 2722-2728). IEEE.
[30] Molckovsky A, Song LM, Shim MG, Marcon NE, Wilson BC. Diagnostic potential of near-infrared Raman spectroscopy in the colon: differentiating adenomatous from hyperplastic polyps. Gastrointestinal endoscopy. 2003;57(3):396-402.
[31] Kendall C, Stone N, Shepherd N, Geboes K, Warren B, Bennett R, Barr H. Raman spectroscopy, a potential tool for the objective identification and classification of neoplasia in Barrett's oesophagus. The Journal of Pathology: A Journal of the Pathological Society of Great Britain and Ireland. 2003;200(5):602-9.
[32] Teh SK, Zheng W, Ho KY, Teh M, Yeoh KG, Huang Z. Diagnostic potential of near-infrared Raman spectroscopy in the stomach: differentiating dysplasia from normal tissue. British journal of cancer. 2008;98(2):457-65.
[33] Bergholt MS, Zheng W, Lin K, Ho KY, Teh M, Yeoh KG, Yan So JB, Huang Z. In vivo diagnosis of gastric cancer using Raman endoscopy and ant colony optimization techniques. International journal of cancer. 2011;128(11):2673-80.
[34] Guo S, Beleites C, Neugebauer U, Abalde-Cela S, Afseth NK, Alsamad F, Anand S, Araujo-Andrade C, Askrabic S, Avci E, Baia M. Comparability of Raman spectroscopic configurations: A large scale cross-laboratory study. Analytical Chemistry. 2020;92(24):15745-56.

PHOTODYNAMIC INACTIVATION OF DORMANT FORMS OF NON-SPORULATING BACTERIA DUE TO ENDOGENOUS PORPHYRINS

DOI 10.24412/cl-36896-2021-1-57-57

ALEXANDER SAVITSKY[1], MARGARITA SHLEEVA[1], IRINA LINGE[2], ALEXANDER APT[2] AND ARSENY KAPRELYANTS[1]

[1]*Federal Research Centre 'Fundamentals of Biotechnology' of the Russian Academy of Sciences, A. N. Bach Institute of Biochemistry, Russia*

[2]*Department of Immunology, Laboratory for Immunogenetics, Central Institute for Tuberculosis, Russia*

e-mail: apsavitsky@inbi.ras.ru

ABSTRACT

For many non-sporulating gram-negative and gram-positive bacteria morphologically differentiated dormant form were described. Different non-sporulating bacteria studied in this work such as *Mycobacterium sp (tuberculosis, smegmatis) and Corynebacterium sp (jeikeium)* in dormant state acquire resistance to all known antibacterial drugs, they are also able to survive in the human body for decades and become active, causing the active form of the disease. The application of photodynamic inactivation (PDI) using exogenously added photosensitizers was recently discussed as an alternative approach for fighting active multidrug-resistant *Mtb in vitro.* In order to cure latent tuberculosis and another disease new approaches need to be developed. The aim of this work is to study the accumulation of porphyrins upon transition of active *Mtb*, *Msm* and *C. jeikeium* to the dormant state, as well as to verify the effectiveness of PDI for such dormant forms. The dormant cells of all these bacteria were obtained under gradual acidification in stationary phase. For *M. tuberculosis* and *C. jeikeium* we did not observe any photodynamic inactivation (PDI) effect on active bacteria *in vitro* as these bacteria do not contain unbound porphyrins in substantial amounts. In the presence of 5-aminolevulinic acid (ALA) an increase in the concentration of porphyrins in stationary phase correlated with the development of gradual acidification of the culture, the beginning of a decrease in metabolic activity and formation of ovoid dormant forms of the bacteria. Dormant cells were exposed to light with the wavelengths of 532 nm or 565 nm, which correspond to the absorption of porphyrins in visible spectral range, for 5-60 minutes. Illumination of bacteria by light resulted in inactivation of dormant forms according to viable bacteria number decrease estimated by MPN assay. At the same time, we observed unpredictable phenomena for active form of *Mtb* in macrophages. After persistence of active *Mtb* cells within macrophages for several days in the presence of ALA, a significant sensitivity of such cells (ca. 99.99%) to light exposure was developed. For the first time we had demonstrated a successful application of PDI for inactivation of dormant *Mycobacterium tuberculosis, smegmatis* and *Corynebacterium jeikeium* due to accumulating a significant amount of endogenous porphyrins. Also, for the first time we have demonstrated the successful application of PDI for inactivation of active *Mtb* located in macrophages due to significant accumulation of endogenous porphyrins.

This work was supported by Russian Science Foundation grant 19-15-00324.

REFERENCES

[1] Shleeva M, Savitsky A, Kaprelyants A. *Corynebacterium jeikeium* Dormant Cell Formation and Photodynamic Inactivation. Front Microbiol. 2020;11:605899. doi: 10.3389/fmicb.2020.605899.

[2] Shleeva M, Savitsky A, Kaprelyants A. Photoinactivation of mycobacteria to combat infection diseases: current state and perspectives. Appl Microbiol Biotechnol. 2021;105(10):4099-4109. doi: 10.1007/s00253-021-11349-0.

[3] Shleeva MO, Savitsky AP, Nikitushkin VD, Solovyev ID, Kazachkina NI, Perevarov VV, Kaprelyants AS. Photoinactivation of dormant Mycobacterium smegmatis due to its endogenous porphyrins. Appl Microbiol Biotechnol. 2019;103(23-24):9687-9695. doi: 10.1007/s00253-019-10197-3.

[4] Shleeva MO, Savitsky AP, Nikitushkin VD, Soloviev ID, Trutneva KA, Keruchenko Ya S, Kaprelyants AS. Effect of Photodynamic Inactivation against Dormant Forms and Active Growing Cells of Mycobacterium smegmatis. Applied Biochemistry and Microbiology, 2020, Vol. 56, No. 3, pp. 285–291. DOI: 10.1134/S000368382003014X

SCALED UP SYNTHESIS OF CURCUMIN, AND PHOTO-LARVICIDAL EFFECTS AGAINST AEDES AEGYPTI LARVAE: WORKING ON DENGUE FEVER, ZIKA AND CHIKUNGUNYA PROBLEM

DOI 10.24412/cl-36896-2021-1-58-58

KLEBER THIAGO DE OLIVEIRA

Department of Chemistry, Federal University of São Carlos – UFSCar, Rod. Washington Luiz km 235, São Carlos-SP, 13.565-905
*www.lqbo.ufscar.br, *kleber.oliveira@ufscar.br*

ABSTRACT

Curcumin is the main natural dye present in turmeric (*Curcuma longa*) and is traditionally used in Indian cooking [1]. Recently, curcuminoids have been shown to have numerous applications in photonic therapies, due to its excellent activity as photosensitizer [2-3]. In this presentation, recent and relevant photo-larvicidal results against *Aedes aegypti* larvae will be presented, showing that the combination of curcumin-formulations with sunlight establishes an extremely effective alternative for larvae control with high environmental safety and low persistence of this molecule [2-3]. This effective protocol has been developed by the CEPOF team and allowed us to work on Dengue fever, Zika and Chikungunya problem. The importance of organic synthesis and enabling technologies for the access from multi-gram to kilogram scale compounds will be also presented [4].

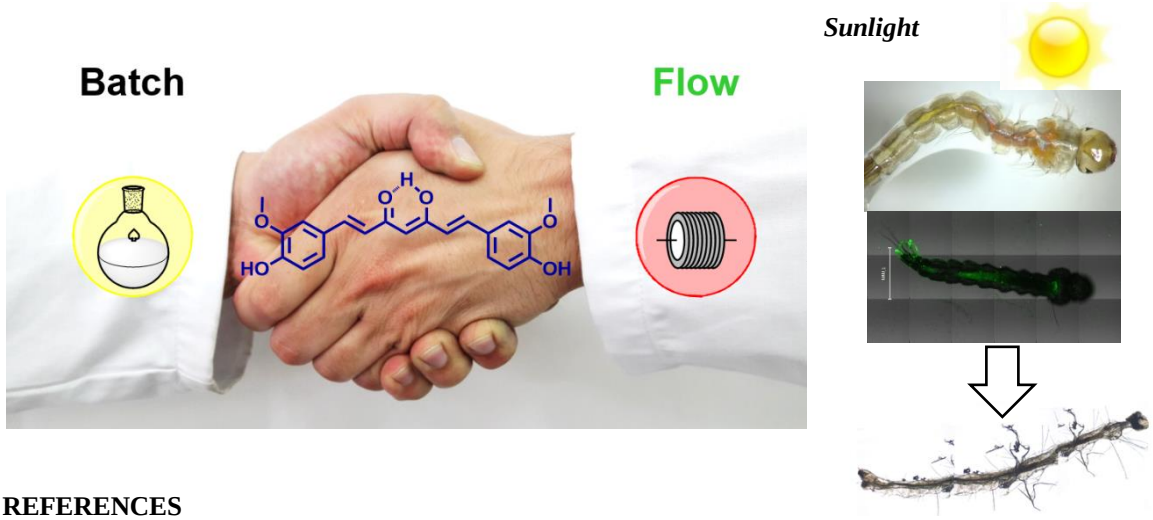

REFERENCES

[1] Esatbeyoglu, T.; Huebbe, P.; Ernst, I. M. A.; Chin, D.; Wagner, A. E.; Rimbach, G. *Angew. Chem. Int. Ed.* **2012**, *51*, 5308 – 5332.
[2] de Souza, L. M.; Inada, N. M.; Venturini, F. P.; Carmona-Vargas, C. C.; Pratavieira, S.; de Oliveira, K. T.; Kurachi, C.; Bagnato, V. S. *J. Asia-Pac. Entomol.* **2019**, *22*, 151–158.
[3] Mezzacappo, N.; Souza, L. M.; Inada, N.M.; Dias, L. D.; Garbuio, M.; Venturini, F. P.; Corrêa, T. Q.; Moura, L.; Blanco, K. C.; de Oliveira, K. T.; Bagnato, V. S. *Pest Manag. Sci.* **2021**, *77*, 2530-2538.
[4] Carmona-Vargas, C. C.; Alves, L. C.; Brocksom, T. J.; de Oliveira, K. T. *React. Chem. Eng.* **2017**, *2*, 366-374.

POTENTIATION OF ANTIMICROBIAL PHOTODYNAMIC INACTIVATION BY INORGANIC SALTS

DOI 10.24412/cl-36896-2021-1-59-60

MICHAEL HAMBLIN

Laser Research Centre, Faculty of Health Sciences, University of Johannesburg, South Africa
Hamblin.lab@gmail.com

ABSTRACT

One of the biggest health problems facing the world today is the inexorable rise of multi-antibiotic resistance amongst a wide range of pathogens, including Gram-positive or Gram-negative bacteria and fungi. Antimicrobial photodynamic inactivation (aPDI) uses visible/NIR excitation of a photosensitizer to produce the reactive oxygen species (ROS) singlet oxygen (Type 2) and hydroxyl radicals (Type1) that are both highly toxic to microbial cells. If the photosensitizer and the light are introduced into the infected area the selectivity is excellent [1]. We have discovered that antimicrobial photodynamic inactivation (aPDI) can be strongly potentiated by addition of the non-toxic salt potassium iodide [2]. This approach works with a wide variety of different photosensitizers including those possessing cationic charges that bind to microbial cells, and those neutral or anionic compounds that are completely ineffective in photoinactivating Gram-negative cells, but can kill > 6 logs in presence of 100 mM KI. The approach is broad spectrum in nature and works with methicillin-resistant Staphylococcus aureus (MRSA), a range of Gram-negative bacteria and Candida albicans. The major mechanism is likely to involve the addition of singlet oxygen to iodide to form peroxyiodide, which then decomposes via two possible routes: (a) formation of the stable species, free iodine and hydrogen peroxide; (b) formation of short-lived radicals I2•- + HOO•. When the PS binds to the microbial cells, killing by the short-lived radicals becomes significant, while for Gram-negative cells with Photofrin [3] or Rose Bengal [4], killing by I3- and H2O2 are dominant [5]. This can be studied by comparing “in” (all ingredients together, “after” cells added after light, and “spin” KI and light added after cells were incubated with PS and centrifuged. KI could potentiate RB-PDT in a mouse model of skin abrasions infected with bioluminescent P. aeruginosa demonstrating possible in vivo applications [4]. We also studied two porphyrins TMPyP4 (tetracationic) and TPPS4 (tetraanionic). Surprisingly TPPS4 was an excellent PS for MRSA and Candida, and could eradicate Gram-negative species when KI and light were added after a spin, showing it was bound to the surface [6]. Another tetraanionic phthalocyanine (ClAlPCS4) did not show this behavior. We conclude that TPPS4 behaves as if it has some cationic character in the presence of bacteria.

One of the applications of KI potentiation of aPDI that may have real clinical relevance, is the treatment of oral candidiasis. Patients with immunosuppression are at risk of developing an infection in the mouth caused by the yeast C. albicans, which is painful and difficult to treat. We showed that methylene blue (MB) plus KI excited by red light could successfully treat oral candidiasisin a mouse model [7]. We went on to carry out a clinical trial conducted on 21 adult AIDS patients with C. albicans oral candidiasis who received two treatments using MB + KI excited by red light, and showed that C. albicans CFUs were significantly reduced [8]. Additional applications of aPDI using MB + KI and red light that showed some success, were endodontic disinfection in root canals in teeth [9], and Gram-negative bacterial cystitis (bladder infection) in female rats [10].

Other inorganic salts such as sodium azide, potassium thiocyanate, potassium selenocyanate, potassium bromide and sodium nitrite also produce increased killing of a broad range of pathogens by up to one million times [11]. The mechanisms of potentiation are different for different salts. At one extreme of the salts is sodium azide, that quenches singlet oxygen but can produce azide radicals (presumed to be highly reactive) via electron transfer from photoexcited phenothiazinium dyes, in a so-called paradoxical potentiation process [12]. As discussed above KI is oxidized to molecular iodine by both Type I and Type II PSs, but may also form reactive iodine species. Potassium bromide is oxidized to hypobromite, but only by titanium dioxide photocatalysis (Type I) [13]. Potassium thiocyanate appears to require a mixture of Type I and Type II photochemistry to first produce sulfite, that can then form the sulfur trioxide radical anion [14]. Potassium selenocyanate can react with either Type I or Type II ROS (or indeed with other oxidizing agents) to produce the semi-stable selenocyanogen (SCN)2 that can attack bacteria [15]. Despite the similar chemical structures of thiocyanate and selenocyanate anions, the mechanisms of potentiation of aPDI turned out to be suprisingly different [16]. Finally, sodium nitrite may react with either Type I or Type II PSs to produce peroxynitrate (again, semi-stable) that can kill bacteria and produce nitrotyrosine by tyrosine nitration [17]. Many of these salts (except azide) are non-toxic, and may be clinically applicable.

REFERENCES

[1] M. R. Hamblin, “Antimicrobial photodynamic inactivation: a bright new technique to kill resistant microbes,” Curr Opin Microbiol, 33, 67-73 (2016).
[2] D. Vecchio, A. Gupta, L. Huang, G. Landi, P. Avci, A. Rodas, and M. R. Hamblin, “Bacterial photodynamic inactivation mediated by methylene blue and red light is enhanced by synergistic effect of potassium iodide,” Antimicrob Agents Chemother, 59(9), 5203-12 (2015).

[3] L. Huang, G. Szewczyk, T. Sarna, and M. R. Hamblin, "Potassium Iodide Potentiates Broad-Spectrum Antimicrobial Photodynamic Inactivation Using Photofrin," ACS Infect Dis, 3(4), 320-328 (2017).
[4] X. Wen, X. Zhang, G. Szewczyk, A. El-Hussein, Y. Y. Huang, T. Sarna, and M. R. Hamblin, "Potassium Iodide Potentiates Antimicrobial Photodynamic Inactivation Mediated by Rose Bengal in In Vitro and In Vivo Studies," Antimicrob Agents Chemother, 61(7), (2017).
[5] M. R. Hamblin, "Potentiation of antimicrobial photodynamic inactivation by inorganic salts," Expert Rev Anti Infect Ther, 15(11), 1059-1069 (2017).
[6] L. Huang, A. El-Hussein, W. Xuan, and M. R. Hamblin, "Potentiation by potassium iodide reveals that the anionic porphyrin TPPS4 is a surprisingly effective photosensitizer for antimicrobial photodynamic inactivation," J Photochem Photobiol B, 178, 277-286 (2018).
[7] F. Freire, C. Ferraresi, A. O. Jorge, and M. R. Hamblin, "Photodynamic therapy of oral Candida infection in a mouse model," J Photochem Photobiol B, 159, 161-8 (2016).
[8] M. Du, W. Xuan, X. Zhen, L. He, L. Lan, S. Yang, N. Wu, J. Qin, R. zhao, J. Qin, J. Lan, H. Lu, C. Liang, Y. Li, M. R Hamblin, and L. Huang, "Antimicrobial photodynamic therapy for oral Candida infection in adult AIDS patients: a pilot clinical trial," Photodiagnosis and Photodynamic Therapy, 102310 (2021).
[9] L. Yuan, P. Lyu, Y. Y. Huang, N. Du, W. Qi, M. R. Hamblin, and Y. Wang, "Potassium iodide enhances the photobactericidal effect of methylene blue on Enterococcus faecalis as planktonic cells and as biofilm infection in teeth," J Photochem Photobiol B, 203, 111730 (2020).
[10] Y. Y. Huang, A. Wintner, P. C. Seed, T. Brauns, J. A. Gelfand, and M. R. Hamblin, "Antimicrobial photodynamic therapy mediated by methylene blue and potassium iodide to treat urinary tract infection in a female rat model," Sci Rep, 8(1), 7257 (2018).
[11] M. R. Hamblin, and H. Abrahamse, "Inorganic Salts and Antimicrobial Photodynamic Therapy: Mechanistic Conundrums?" Molecules, 23(12) (2018).
[12] L. Huang, T. G. St Denis, Y. Xuan, Y. Y. Huang, M. Tanaka, A. Zadlo, T. Sarna, and M. R. Hamblin, "Paradoxical potentiation of methylene blue-mediated antimicrobial photodynamic inactivation by sodium azide: role of ambient oxygen and azide radicals," Free Radic Biol Med, 53(11), 2062-71 (2012).
[13] X. Wu, Y. Y. Huang, Y. Kushida, B. Bhayana, and M. R. Hamblin, "Broad-spectrum antimicrobial photocatalysis mediated by titanium dioxide and UVA is potentiated by addition of bromide ion via formation of hypobromite," Free Radic Biol Med, 95, 74-81 (2016).
[14] T. G. St Denis, D. Vecchio, A. Zadlo, A. Rineh, M. Sadasivam, P. Avci, L. Huang, A. Kozinska, R. Chandran, T. Sarna, and M. R. Hamblin, "Thiocyanate potentiates antimicrobial photodynamic therapy: in situ generation of the sulfur trioxide radical anion by singlet oxygen," Free Radic Biol Med, 65, 800-810 (2013).
[15] L. Huang, W. Xuan, A. Zadlo, A. Kozinska, T. Sarna, and M. R. Hamblin, "Antimicrobial photodynamic inactivation is potentiated by the addition of selenocyanate: Possible involvement of selenocyanogen?" J. Biophotonics, 11(8), e201800029 (2018).
[16] L. Huang, W. Xuan, T. Sarna, and M. R. Hamblin, "Comparison of thiocyanate and selenocyanate for potentiation of antimicrobial photodynamic therapy," J. Biophotonics, 12(1), e201800092 (2019).
[17] Y. Y. Huang, P. J. Rajda, G. Szewczyk, B. Bhayana, L. Y. Chiang, T. Sarna, and M. R. Hamblin, "Sodium nitrite potentiates antimicrobial photodynamic inactivation: possible involvement of peroxynitrate," Photochem Photobiol Sci, 18(2), 505-515 (2019).

BREATHOMICS USING LASER PHOTO-ACOUSTIC SPECTROSCOPY AND MACHINE LEARNING

DOI 10.24412/cl-36896-2021-1-61-61

YURY V.KISTENEV, ALEXEY V. BORISOV, VLADIMIR V. PRISHEPA, DENIS A. VRAZHNOV

LMIML laboratory, Tomsk State University, Russia

yv.kistenev@gmail.com

ABSTRACT

Analysis of volatile molecular biomarkers in the exhaled air, called breathomics, is suitable for operative non-invasive medical screening tests. The report is devoted to applications of laser spectroscopy and machine learning for evaluation of volatile molecular biomarkers' profile to detect a specific disease. Breath air analysis can be conducted through the pattern-recognition-based and chemical-composition-based approaches. The former approach is typical for supervised machine learning algorithms.

A content analysis of gas mixtures can be conducted through an inverse spectroscopy problem solution. The multivariate curve resolution (MCR) methods are widely used for decoding the spectra of complex mixtures, including overlapping spectra, and are based on a bilinear model of the complex spectrum in the form of a superposition of contributions of individual components [2] -[4] . One of the main problems is to find the optimal set of components and concentrations that best approximates the experimental spectrum. For example, MCR needs a knowledge about probable composition of a gas sample [4] .

For the chemical-composition-based approach implementation, we use deep neural networks [[1]] and original chemometrics' methods, including criterium based on reducing a spectrum complexity (RSC) [2] which corresponds to the minimum of the derivative's difference between the whole spectrum and the subtracted component spectrum, to provide exhaled air chemical composition. The example of RSC method application is shown in Fig.1. Here, we used a combination of an exhaled air sample combined with CH_4 addition in concentration of $7.1 \cdot 10^{-04}$ %.

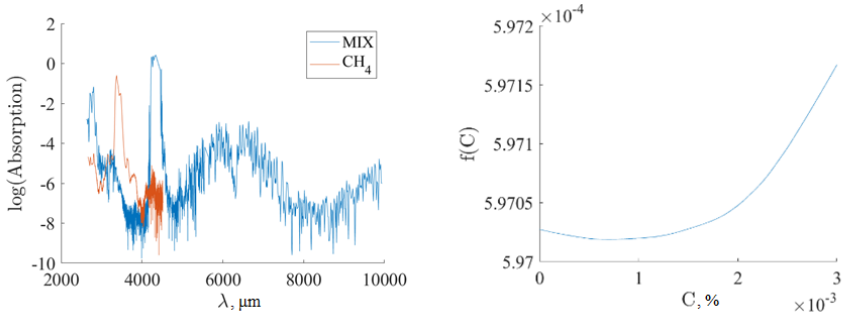

Figure 1. *(a) Absorption spectra of an exhaled air sample (MIX) and CH_4; (b) the value of the criterium based on RSC depending on the concentration of CH_4 addition.*

The research was carried out with the support of a grant under the Decree of the Government of the Russian Federation No. 220 of 09 April 2010 (Agreement No. 075-15-2021-615 of 04 June 2021).

REFERENCES

[1] V. V. Prischepa, et al. Proc. SPIE 11582. 115821J, 2020.
[2] Tauler De Juan Multivariate Curve Resolution-Alternating Least Squares for Spectroscopic Data. Chapter 2. Data Handling in Science and Technology. Elsevier B.V. 2016
[3] Pohl A, Deßmann N, Dutzi K *et al.* Identification of Unknown Substances by Terahertz Spectroscopy and Multivariate Data Analysis *J. Infrared Millim. Terahertz Waves.* 37(2). 175–88, 2016.
[4] Ruckebusch C, Blanchet L Multivariate curve resolution: A review of advanced and tailored applications and challenges *Anal. Chim. Acta.* 765, 28-36, 2013.
[5] A.Borisov, et al. *Journal of Breath Research.* 027104. *2021.*

IMAGING BY PHOTOACOUSTIC MICROSCOPY AND TOMOGRAPHY WITH PLASMONIC TIN NANOPARTICLES

DOI 10.24412/cl-36896-2021-1-62-62

ANDERSON S. L. GOMES[1,3] AVISHEK DAS [1], ARTHUR CESARE [1], ANTON A. POPOV [2], ANDREI PASTUKHOV [2] AND ANDREI KABASHIN [2,3]

[1]Departamento de Física, Universidade Federal de Pernambuco, Recife, 50670-901, PE, Brazil; avishek55das@gmail.com (A. D); arthurcmvp@gmail.com (A. C); anderson.lgomes@ufpe.br (A. G)

[2]Aix Marseille University, CNRS, LP3, 163 Ave. De Luminy, Case 917, 13288 Marseille, France; kabashin@lp3.univ-mrs.fr (A.V.K.)

[3]Bio-Nanophotonics Laboratory, MEPhI, Institute of Engineering Physics for Biomedicine (PhysBio), 31 31 Kashirskoe sh., 115409 Moscow, Russia

ABSTRACT

Photoacoustic imaging (PAI) is enabled by a hybrid of optical excitation and acoustic detection which comprises both the advantages of high optical contrast and ultrasonic resolution. Some PAI techniques are mostly advantageous for pre-clinical or clinical non-invasive biomedical imaging. In this talk, we shall highlight the basics and state-of-the-art in PAI methods with particular emphasis on the use of exogenous contrast agents. We will describe how we have exploited Titanium Nitride (TiN) nanoparticles for PAM (Photoacoustic Microscopy) and PAT (Photoacoustic Tomography) prepared by the laser ablation technique [1]. Following a structural and optical characterization, TiN nanoparticles ranging from 50-100nm in size were employed. The absorption spectra of the nanoparticles confirmed the presence of a broad plasmonic band covering both parts of the visible and near-infrared (NIR) spectrum. Recent characterization of the nonlinear optical properties of such nanoparticles has been recently published [2]. For the photoacoustic imaging, a lab-made setup was developed by employing a Q-switched Nd: YAG laser (fundamental and second harmonic), high-frequency ultrasonic transducer, customized two-dimensional (2D) scanning stage and real-time data acquisition computer program. The PAM system was used to image the TiN nanoparticles with a resolution of ~ 50 μm, underneath 1 mm chicken breast tissue. For the PAT results, lower resolution (~400 μm) was measured, but the penetration depth of 2cm was observed. Future applications will be discussed.

The authors thanks CNPq, FACEPE and CAPES for financial support for this work.

REFERENCES

[1] Popov, A.A., Tselikov, G., Dumas, N. et al. Laser-synthesized TiN nanoparticles as promising plasmonic alternative for biomedical applications. Sci Rep 9, 1194 (2019).

[2] Melissa E. Maldonado, Avishek Das, Anderson S. L. Gomes, Anton A. Popov, Sergey M. Klimentov, Andrei V. Kabashin, Nonlinear Photoacoustic Response of Suspensions of Laser-Synthesized Plasmonic Titanium Nitride Nanoparticles, Opt. Lett. 45, 6695-6698 (2020).

LIGHT AND ULTRASOUND TO TREAT IN A NON-INVASIVE WAY NODULAR AND PIGMENTED SKIN LESIONS

DOI 10.24412/cl-36896-2021-1-63-63

ERIKA TONETH PONCE AYALA, MURILO DE OLIVEIRA SOUZA, CAMILA APARECIDA ANTUNES, MARLON RODRIGUES GARCIA, MICHELLE BARRETO REQUENA, FERNANDA ALVES DIAS DE SOUSA, LILIAN TAN MORIYAMA, CRISTINA KURACHI, ANA GABRIELA SALVIO, VANDERLEI SALVADOR BAGNATO, SEBASTIÃO PRATAVIEIRA

São Carlos Institute of Physics, University of São Paulo

ABSTRACT

Despite all the efforts and scientific-technological advances in recent years, deaths from any types of cancer are still among the top 3 causes of death in the world. Among the factors for this, we can mention the increase in life expectancy, the growth in the world population, and exposure to carcinogens. Nevertheless, lack of medical assistance is also aggravating for these deaths.

In BRICS countries with large populations and few resources, it is extremely necessary to develop efficient and low-cost treatments to be widely adopted. For example, some types of skin lesions, such as pigmented lesions, nodular lesions, and especially melanoma, are a relevant health problem due to the difficulty in treating them in a non-invasive and painless way. The standard treatment for these types of injuries is surgical resection, however, it is very invasive and aggressive, and the aesthetic result is poor. Therefore, several treatment possibilities are being developed and tested to change this clinical reality. One option is Photodynamic Therapy, which has proven to be very efficient for treating superficial non-melanoma skin lesions. In these cases, PDT is a non-invasive procedure and uses a combination of light, a light-sensitive drug - called a photosensitizer (FS), and molecular oxygen (O_2), after the interaction of these three ingredients, reactive oxygen species are generated resulting in cell death. This technique has been successfully implemented in Brazil and worldwide, with efficient, safe, and better aesthetic results in comparison with other used methods.

However, there are still lesions that need alternative methods to the current ones, such as nodular and pigmented lesions where the delivery of light in a non-invasive way is a challenge, due to the light-tissue interaction properties, the light penetration necessary to initiate the photodynamic effect is limited to a few millimeters. An alternative method to overcome these challenges is the sonodynamic therapy (TSD), which consists of using low frequency ultrasound waves (US) and now a molecule that is activated by ultrasound - a sonosensitizer (SS). SDT has an application protocol like PDT, in which the SS applied to the patient interacts with the US waves leading to cell death. Unlike light, US easily crosses biological tissues due to its low attenuation, which allows this therapy to reach deeper tumors.

In this talk, we will present study that aims to evaluate the ability of 5-aminolevulinic acid (5-ALA) mediated SPDT to reduce the size of B16-F10 melanoma tumors in mice. B16-F10 tumor cells ($1x10^6$ cells) were implanted subcutaneously on the right-side flanks of nude mice. When the tumor reached an average volume of $\approx 100 mm^3$, mice were treated with 1 daily session of PDT, SDT or SPDT for 5 days. Mice were intraperitoneally injected with 5-ALA at the dose of 250 mg/kg weight, after 3h of injection, mice were irradiated with light (red laser, 100 mW/cm^2), ultrasound (1MHz, 1.5 W/cm^2, 20,50 %) and both sources. For these procedures, a single probe capable of irradiating light and ultrasound individually and simultaneously was developed. Tumor volume was measured at the time of each treatment and daily after the treatment for 6 days. Tissue sections will be analyzed through histological processing.

It was observed in SDT group, a decrease in tumor size after the first session as well as in tumor growth rate after treatment. Results obtained so far (SDT group) suggest that the combination of SDT and PDT can improve the effectiveness of each treatment applied individually. The combination of PDT and SDT could be very useful non-invasive technique for treatment of melanoma skin cancer.

ENHANCED ANTIBACTERIAL ACTION OF SILVER NANOPARTICLES LOADED ON REDUCED GRAPHENE OXIDE SHEETS UNDER BLUE-LIGHT IRRADIATION

DOI 10.24412/cl-36896-2021-1-64-64

ANDERSON R. L. CAIRES*

Optics and Photonics Group, Institute of Physics, Federal University of Mato Grosso do Sul, Campo Grande, Mato Grosso do Sul, 79070-900, Brazil.

anderson.caires@ufms.br

ABSTRACT

The main motivation is to show that an efficient process of bacterial inactivation can be achieved by using silver nanoparticles (AgNPs) anchored on graphene oxide (GO) sheets under blue light illumination. It will be presented general motivations on: multi-drug microorganisms; antimicrobial photodynamic therapy (aPDT); nanoparticles in aPDT; photodynamic action of AgNPs; and enhanced photodynamic effect of AgNPs loaded on graphene oxide (GO). Finally, it will be shown a recent published study, which demonstrates that an enhanced antibacterial action of AgNPs-GO, against *Staphylococcus aureus*, under blue-light illumination can be achieved because of three different bacterial killing processes: (i) chemical effect promoted by Ag+ ion release from AgNPs; (ii) photodynamic activity induced by AgNPs-GO, enhancing the bacterial photoinactivation due to the excited-Plasmons of the AgNPs when anchored on r-GO; and (iii) photodynamic effect promoted by bacterial endogenous photosensitizers under blue-light irradiation.

Keywords: Antimicrobial photodynamic therapy; Silver nanoparticle; Graphene oxide; Blue light; *Staphylococcus aureus*.

PROTEIN PROFILE STUDY OF NEONATAL TEAR FLUIDS

DOI 10.24412/cl-36896-2021-1-65-65

ALISHA RIZVI[1], SPHURTI S ADIGAL[1], SULATHA V BHANDARY[1], AND SANTHOSH CHIDANGIL[2]

1. Department of Ophthalmology, Kasturba Medical College, Manipal Academy of Higher Education, Manipal

2. Department of Atomic and Molecular Physics, Manipal Academy of Higher Education, Manipal

sphurti777@gmail.com

ABSTRACT

Newborn babies (neonates) begin to secrete tears in the first 24 hours of life and it produces enough aqueous to maintain clear vision and humidify the ocular surface. Neonatal tear analysis can provide information about the health condition of eyes since it contains specific molecules, proteins and their relative concentrations may alter under abnormal conditions. Neonatal tear protein content has not been studied as much as in adults tear sample due to the difficulty of collecting samples without causing reflex tearing. To explore the neonatal tear samples extensively, spectroscopic, proteomic, lipidomic, and metabolomics studies are necessary. The present objective of the study is to investigate the unstimulated neonatal tear fluid by collecting samples using non-invasive method (Schirmer strip) and analyze the protein patterns of term and pre-term babies tear fluids using high performance liquid chromatography with light emitting diode-induced fluorescence system (HPLC-LED-IF) developed in our laboratory. The studies have reported concentration of standard protein markers (lysozyme, lactoferrin and serum albumin) in neonatal tear fluid are of the order of micromolar concentration. The detection limits of these standard proteins obtained for the present system are of the order of nanomolar concentrations. The protein profiles of term and preterm tear fluid samples has been analyzed and found noticeable differences between each category.

WHOLE BLOOD RAMAN SPECTROSCOPY ANALYSIS FOR MYOCARDIAL INFARCTION

DOI 10.24412/cl-36896-2021-1-66-66

REENA V JOHN[1], TOM DEVASIA[2], MITHUN N1, JIJO LUKOSE[1], SANTHOSH CHIDANGIL[1]

1Centre of Excellence for Biophotonics, Department of Atomic and Molecular Physics,
Manipal Academy of Higher Education, Manipal, Karnataka, India-576104
2Department of Cardiology, Kasturba Medical College, Manipal,
Manipal Academy of Higher Education, Manipal, Karnataka, India-576104

santhosh.cls@manipal.edu

ABSTRACT

The myocardial infarction (MI) has major effect on the mortality rate of the society. Diabetes mellites, hypertension, inflammation are some of the risk factors of MI. The studies have shown that presence of inflammation, alters activity of tetrahydrobiopterin (BH4) cofactor. A positive correlation between inflammatory marker, C-reactive protein (CRP) and BH4 is also reported. The direct measurement of BH4 in blood is tedious, thus making it less suitable for clinical application. Here in this study, variation in BH4 is indirectly estimated using phenylalanine to tyrosine ratio in MI blood samples. Phenylalanine is an essential amino acid, and tyrosine is a non-essential amino acid. Since it can be synthesized by hydroxylation of phenylalanine in body through phenylalanine hydroxylase (PAH) enzyme. The activity of PAH enzyme is regulated by tetrahydrobiopterin (BH4) cofactor. Thus, the deficiency in BH4 cofactor is reflected in phenylalanine to tyrosine ratio.

Raman spectroscopy is promising method, for clinical application. In the present Raman spectral study of whole blood samples, the intensity ratio corresponding to phenylalanine (1000cm^{-1}) and tyrosine (825cm^{-1}) is calculated to predict the changes in availability BH4 cofactor. Principal component analysis (PCA) was carried out and has showed good clustering among the different categories. The technique can be utilized to investigate the level of inflammation in MI samples by indirectly assessing BH4 availability.

BIOPHOTONIC APPROACHES TOWARDS CIRCULATING TUMOR CELL DETECTION AND PHOTODYNAMIC CANCER THERAPY

DOI 10.24412/cl-36896-2021-1-67-68

HEMA SANTHAKUMAR, KUNNUMPURATHU JIBIN, RAMAPURATH. S. JAYASREE
Sree Chitra Tirunal Institute for Medical Sciences and Technology, BMT Wing,
Thiruvananthapuram, Kerala, India
jayasree@sctimst.ac.in

ABSTRACT

Although, cancer is considered as a localized disease in its pre-mature stages, in certain types of cells, it often is innate with patient becoming symptomatic and results in metastasis. Cancer cells are showered from the primary tumor cells into the circulating blood stream that finally forms metastasis. Thus, it becomes critical to identify and quantify the circulating tumor cells (CTC) during the early stages of tumorigenesis.

Here, we discuss about the design and fabrication of a user-friendly custom-designed nanotag enabled portable system for the selective separation and isolation of CTCs from whole blood. The detection should be followed by treatment. Gold nanoclusters of ultrasmall size comprising a few atoms are known for its unique feature of excellent fluorescent property. Herein, simple one step green synthesis method for the preparation of highly fluorescent silver doped gold nanoclusters using custom synthesized tripeptide Asp-Cys-Gly and its potential in generating ROS towards cancer treatment, and simultaneous imaging is discussed. Because invasive tissue biopsy data obtained from limited amount of collected tissues are often expensive and biased, "liquid biopsy" has gained significant attention as a promising diagnostic procedure for the identification and quantification of cancer driven materials present in the blood stream. The key targets employed in liquid biopsy include various circulating biomarkers such as circulating tumor cells, circulating vesicles, circulating nucleic acids and circulating proteins. Conventionally, these biomarkers are detected either by traditional protein or nucleic acid-based assays. Among various circulating biomarkers, CTC show great promise in the early detection of cancer and more specifically cancers of metastatic nature, since they are prognostic markers which are present in the blood plasma. However, it is extremely challenging to develop a system to count and detect the CTC in cancer patients as its presence is as low as 1-10 CTC/mL of blood plasma. Herein with the aid of nanotechnology, we present a custom-designed SERS nanotag enabled portable filter-based sensor platform which exploits both tumor cell target specificity and size based centrifugal force for the separation and isolation of circulating breast cancer cells (SKBR3 cells) from peripheral blood sample. Towards this goal, we designed a simple and easy-to-handle custom made centrifugal prototype comprising of three independent chambers (figure 1b), all of which are made transparent for clear internal visibility, detachability of components for ease of use, reusability and autoclavability. The single prototype can serve the purposes starting from collecting blood along with SERS nanotag, centrifugation, size and antibody-based cell separation and finally the detachable filter taken out for SERS and microscopic analysis.

Considering the unique roles that could perform within the single prototype, it is hereafter named as a 'lab-on-a-filter' system. The 'lab-on-a-filter' system is equipped with an anti-EpCAM immobilized flexible and transparent track-etched polycarbonate (PC) membrane filter with pore size 8μM. To rely on the SERS technology to detect breast cancer cells in peripheral blood, a highly sensitive and target specific sandwich system of SERS nanotag (Au-rGO@anti-ErbB2) is prepared and incubated with the collected blood before using it in the developed system. As we have used SKBR3 cells as model CTCs, which has both EpCAM and ErbB2 over expression, we have used two different antibodies, anti-EpCAM conjugated over the polycarbonate filter sheets and anti-ErbB2 antibody for the SERS tag preparation. This dual functionalization increases the specificity of the 'lab-on-a filter' system towards the capturing of the cancer cells for an efficient isolation and detection. The PC membrane filter is placed in the centrifugal prototype in such a way that, it can be detached and mounted for SERS imaging analyses after the selective isolation of CTCs on top of it. Taken together, the lab-on-a-filter system will serve as a potential candidate for the identification, isolation and accurate quantification of CTC, which may have huge impact in translational clinical research.

In another study we have utilized gold nanoclusters which has unique features arising from quantum size effect for the imaging and cancer therapy. Gold cluster is a material of interest with ultrasmall size with a few atoms (< 3 nm), has excellent fluorescent property, tremendous catalytic activities, two-photon absorptions and long lifetime. Its physico-chemical and biological properties are extremely favourable for drug delivery and therapeutic applications due to its high inertness, low toxicity with good renal clearance and long blood circulation time. The fluorescence of the gold nanoclusters can be tuned with different core size and ligand functionalization. Here, we have synthesized a novel cluster using simple one step method to get highly fluorescent silver doped gold nanoclusters (DCG-GNC) using custom synthesized tripeptide Asp-Cys-Gly (DCG) as reducing cum stabilizing agent. The peptides were designed to contain cysteine residue to facilitate interaction with gold ions, thereby to achieve biomineralization of gold clusters. Unlike the case of gold nanoparticles which is known for its surface plasmon resonance peak in the visible range, gold nano cluster shows no sharp absorption. Moreover, it exhibits strong fluorescence which can be tuned in the desired region (figure 2a). DCG-GNC displayed strong fluorescent property, large Stokes shift and good photostability, thereby making them promising bioimaging agents. The cytocompatibity and cellular uptake of DCG-GNC were investigated in MCF-7 breast cancer cells. In addition, the anti-cancer activity of DCG-GNC was also explored with the photoinduced generation of

increased intracellular ROS followed by stimulation of mitochondrial apoptotic pathway in cancer cells. Photodynamic therapy (PDT) works with the accumulation of photosensitizer (PS) in tumours, which upon light irradiation generate singlet oxygen ($^1O_2$) and other reactive oxygen species (ROS) to induce cell death. ROS, a specific type of oxygen-containing reactive molecules plays important roles in different cellular processes, including cell proliferation at basal level, but at high concentration, ROS can be cytotoxic and induce apoptosis/necrosis. The photodynamic potential of DCG-GNC by acting as a photosensitizer or induce ROS generation under laser irradiation was evaluated by H2-DCFDA staining method. H2-DCFDA is a nonfluorescent cell-permeable dye, which is activated by intracellular esterases through cleavage of acetate groups and becomes fluorescent (λ_{em} = 525 nm) upon oxidation by ROS. The ROS production in the presence and absence of laser irradiation performed in breast cancer cells is shown in figure 2b. The study points to the fact that peptide stabilized silver doped gold cluster in general and specifically, DCG-GNC can act as a promising cancer theranostic agents and the potential of their use could be ventured into for future clinical applications.

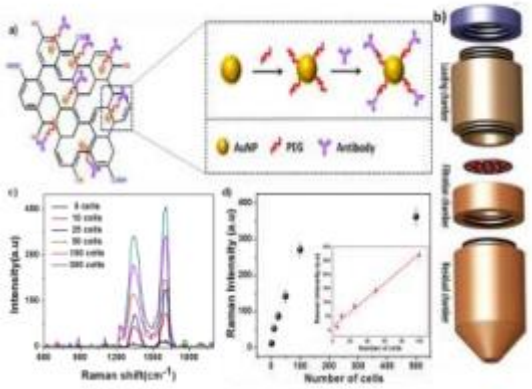

Figure 1. *a) Formation of Au-rGO@anti-ErbB2 nanotag. b) Design of centrifugal prototype and c) Detection specificity of SKBR3 cells in whole blood and d) Raman intensity against number of SKBR3 cells for limit of detection.*

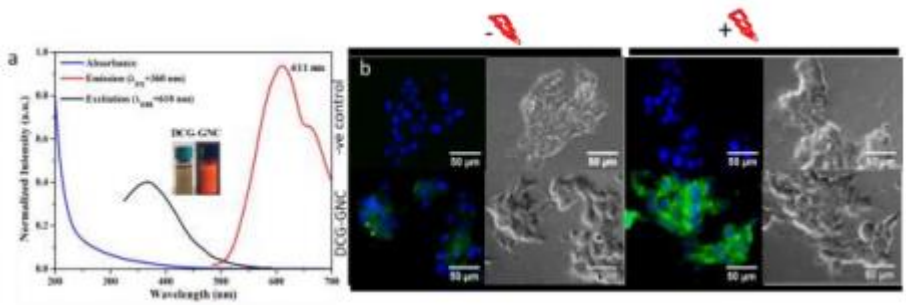

Figure 2. *UV-Vis Absorption, Emission & Excitation spectra of TPGNCsDCG-GNC and DCS-GNC. Insets show the photographic image of gold nanoclusters under visible (left) and UV light, 365nm (right) illumination. Microscopic images of ROS generation in DCG-GNC and DCS-GNC treated cancer cells with and without laser irradiation*

REFERENCES

[1] Brock, G.; Castellanos-Rizaldos, E.; Hu, L.; Coticchia, C.; Skog, J. Liquid Biopsy for Cancer Screening, Patient Stratification and Monitoring. Transl. Cancer Res. 2015, 4, 280-290 DOI: 10.21037/4546.

[2] Cristofanilli, M.; Budd, G. T.; Ellis, M. J.; Stopeck, A.; Matera, J.; Miller, M. C.; Reuben, J. M.; Doyle, G. V.; Allard, W. J.; Terstappen, L. W. M. M.; Hayes, D. F. Circulating Tumor Cells, Disease Progression, and Survival in Metastatic Breast Cancer. N. Engl. J. Med. 2004, 351, 781–791. DOI:10.1056/NEJMoa040766

[3] Jibin, K.; Prasad, J. S.; Saranya, G. et al. Optically Controlled Hybrid Metamaterial of Plasmonic Spiky Gold Inbuilt Graphene Sheets for Bimodal Imaging Guided Multimodal Therapy. Biomater. Sci. 2020, 8, 3381–3391. DOI:10.1039/D0BM00312C.

[4] Jibin, K.; Victor, M.; Saranya, G. et al. Nanohybrids of Magnetically Intercalated Optical Metamaterials for Magnetic Resonance/Raman Imaging and In Situ Chemodynamic/Photothermal Therapy. ACS Appl. Bio Mater. 2021. DOI:10.1021/acsabm.1c00510.

[5] Liu, G., Shao, Y., Ma, K. et al. Synthesis of DNA-templated fluorescent gold nanoclusters. Gold Bull, 2012, 45, 69–74. doi.org/10.1007/s13404-012-0049-6

[6] Akram Yahia-Ammar, Daniel Sierra, Fabienne Mérola et al.Self-Assembled Gold Nanoclusters for Bright Fluorescence Imaging and Enhanced Drug Delivery, ACS Nano 2016, 10, 2, 2591–2599, doi.org/10.1021/acsnano.5b07596

PHOTOACOUSTIC BREATH ANALYSER FOR THE DIAGNOSIS OF ASTHMA

DOI 10.24412/cl-36896-2021-1-69-69

NIDHEESH V.R[1], ASWINI KUMAR MOHAPATRA[2], RJAESH NAYAK[1], UNNIKRISHNAN V.K.[1], RAJEEVKUMARSINHA[1], VASUDEVAN BASKARAN KARTHA[1] AND SANTHOSH CHIDANGIL[1]

[1]Centre of Excellence for Biophotonics, Department of Atomic and Molecular Physics, Manipal Academy of Higher Education, Manipal, Karnataka, India-576104

[2]Department of Respiratory and Pulmonary Medicine, Kasturba Medical College, Manipal, Manipal Academy of Higher Education, Manipal, Karnataka, India-576104

Corresponding author: santhosh.cls@manipal.edu

Presenting author: nidheeshvr1995@gmail.com

ABSTRACT

Breath analysis is getting important for the diagnosis of lung-related diseases due to the possibility of volatile organic compounds (VOC) as a biomarker for different diseases and the technique is non-invasive. Photoacoustic spectroscopy (PAS) is a well-known absorption method, which can be implemented for the study of VOCs. In the PAS technique, an increase in acoustic intensity generated from the PA cell by the absorption of light by the VOC is measured. We have designed and assembled a Photoacoustic breath analyser for the study of VOCs. The device has got the detection limit in ppb/ppm for different VOCs such as acetone, acetonitrile, benzene and toluene. A preliminary study on exhaled breath samples from asthma and normal subjects has been performed using the device. Principal component analysis has been carried out to find out the classification of asthma and normal samples. Noticeable differences observed in the PA signals of normal and asthma breath samples, due to the VOC biomarkers present in the asthma samples. Nitric oxide is the breath biomarker that has been used for the diagnosis of asthma in hospitals. This study demonstrates that the application of Photoacoustic breath analyser to study exhaled breath samples for the diagnosis of asthma. Experiment is in progressto analyse the breath samples of different lung diseases.

NANO SCALE TISSUE MULTIFRACTAL ANISOTROPY IN POLARIZED LIGHT SCATTERING: NOVEL BIOMARKER FOR PRECANCER DETECTION

DOI 10.24412/cl-36896-2021-1-70-72

NIRMALYA GHOSH[1], IGOR MEGLINSKI[2], NANDAN DAS[3] AND RAJIB DEY[1]

[1]Department of Physical Sciences, IISER Kolkata, India
[2]School, of Engineering and Applied Sciences, Aston University, UK

ABSTRACT

Studies on structures and processes that exhibit self-similarity has evoked intensive investigations recently because of their fundamental nature and potential applications in diverse areas ranging from complex biological systems, material structures, electrical circuits to various optical phenomena [1]. While most of the self-similar processes typically exhibit monofractal behaviour that can be adequately described by a single scaling exponent, a few special class of complex processes are associated with more complicated scaling behaviour which may be thought of as consisting of many interwoven fractal subsets, each of them characterized by their own local scaling exponent [2]. Such complex self-affine processes are also ubiquitous in nature, and are extensively studied for diverse applications, for example in physiological time series of heartbeat, turbulence, Sun's magnetic field dynamics, stock market fluctuations and so forth [2]. We have recently shown that the spatial distribution of refractive index (RI) in biological tissues exhibits multifractality, indicative of its morphological and ultra-structural tissue content [3, 4]. We have subsequently developed a novel light scattering-based inverse method for in-situ determination of multifractality of tissue RI fluctuations [3].

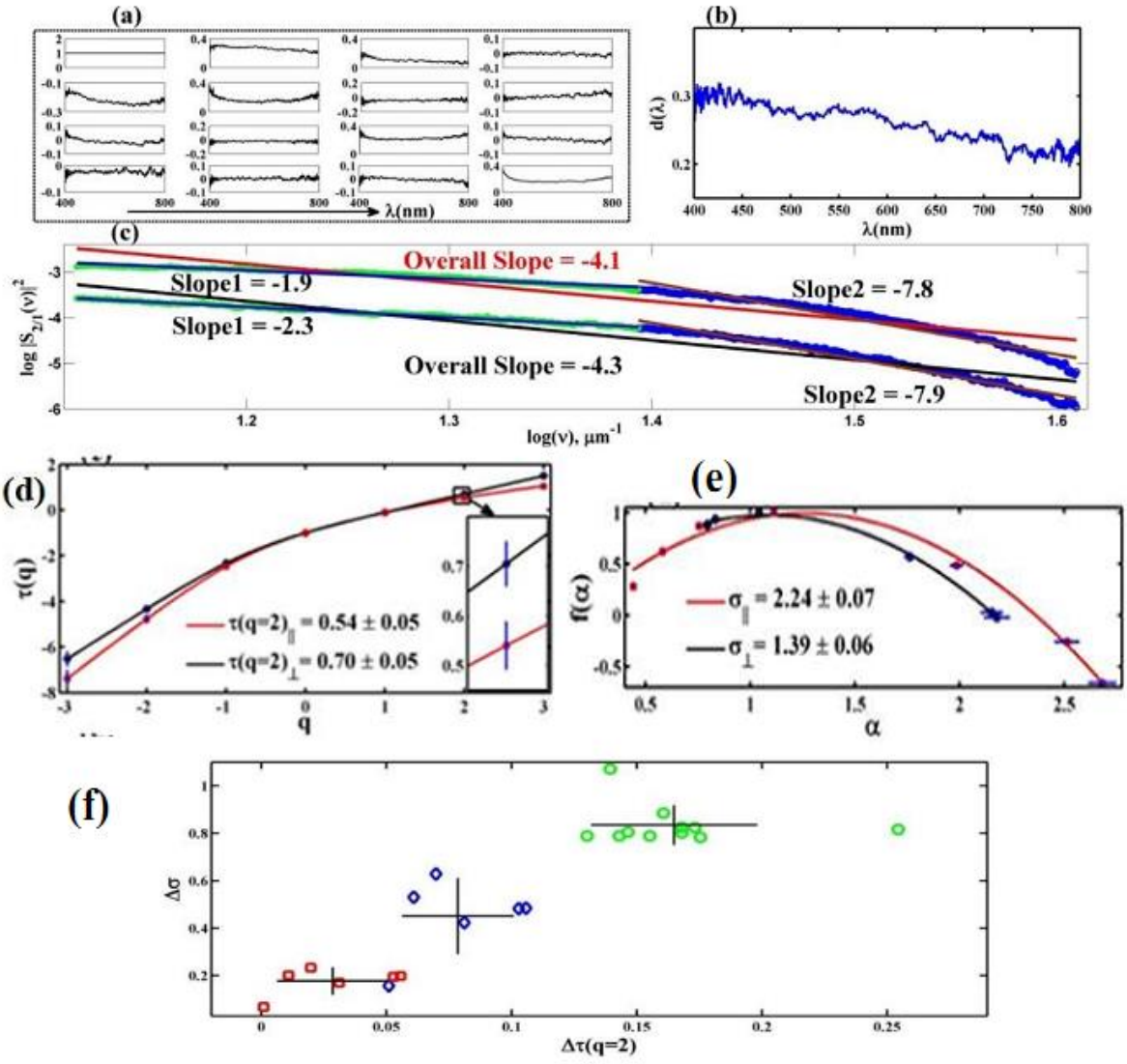

Figure 1: *(a, b, c): Manifestation of multifractal anisotropy in the wavelength variation of scattering Mueller matrix elements of a Grade I precancerous tissue. (a) Wavelength variation of the scattering Mueller matrix elements*

(normalized by the $M_{11}(\lambda)$ element). (b) Wavelength dependence of the derived linear diattenuation parameter (λ). (c) The spatial frequency (ν) distribution of the Mueller matrix-derived light scattering parameters $|s_2(\nu)|^2$ and $|s_1|(\nu)|^2$ (log-log plot). Fitting at two selected ν -ranges (lower (blue) and higher (brown)) and overall fitting (red for $|s_2(\nu)|^2$ and black for $|s_1|(\nu)|^2$ are shown and the corresponding values for the exponents are noted. (d, e): Inverse analysis of multifractal anisotropy. (d) The moment (q)-dependence of the classical multifractal scaling exponent (q) (inset highlights the anisotropy or difference in τ around $q = 2$) and (e) the corresponding singularity spectra $f(\alpha)$ derived from $\eta_{||}(\rho)$(red square) and $\eta_{\perp}(\rho)$(black circle). The values for ($q = 2$) and σ are noted. In (c) and (d) lines are guide for eye and the error bars represent standard deviations of the parameters for measurements on ten non-overlapping spots. (f) Differentiating different grades of precancers based on the Mueller matrix-derived multifractal anisotropy parameters. The three different precancerous grades (Grade I – green circle, II – blue diamond and III – red square) are mapped by their differential classical multifractal scaling exponent, $\Delta\tau = |\tau(q = 2)_{||} - \tau(q = 2)_{\perp}|$; and differential width of singularity spectrum $\Delta\sigma = |\sigma_{||} - \sigma_{\perp}|$ for orthogonal linear polarizations. Higher grades of precancers are associated with decrease of both h and $\Delta\sigma$ parameters, implying reduction in multifractal anisotropy. (Adopted from [15].)

The method is based on Fourier domain pre-processing of light scattering signal via the Born approximation, followed by the Multifractal Detrended Fluctuation Analysis. After successful validation of this inverse approach in synthetic multifractal scattering phantoms, it was initially explored for precancer detection. Following these findings of multifractal nature of tissue RI fluctuations, we have extended this method to extract microscopic anisotropy in tissue ultra-structure using polarized light scattering measurements. Note that conventional polarimetric methods lack the desirable sensitivity towards changes in the microscopic anisotropy because the tissue structural anisotropy metrics derived using these methods typically represents macroscopic properties. Yet, the morphological changes associated with precancer are rather subtle, typically associated with alterations in the microscopic anisotropy of tissue ultra-structure (anisotropy at sub-micron to nanometer length scales). In order to address this outstanding challenge in tissue polarimetry research, we have used spectroscopic Mueller matrix measurements [5-13] and its inverse multifractal analysis to quantify nanometer scale anisotropy in tissue structure, which is otherwise hidden in conventional light scattering and Mueller matrix measurements. The method is based on processing the relevant Mueller matrix elements in Fourier domain using Born approximation followed by multifractal analysis [14-18]. Application of this method on ex-vivo tissues of human cervix demonstrated the sensitivity of the multifractal anisotropy parameters towards tissue structural anisotropy at the nanometer length scales [14, 15]. These results are summarized in Figure 1. These results also demonstrated the potential of the developed methodology for novel precancer biomarker identification / tissue assessment diagnostic tool. In this talk, I shall briefly present the results of our observation on tissue multifractality and nano scale multifractal anisotropy, the developed inverse polarized light scattering model for extraction/quantification of multifractal anisotropy, its validation and exploration for precancer detection.

REFERENCES

[1] Mandelbrot, B. The Fractal Geometry of Nature (W. H. Freeman, New York, 2000).
[2] Stanley, H. Eugene. and Meakin, Paul, Nature 335, 405-409 (1988).
[3] Nandan Das, Subhasri Chatterjee, Satish Kumar, Asima Pradhan, Prasanta Panigrahi, I. Alex Vitkin and Nirmalya Ghosh, Scientific Reports, 4, 6129 (2014).
[4] N. Das,S. Chatterjee, J. Soni,J. Jagtap,A. Pradhan,T.K. Sengupta,P.K. Panigrahi, I. A. Vitkin, and N. Ghosh, Optics Letters, 38, 211-213 (2013).
[5] Subir K. Ray, Ankit K. Singh, Ajmal, Shubham Chandel, Partha Mitra, and Nirmalya Ghosh, Phys. Rev. A 100,
[6] 033805 (2019)
[7] Subir Kumar Ray, Shubham Chandel, Ankit Kumar Singh, Abhishek Kumar, Arpita Mandal, Subhradeep Misra, Partha Mitra, and Nirmalya Ghosh, ACS Nano, 11, 1641-1648 (2017).
[8] Mandira Pal, Sudipta Saha, Athira B S, Subhasish Dutta Gupta, and Nirmalya Ghosh, Phys. Rev. A, 99, 032123 (2019).
[9] Ankit Kumar Singh, Subir Kumar Ray, Shubham Chandel, Angad Gupta, Semanty Pal, Partha Mitra, and Nirmalya Ghosh, Phys. Rev. A, 97, 053801 (2018).
[10] Krishnendu Maji, Sudipta Saha, Rajib Dey, Nirmalya Ghosh and Debasish Haldar, J. Phys. Chem. C, 121, 19519−19529 (2017).
[11] Shubham Chandel, JalpaSoni, Subirkumar Ray, Anwesh Das, AnirudhaGhosh, Satyabrata Raj and Nirmalya Ghosh, Scientific Reports, 6, 26466 (2016).
[12] SudiptaSaha, JalpaSoni, Shubham Chandel, Uday Kumar, and NirmalyaGhosh, Journal of Biomedical Optics, 20(8), 085005 (2015).
[13] Soumitra Satapathi, Jalpa Soni, and Nirmalya Ghosh, Applied Physics Letters, 104, 131902 (2014).

[14] J. Jagtap, S. Chandel, N. Das, J. Soni, S. Chatterjee, A. Pradhan, and N. Ghosh, Optics Letters, 39, 243-246 (2014).
[15] Nandan Das, Rajib Dey, Semanti Chakraborty, Prasanta Panigrahi, Igor Meglinski, Nirmalya Ghosh, Optics Communications, 413, 172-178 (2018).
[16] N Das, R Dey, S Chakraborty, P K Panigrahi, P K Panigrahi, I Meglinski, N Ghosh, Laser Physics Letters, 15, 035601 (2018).
[17] Nandan Das, Sabyasachi Mukhopadhyay, Nirmalya Ghosh, Jay Chhablani, A. Richhariya, K. Divakar Rao, N. K. Sahoo, Journal of Biomedical Optics, 21, 096004 (2016).
[18] Nandan Das, Rajib Dey, S. Chakraborty, P. K. Panigrahi and N. Ghosh, Journal of Optics, 18, 125301 (2016).
[19] Nandan Das, Rajib Dey and N. Ghosh, Journal of Biomedical Optics, 21, 095004 (2016).

IDENTIFICATION OF NON-COMMUNICABLE DISEASES WITH RAMAN-BASED OPTICAL AND LIQUID BIOPSY

DOI 10.24412/cl-36896-2021-1-73-75

IVAN BRATCHENKO[1], LYUDMILA BRATCHENKO[1] YULIA KHRISTOFOROVA[1], ELENA TUPIKOVA[2], SAHAR AL-SAMMARRAE[1], PETER LEBEDEV[3], DARIA KONOVALOVA[3]AND VALERY ZAKHAROV[1]

[1]*Laser and biotechnical systems department, Samara university, Russia*
[2]*Chemistry department, Samara university, Russia*
[3]*Therapy department, Samara state medical university, Russia*
iabratchenko@gmail.com

ABSTRACT

We utilized conventional Raman spectroscopy technique for the analysis of skin tissues and surface enhanced Raman spectroscopy (SERS) for the analysis of blood serum. When classifying subjects by the presence of kidney failure using the PLS-DA method, the most informative Raman spectral bands are 1315 to 1330, 1450 to 1460, 1700 to 1800 cm^{-1}. In general, the performed study demonstrates that for *in vivo* skin analysis, the conventional Raman spectroscopy can provide the basis for cost-effective and accurate detection of kidney failure and associated metabolic changes in the skin. Application of SERS technique for the analysis of blood serum led to the ROC AUC of 0.983 (0.969 – 0.997; 95%CI) for the discrimination of healthy individuals and patients with kidney failure. For SERS we observe strongly enhanced bands which may be attributed to biochemical components such as nucleic acids (641, 724, 813, 1003, 1210, 1132 and 1450 cm^{-1}), carbohydrates (641, 890 and 1094 cm^{-1}) and lipids (1278 and 1327 cm^{-1}). Raman-based liquid biopsy may be promising in non-communicable diseases identification, as it provides fast and rapid diagnosis.

INTRODUCTION

In modern world practice, promising diagnostic methods are emerging, such as "optical biopsy" and "liquid biopsy", which are used for specific diseases biomarkers detection in biological tissues and fluids [1]. Optical methods have the potential to overcome the limitations of traditional methods of clinical analysis. One of the most promising methods of optical analysis (and optical biopsy) is a Raman spectroscopy, which can contribute to understanding of molecular basis of diseases and creation of new bioanalytical tools for the diagnosis of diseases [2]. Since each type of biological tissue and biofluid has an individual molecular composition and, thus, a unique spectral profile resulting from the transition of a molecule from one vibrational-rotational state to another, a set of such individual states of functional groups of nucleic acids, proteins, lipids and carbohydrates makes it possible to characterize component composition of tissues, which ultimately makes it possible to isolate disease markers.

Along with the use of optical biopsy methods, it is possible to apply a supersensitive technique for analyzing biofluids based on surface-enhanced Raman spectroscopy, which will be most effective for detecting low concentrations of disease markers in biological fluids [3]. In the last decade, the development of nanotechnology has led to the creation of promising tools for solving new problems in the study of various human diseases, which is especially important for effective and targeted treatment and a deeper fundamental understanding of the biochemistry of diseases.

In this study we demonstrate application of conventional Raman spectroscopy for the analysis of skin and application of SERS for serum analysis to determine the presence of non-communicable diseases.

MATERIALS AND METHODS

The study of skin optical biopsy was performed for three groups of subjects: the target group consisting of 85 hemodialysis patients with kidney failure (90 spectra series), the adult control group constituted by 40 healthy volunteers (80 spectra) without systemic diseases and the young control group constituted by 84 healthy volunteers (168 spectra) without systemic diseases. Stimulation of the collected spectra was performed by the laser module (LuxxMaster LML-785.0RB-04, PD-LD, New Jersey) with the central wavelength of 785 nm. The Raman probe (RPB785, InPhotonics, Massachusetts) is able to focus the exciting radiation, as well as to collect and filter the scattered radiation. The focal length of the utilized Raman probe was 7.5 mm with the distance between the tested skin sample and the output lens of the Raman probe of 7 mm. The collected signal was decomposed into a spectrum using a portable spectrometer (QE65Pro, Ocean optics, Florida). Details of the utilized Raman setup and cohort of studied patients maybe found elsewhere [4].

In SERS analysis of blood, we estimated 58 patients with kidney failure and 78 healthy individuals. The collected samples were placed in sterile tubes. Between sampling and direct recording of spectral characteristics, the samples were stored at -14 °C. The experimental setup for blood liquid biopsy includes a spectrometric system (EnSpectr R785, Spektr-M, Chernogolovka, Russia) and a microscope (ADF U300, ADF, China). Focusing the exciting radiation and collecting the scattered radiation were implemented using 50x Objective LMPlan. The stimulation of collected spectra was performed by the laser module with central wavelength 785 nm. A yellow-green sol with a silver concentration of 0.05-0.1 g/l was obtained by reduction from an aqueous solution of silver nitrate with sodium citrate at a temperature of 95°C

for 10 minutes. For SERS testing, a 1/1 silver colloid is added to the serum sample. Initial serum samples and samples of serum solutions with silver sol in a volume of 6 µl are applied to aluminum foil and dried for 60 minutes at room temperature.

All spectral data were processed by means of regression analysis. The fact that each tested subject is characterized by spectral data and a priori information on a particular class (the target or the control group) helped us to solve the supervised classification problem. The obtained experimental dataset was subjected to discriminant analysis with the projection on latent structures (PLS-DA). Since the analyzed spectral data are multicollinear, the projection analysis methods can provide a statistically reliable result. The PLS-DA is one of the most common approaches to solving such problems. When constructing the regression model, the informative spectra bands were defined by analyzing the variable importance in the projection (VIP) distribution. VIP makes it possible to assess the impact of individual variables of the predicate matrix array on the model [5].

RESULTS AND DISCUSSION

Figure 1 demonstrates the VIP scores of the Raman spectra matrices in the constructed regression models. Analysis of Figure 1 graphically demonstrates that the spectral bands characteristic of kidney failure does not overlap with the bands that are informative when discriminating healthy skin tissues by age. Application of Raman spectroscopy to investigate the forearm skin has yielded the accuracy of 0.96, sensitivity of 0.94 and specificity of 0.99 in terms of identifying the target subjects with kidney failure. The autofluorescence analysis in the near infrared region identified the patients with kidney failure among healthy volunteers of the same age group with specificity, sensitivity, and accuracy of 0.91, 0.84, and 0.88, respectively. When classifying subjects by the presence of kidney failure using the PLS-DA method, the most informative Raman spectral bands are 1315 to 1330, 1450 to 1460, 1700 to 1800 cm^{-1}. In general, the performed study demonstrates that for *in vivo* skin analysis, the conventional Raman spectroscopy can provide the basis for cost-effective and accurate detection of kidney failure and associated metabolic changes in the skin.

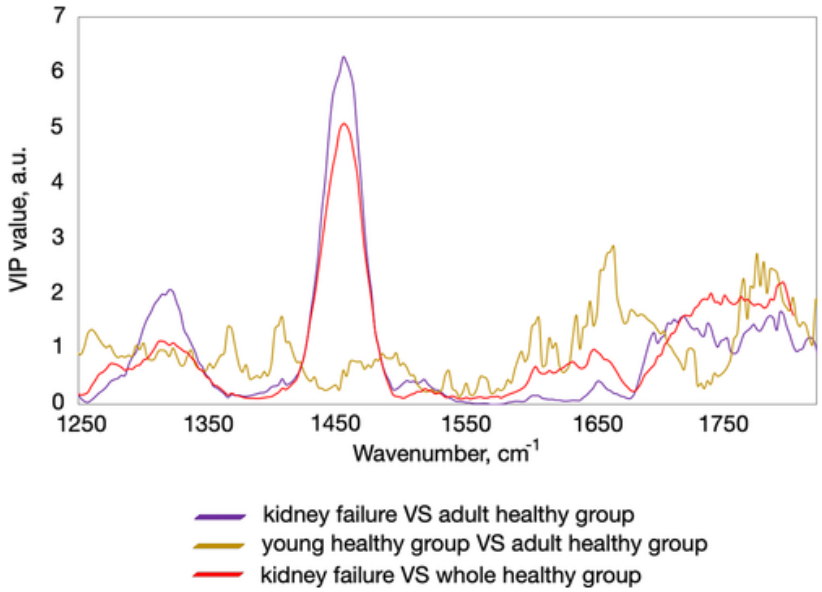

***Figure 1**: VIP-scores of the Raman spectra matrices for: "kidney failure vs adult healthy group" PLS-DA model, "young healthy group vs adult healthy group" PLS-DA model, "kidney failure vs whole healthy group" PLS-DA model*

Application of SERS technique for the analysis of blood serum led to the ROC AUC of 0.983 (0.969 – 0.997; 95%CI) for the discrimination of healthy individuals and patients with kidney failure. The most important Raman bands that helps to achieve such performance of PLS-DA classification models are highlighted in Figure 2. For SERS we observe strongly enhanced bands which may be attributed to biochemical components such as nucleic acids (641, 724, 813, 1003, 1210, 1132 and 1450 cm^{-1}), carbohydrates (641, 890 and 1094 cm^{-1}) and lipids (1278 and 1327 cm^{-1}). Several of these bands clearly stand out by the impact of SERS technique at (724, 813, 890, 961 and1132 cm^{-1}) because such bands were undetectable by conventional Raman spectroscopy due to weak intensity. The SERS spectrum of serum with silver nanoparticles showed many dominant vibration bands, indicating a strong interaction between the silver colloids and the serum substances.

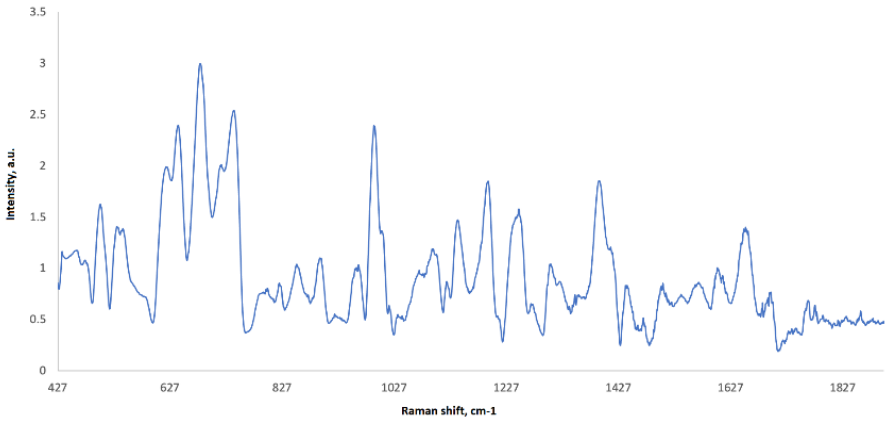

***Figure 2**: VIP-scores of the Raman spectra matrices for discrimination of kidney failure and healthy individuals based on SERS analysis of blood serum*

CONCLUSION

Raman-based optical and liquid biopsy may be promising in non-communicable diseases identification, as it provides fast and rapid diagnosis. The classification performance can be further improved by using more complex analysis approaches as neural network algorithms of Raman spectra analysis [6] or by adding complementary information to the analysis (such as patients' demographics [7]). Important to note, that the proposed approach may be combined with other optical techniques for more precise diseases detection. Proposed Raman systems can be tested for their ability to detect other illness (track diabetes [8, 9] or find cancers [10]) and to find tumors in other organs. However, such novel approaches need to be tested in future large multicenter trials.

ACKNOWLEDGEMENTS

This study was supported by Russian Science Foundation grant No. 21-75-10097.

REFERENCES

[1] R.R. Alfano, Y. Pu, Optical biopsy for cancer detection. In: Jelinkova H, editor. Laser for Medical Applications, Cambridge: Woodhead Publishing Limited, p. 325–367. 2013. https://doi.org/10.1001/archderm.137.12.1627.

[2] Y.A. Khristoforova, I.A. Bratchenko, O.O. Myakinin, D.N. Artemyev, A.A. Moryatov, A.E. Orlov, S.V. Kozlov, V.P. Zakharov, Portable spectroscopic system for in vivo skin neoplasms diagnostics by Raman and autofluorescence analysis, Journal of Biophotonics, 12, e201800400, 2019. https://doi.org/10.1002/jbio.201800400.

[3] W. R. Premasiri, J. C. Lee, L. D. Ziegler, Surface Enhanced Raman Scattering of Whole Human Blood, Blood Plasma and Red Blood Cells: Cellular Processes and Bioanalytical Sensing, J Phys Chem B, 116(31), 9376–9386, 2012.

[4] L.A. Bratchenko, I.A. Bratchenko, Y.A. Khristoforova, D.N. Artemyev, D.Y. Konovalova, P.A. Lebedev, V.P. Zakharov, Raman spectroscopy of human skin for kidney failure detection, Journal of Biophotonics, 14(2), e202000360, 2021. https://doi.org/10.1002/jbio.202000360.

[5] D.M. Haaland, E.V. Thomas, Partial least-squares methods for spectral analyses. 1. Relation to other quantitative calibration methods and the extraction of qualitative information, Analytical Chemistry, 60, 1193–1202, 1988. https://doi.org/10.1021/ac00162a020.

[6] R. Arnaout, L. Curran, Y. Zhao, J.C. Levine, E. Chinn, A.J. Moon-Grady, An ensemble of neural networks provides expert-level prenatal detection of complex congenital heart disease, Nature Medicine, 27, 882–891, 2021. https://doi.org/10.1038/s41591-021-01342-5.

[7] J. Zhao, H. Zeng, S. Kalia, H. Lui, Incorporating patient demographics into Raman spectroscopy algorithm improves in vivo skin cancer diagnostic specificity. Translational Biophotonics, 1(1-2), e201900016, 2019. https://doi.org/10.1002/tbio.201900016.

[8] E. Guevara, J.C. Torres-Galván, M.G. Ramírez-Elías, C. Luevano-Contreras, F.J. González, Use of Raman spectroscopy to screen diabetes mellitus with machine learning tools, Biomedical Optics Express, 9(10), 4998–5010, 2018. https://doi.org/10.1364/BOE.9.004998.

[9] F.R. Paolillo, V.S. Mattos, A.O. de Oliveira, F.E.G. Guimarães, V.S. Bagnato, J.C. de Castro Neto, Noninvasive assessments of skin glycated proteins by fluorescence and Raman techniques in diabetics and nondiabetics, Journal of Biophotonics, 12(1), e201800162, 2019. https://doi.org/10.1002/jbio.201800162.

[10] I.A. Bratchenko, L.A. Bratchenko, A.A. Moryatov, Y.A. Khristoforova, D.N. Artemyev, O.O. Myakinin, A.E. Orlov, S.V. Kozlov, V.P. Zakharov, In vivo diagnosis of skin cancer with a portable Raman spectroscopic device. Experimental Dermatology, 30(5), 652-663, 2021. https://doi.org/10.1111/exd.14301.

IMPROVING STEM CELL DIFFERENTIATION USING NEAR-INFRARED AND GREEN IRRADIATION

DOI 10.24412/cl-36896-2021-1-76-76

ANINE CROUS, DANIELLA DA SILVA, MADELEEN JANSEN VAN RENSBURG and HEIDI ABRAHAMSE

[1]*Laser Research Centre, Faculty of Health Sciences, University of Johannesburg, South Africa*

acrous@uj.ac.za

ABSTRACT

Degenerative disorders, which include osteoporosis and Alzheimer's disease, are characterized by a progressive decline in normal cell or tissue function. Transdifferentiation of adipose-derived mesenchymal stem cells (ADMSCs) into multiple cell lineages, including neurons and osteoblasts, is possible. It has been demonstrated that photobiomodulation can optimize this process (PBM). The use of genetically modified immortalized ADMSCs (iADMSCs) cells provides accessibility by overcoming ethical problems and facilitates continuous cell culture proliferation. In this comparative study, the effects of PBM, using 5 J/cm^2 at 825 nm and/or 525 nm consecutively were determined on the differentiation potential of iADMSCs to determine the most effective wavelength of PBM to induce differentiation into neurons and osteoblasts. iADMSCs were characterized using their surface protein markers CD44/90/166 and induced to differentiate into neuronal cells or osteoblasts. iADMSCs stem cell markers were characterized using flow cytometry. Morphological changes were examined, and biochemical assays performed including LDH cytotoxicity assay, reactive oxygen species (ROS) production, trypan blue viability and ATP proliferation. Transdifferentiation of iADMSCs using various trans-differentiation inducers and PBM therapy showed promise. Neuronal transdifferentiation was observed through the decrease in stem cell markers after characterization. Observations of morphology showed changes in PBM treated groups from that of the standard, where the cells showed rounding and synaptic protrusion development. There was an overall increase in cytotoxicity indicative of membrane permeabilization when using all irradiation parameters, signifying transdifferentiation. An increase in ROS production was noted when using 525 nm irradiation, cell viability was maintained throughout the experimental groups, with a significant increase when using consecutive irradiation. Cell proliferation was increased when subjected to 825 nm irradiation, however the use of 525 nm and the consecutive use of 825 nm and 525 nm did lead to a decrease in proliferation, signifying differentiation. Osteoblast transdifferentiation was also seen by a decrease in stem cell marker expression. A noticeable change in cell morphology started to occur for all experimental groups after 24 hours, over time it was seen that 525 nm and consecutive PBM treatments had the most change in morphology seen by a rounded-up cell shape like that of osteoblasts. Biochemical analysis revealed no increase in cytotoxicity or ROS for all experimental groups after 48 hours, after 7 days significant increases where noted, that can be ascribed to contact inhibition. Cell viability was maintained over time and a decrease in cell proliferation was noted in experimental samples where 525 nm and consecutive irradiation had the greatest decrease in proliferation. We suggest that consecutive use of green and NIR PBM along with growth inducers offer a better solution of transdifferentiating iADMSCs to neurons and osteoblasts. Findings from this research will serve as contribution toward validating stem cell technology for application in in vivo, pre-clinical and clinical research settings.

KEYWORDS: Photobiomodulation; Transdifferentiation; Adipose Derived Mesenchymal Stem Cells; Osteoblasts; Neurons

ACKNOWLEDGEMENTS

This work was supported by the National Research Foundation (NRF) S&F -Scarce Skills Postdoctoral Fellowship (Grant no: 120752) received by Anine Crous; the Global Excellence and Stature, Fourth Industrial Revolution (GES 4.0) Postgraduate Scholarship received by Madeleen Jansen van Rensburg and the South African Research Chairs Initiative of the Department of Science and Technology and National Research Foundation of South Africa (SARChI/NRF-DST) (Grant no: 98337), received by Heidi Abrahamse and Daniella Da Silva.

VORTEX BEAM-BASED RAMAN SPECTROSCOPY FOR CELL MEMBRANE STUDIES

DOI 10.24412/cl-36896-2021-1-77-77

GHANASHYAM C, ASEEFHALI BANKAPUR*, SANTHOSH CHIDANGIL
Department of Atomic and Molecular Physics, Manipal Academy of Higher Education, Manipal-576104, India
asif.bankapur@manipal.edu

ABSTRACT
Spiral phase plate (SPP) is an optical element with an optical thickness that varies with azimuthal angle so that the incident beam arises with a spiral phase front. Thus, a Gaussian beam incident on SPP emerges out as a vortex beam having a central null region with doughnut shape intensity distribution. Herein we mainly concentrate on initial result obtained when an SPP is introduced into a micro-Raman setup. Beam profiling of the vortex beam was done at focus of a biconvex lens and compared with the Gaussian beam profile obtained at the same point. Images of the vortex beam were taken at the focus of the microscope objectives using the NIS-D elements software. The inner and outer diameter was measured to choose the appropriate sample for our studies. Raman spectrum of Tylenol was obtained using vortex beam and found that vortex beam was able to reproduce all the peaks recorded using the Gaussian beam. A dye-polystyrene system was prepared, and experiments were performed to show that using vortex beam Raman signals can be obtained exclusively from the boundaries.
Keywords: Spiral Phase Plate, Vortex beam, Raman spectrum, Dye-polystyrene system

A MULTIMODAL APPROACH TO NON-INVASIVE DIAGNOSIS OF BASAL CELL CARCINOMA: A PILOT STUDY

DOI 10.24412/cl-36896-2021-1-78-80

ELINA GENINA[1,2], YANA KUZINOVA[3], YURY SURKOV[1,2], ISABELLA SEREBRYAKOVA[1,2], EKATERINA LAZAREVA[1,2], OLGA KONOPATSKOVA[3], ALI ANSARY[4], VALERY TUCHIN[1,2,5]

[1]*Optics and Biophotonics Department, Saratov State University, Saratov, Russia*
[2]*Laboratory of laser molecular imaging and machine learning, Tomsk State University, Tomsk, Russia*
[3]*Department of Faculty Surgery, Saratov State Medical University, Saratov, Russia*
[4]*Laser and Plasma Research Institute, Shahid Beheshti University, Tehran, Iran*
[5]*Laboratory of Laser Diagnostics of Technical and Living Systems, Institute of Precision Mechanics and Control, FRC "Saratov Scientific Centre"of the Russian Academy of Sciences, Saratov, Russia*
eagenina@yandex.ru

ABSTRACT

Despite the development of medicine, cancer remains one of the most dangerous diseases nowadays. The detection and treatment of cancer is one of the most challenges for medicine in the twenty-first century. An effective solution of the problem is the use of modern interdisciplinary technologies. Most often, if the tumor is diagnosed earlier and treated, the patient will have a better prognosis and much greater opportunities for complete recovery. Many recent technological innovations have used physics principles, such as optics and coherent photonics, to improve early diagnostic and therapeutic procedures to reduce cancer incidence and mortality [1]. In this study, the development of technologies for biomedical imaging of skin cancer is presented.

Skin cancers are due to the development of abnormal cells that have the ability to invade or spread to other parts of the body. There are three main types of skin cancers: basal-cell carcinoma (BCC), squamous-cell carcinoma (SCC), and melanoma. BCC is the most common epithelial neoplasms of the skin, accounting for 45-90% of all malignant epithelial tumors of this localization [2]. BCC consists of cells similar to the cells of the basal layer of the epidermis. It differs from other skin cancers by extremely rare metastasis, but it is capable of extensive local growth, which leads to significant cosmetic and functional disorders [3].

In this pilot study, a combination of high–resolution ultrasound examination and optical methods (Raman spectroscopy, optical coherence tomography (OCT), and diffuse reflectance spectroscopy) were used.
The study involved light-skinned volunteers with basal cell carcinoma and benign neoplasms and volunteers with high pigmented health skin. Informed consents were acquired from all patients prior to the study. Enrolled patients' age ranged from 48 to 78 years. Enrolled patients were 2 Caucasian males and 7 females. Differentiation of neoplasms was carried out using morphological research: basal cell carcinoma (7 lesions) and benign neoplasms (2 lesions).

Ultrasound DUB SkinScanner (tpm taberna pro medicum GmbH, Germany) was used in the initial management of neoplasms (including helping in the differential diagnosis and measurement of thickness). High resolution ultrasound imaging systems enabled ultrasound to differentiate structures of less than 100 microns on the beam axis (axial resolution) and 200 microns on the scan axis (resolution axis). The frequency ranges 33 and 75 MHz, allowed visualisation of the superficial layer of the skin (epidermis and dermis, and the upper part of hypodermis), where the majority of lesions and skin tumors were located. Figures 1 show photography of the superficial BCC from smartphone and dermascope, and ultrasonic images with different resolutions.

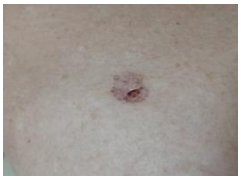

Real photo of BCC
(a)

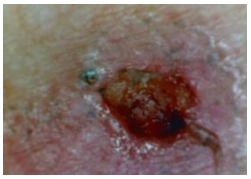

Macro-photo
(b)

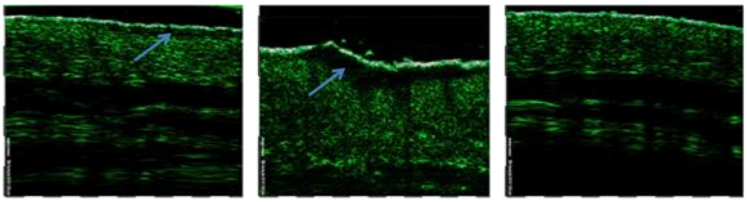

(c)

Figure 1: *Photography of the superficial BCC from (a) smartphone and (b) dermascope, and (c) ultrasonic images with different resolutions.*

It is well seen the borders of the tumors. Real sizes were evaluated. For example, for the superficial BCC the depth was evaluated from 0.45 to 0.74 mm in different sites, for pigmented BCC it was from 0.2 to 0.71 mm, and for pigmented benign neoplasm it was about 2.22 mm.

Neoplastic cells are characterized by increased nuclear material, an increased nuclear-to-cytoplasmic ratio, increased mitotic activity, abnormal chromatin distribution, and decreased differentiation. There is a progressive loss of cell maturation, and proliferation of these undifferentiated cells results in increased metabolic activity. General features of neoplastic cells result in specific changes in nucleic acid, protein, lipid, and carbohydrate quantities and/or conformations. For the study we used Raman spectrometer QE65000 (Ocean Optics, USA) with diode laser 785 nm (Ocean Optics, USA) and probe.

The original analyses for Raman signals are based on differences in intensity, shape, and location of the various Raman bands between normal and cancerous cells and tissues. However, there are no distinctive Raman peaks or bands that can be uniquely assigned to BCC by visual inspection alone. The development of the malignant skin disease increases the content of metabolic products in the pathological areas of the skin, changes the concentration of proteins and lipids. Proteins predominantly contributes to the appearance of bands in the spectral range 1240–1270, 1340, 1440–1460, and 1665 cm^{-1}, the spectral features arising from the contribution of lipids, are observed in the 1271–1301, 1440, 1650–1660 cm^{-1} bands. One of the significant differences between malignant and benign formations is the process of metabolism and destruction of collagen. Cells of malignant tumors form fast-growing, low-differentiated structures, and the development of such structures is accompanied by the increased activity of collagenase. Collagenase destroys the molecular bonds of collagen fibers, and changes in Raman spectra of skin tissue can be observed in 1248, 1454, and 1665 cm^{-1} bands associated with peaks of collagen [4].

In the BCC, there was an increased content of proteins (430, 475) and nucleic acids (622, 685), a decreased content of lipids (1287, 1419) and keratin (1463, 1670). Increased peaks associated with DNA (755) and cell nuclei (831).
Optical coherence tomography is used for preoperative determination of the peripheral boundaries of BCC in order to choose the optimal treatment method and minimize the invasiveness of surgical intervention. OCT is characterized by high efficiency for the *in vivo* diagnosis of malignant and benign skin tumors. OCT B-scans were obtained using the GAN930V2-BU spectral OCT (Thorlabs, USA) operating at a central wavelength of 930 nm with axial and lateral resolutions of 6.00 and 7.32 μm, respectively, and a scanning depth of 2 mm. OCT was used for *in vivo* differential diagnosis between benign skin neoplasms and BCC. It was well seen different heterogeneity of skin structures. We used aqueous 70%-glycerol solution for increasing the probing depth of OCT. Enhancers of epidermis permeability was not used because the epidermal barrier was injured and not prevented diffusion of OCA and water. It was well seen that after 10 minutes the optical probing depth increased in 1.5-2 times and visualization of heterogeneities characteristic of basal cell carcinoma has been improved (fig. 2).

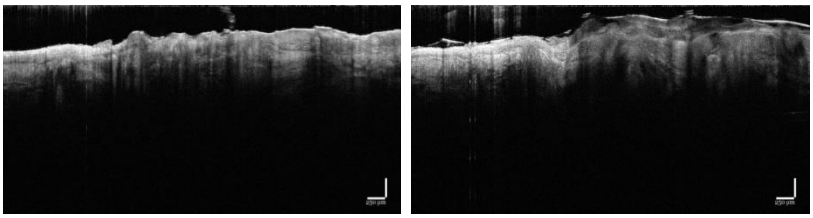

(a) (b)

Figure 2: *OCT-scans of skin with BCC (a) before optical clearing and (b) in 10 min after 70%-glycerol application.*

Diffuse backscattered spectroscopy is well suited for use in biomedical applications due to its low instrumentation cost and easy implementation. Reflectance measurement is a function of optical scattering and absorption. The primary sources of scattering in skin include collagen, mitochondria, melanin, and cell nuclei. Hemoglobin and melanin are the primary sources of absorption in skin. Diffuse reflectance was measured in the range of 400 - 2150 nm using both USB4000-UV-VIS and NIRQUEST spectrometers (Ocean Optics, USA) equipped with QR400-7-VIS-NIR fiber optic

probes (Ocean Optics, USA). Determined by visual inspection, BCC contributed to reflectance spectral intensity and spectral slope. It was founded that areas of the skin most affected by basal cell carcinoma had lower reflectance intensities compared with normal skin.

Thus, the sizes of neoplasms were evaluated using ultrasound examination, and their internal structure was visualized using OCT in combination with optical clearing. Diffuse reflectance extracted physiological parameters such as hemoglobin content, oxygen saturation, and tissue microarchitecture. Raman spectroscopy was helpful for determining lipid, nuclear, and protein content. Our results demonstrated the ability of these modalities to quantitatively assess tissue biochemical, structural, and physiological parameters that could be used to determine tissue pathology.

The study was funded by RFBR, project number 20-52-56005, and the grant under the Degree of the Government of the Russian Federation No. 220 of 09 April 2010 (Agreement No. 075-15-2021-615 of 04 June 2021).

REFERENCES

[1] L. Lim, B. Nichols, M.R. Migden, N. Rajaram, J.S. Reichenberg, M.K. Markey, M.I. Ross, J.W. Tunnell, Clinical study of noninvasive in vivo melanoma and nonmelanoma skin cancers using multimodal spectral diagnosis, J. Biomed. Opt. 117003, 2014.

[2] MedElement. Clinical protocols. Skin Cancer. https://diseases.medelement.com/disease/рак-кожи-2018/16198, 2021.

[3] G. Paolino, M. Donati, D. Didona, S.R. Mercuri, C. Cantisani, Histology of Non-Melanoma Skin Cancers: An Update, Biomedicines, 71, 2017.

[4] I.A. Bratchenko, L.A. Bratchenko, A.A. Moryatov, Yu.A. Khristoforova, D.N. Artemyev, O.O. Myakinin, A.E. Orlov, S.V. Kozlov, V.P. Zakharov, In vivo diagnosis of skin cancer with a portable Raman spectroscopic device, Experimental Dermatology, 652–663. 2021.

MATHEMATICAL MODEL OF CALCIUM-DEPENDENT GLYCEMIC CONTROL COMPONENTS IN HEPATOCYTES

DOI 10.24412/cl-36896-2021-1-81-83

OKSANA TILINOVA[1], ARINA MARTYSHINA[1], SOFIA KISIL[2], MIKHAIL YAMASHEV[3], IRINA DOKUKINA[1], AND EUGENE GRACHEV[3]

[1] *Physics department Sarov Physics and Technology Institute, National Research Nuclear University MEPhI, Russia*
[2]*Biology department, Lomonosov Moscow State University, Russia*
[3]*Physics department, Lomonosov Moscow State University, Russia*

ivdokukina@mephi.ru

ABSTRACT

The liver can adjust to the current state of the body. The metabolic flexibility of the liver is a mechanism that allows it to keep the glucose level in the blood stable, both in the fasting state and after a meal [1]. In this work, we improved our previously published model of Ca2+-signaling in hepatocytes [2] by including glucose and lipid metabolism. The new model follows principles of the law of acting masses and chemical kinetics. The influence of dysfunctional Ca2+-signaling and deviations of the major lipid metabolism processes from normal on the plasma glucose level and other components of the glycemic control system are studied. The key factors leading to deviations in the work of the glycemic control system in hepatocytes, the connection between them, and possible consequences are identified.

In response to an increase in the blood glucose level, beta-cells of the pancreas produce insulin through exocytosis. There are three insulin-dependent mechanisms of lowering blood glucose levels: the transition of excess glucose to glycogen, glucose oxidation (glycolysis), and synthesis of fatty acids (lipogenesis). The result of lipogenesis is the release of very-low-density lipoproteins in the blood plasma, which will be used by the body to meet its energy needs [3].
During fasting, the blood glucose level gradually decreases, and insulin doesn't affect hepatocytes anymore. Instead, glucose is released from glycogen stores. In addition, the synthesis of glucose from alternative substrates, such as, for example, glycerol, known as gluconeogenesis, is started. Ca2+ ions are also one of the critical regulators of glucose metabolism in hepatocytes [4] (Fig.1).

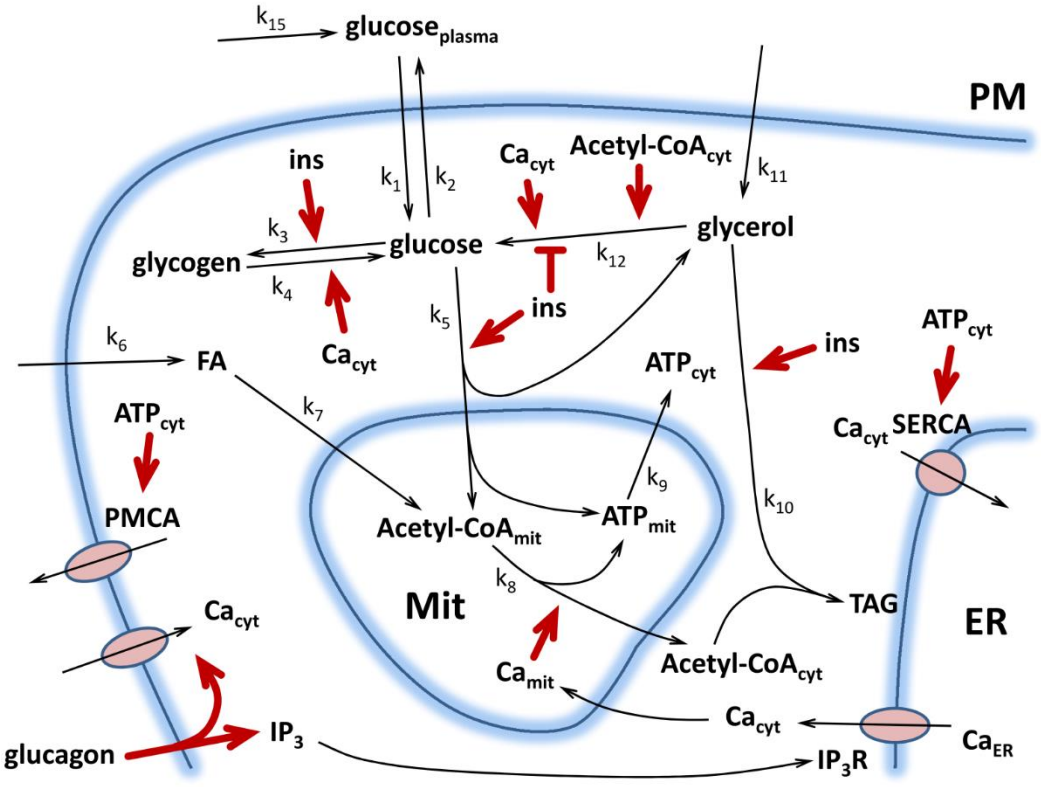

Figure 1: *Process diagram of the hepatocyte.*

The present model is based on one of our previous models. Insulin resistance in hepatocytes is one of the earliest factors of developing type II diabetes. Previously we studied key factors in developing insulin resistance in hepatocytes and suggested the hypothesis about the dominant role of both the modulation of IP3-receptors and the inability of mitochondria to form mitochondria-associated membranes (MAMs) with the endoplasmic reticulum in the disease development. The combination of the modulation of IP3-receptors and the inability of the mitochondria to form MAMs leads to a significant increase in the concentration of cytosolic Ca2+. We assumed that the increase in cytosolic Ca2+ leads to an increase in hepatic glucose release. To check this, we improved the model [2] by taking both glucose and lipid metabolisms into account.

In the previous work, we constructed a mathematical model that allowed us to study the individual contribution of each of the assumed factors to the development of hepatocyte insulin resistance. It was assembled from a combination of well-established models of IP3-receptor dynamics and mitochondrial impact on cytosolic Ca2+ signaling. The present mathematical model is based on a process diagram using the principles of the law of acting masses and chemical kinetics. Sigmoidal functions were used to describe the dependencies of major processes rates on insulin and other factors. The influence of the parameters of these functions, which are responsible for the amplitude and sharpness of the transition, was investigated in this work. The influence of deviations in calcium signaling and the regulation of lipid metabolism from the norm was studied. In particular, we investigated the effect of insulin on:

- the glycolysis rate;
- the glycogen synthesis rate;
- the gluconeogenesis rate.

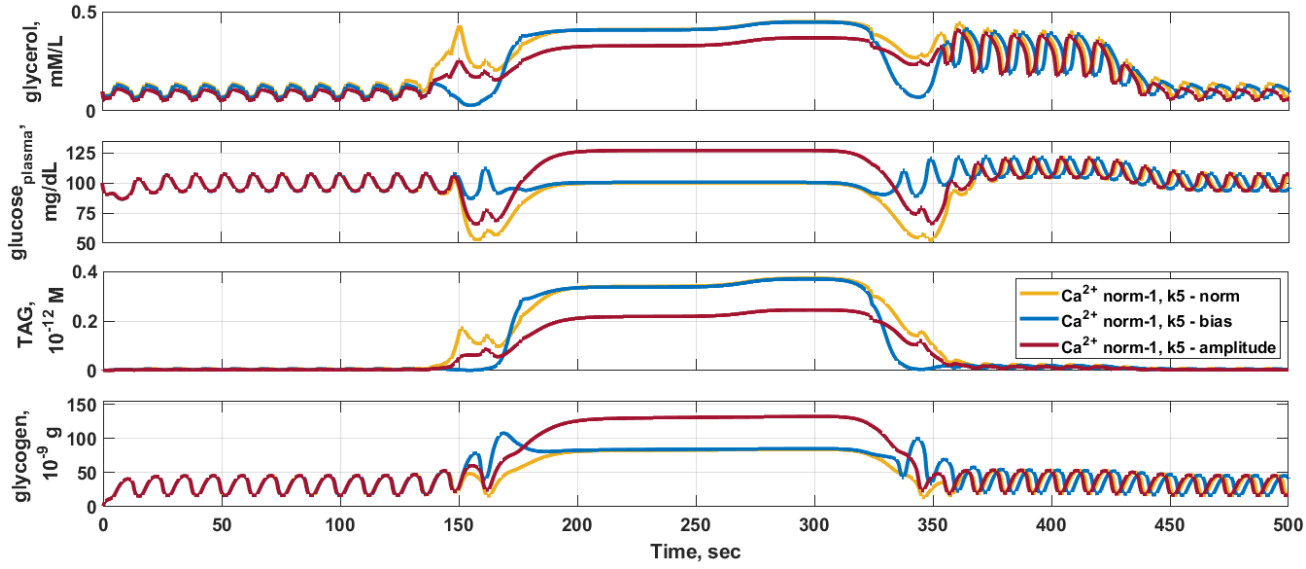

Figure 2: *The effect of insulin on glycolysis rate at normal Ca2+ signalling.*

The modeling results agree with modern concepts of the processes of synthesis, storage, and metabolism of glucose in hepatocytes. It was shown (Fig. 2) that:

- only the rate of glycolysis in dependence on insulin has a significant effect on the plasma glucose level (100 -> 125);
- a decrease in the effect of insulin on glycolysis leads not only to an increase in the concentration of glucose in the blood but also to an increase in glycogen stores during the meal and a decrease in the concentration of glycerol and triacylglycerol (TAG), in other words, to a decrease in further lipid storage.

It was also shown (Fig. 3) that:

- a decrease in the amplitude of the dependence of the glycolysis rate on insulin combined with dysfunctional Ca2+-signalling leads to an even greater increase in the concentration of glucose in the blood (100 -> 150);
- by themselves, dysfunctional Ca2+-signalling during normal insulin action does not cause any changes in blood glucose levels. Still, it does stimulate the production of glycerol and TAG; in other words, it leads to a potential increase in lipid storage and further obesity development.

Thus, in this work, the previously published model of Ca2+-signalling in hepatocytes has been improved by modifying the model, so that glycolipid metabolism is included. Modeling results are well reconciled with known concepts of hepatocytes storage, release, and metabolism. The model allows improving our understanding of metabolic pathologies.

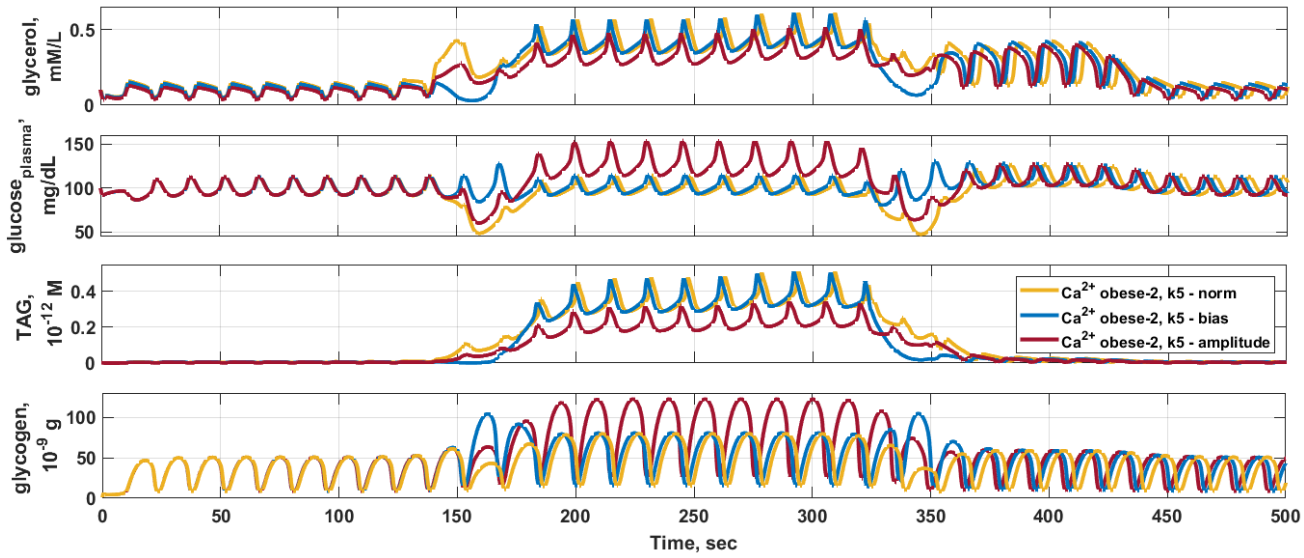

Figure 3: *The effect of insulin on glycolysis rate at dysfunctional Ca2+ signalling.*

REFERENCES

[2] Theurey, P., Tubbs, E., Vial, G., Jacquemetton, J., Bendridi, N., Chauvin, M.A., Alam, M.R., Le Romancer, M., Vidal, H., Rieusset, J., 2016. Mitochondria-associated endoplasmic reticulum membranes allow adaptation of mitochondrial metabolism to glucose availability in the liver. J. Mol. Cell Biol. 8 (2), 129–143. https://doi.org/10.1093/jmcb/mjw004

[3] Dokukina, I.V., Yamashev, M.V., Samarina, E.A., Tilinova, O.M., Grachev, E.A., 2021. Calcium-dependent insulin resistance in hepatocytes: mathematical model. J. Theor. Biol. 522, 110684 https://doi.org/10.1016/j.jtbi.2021.110684

[4] Wang, J., He, W., Tsai, P.J., Chen, P.H., Ye, M., Guo, J., Su, Z., 2020. Mutual interaction between endoplasmic reticulum and mitochondria in nonalcoholic fatty liver disease. Lipids in Health and Disease. 19:72 https://doi.org/10.1186/s12944-020-01210-0Bg

[5] Samuel, V., Shulman, G., 2016. The pathogenesis of insulin resistance: integrating signaling pathways and substrate flux. J. Clin. Invest. 126 (1), 12–22. https://doi.org/10.1172/JCI77812

OPTICAL CLEARING AS A TOOL FOR MULTIMODAL TISSUE IMAGING

DOI 10.24412/cl-36896-2021-1-84-85

VALERY TUCHIN

Science Medical Center, Saratov State University, Saratov, Russia
Laboratory of Laser Molecular Imaging and Machine Learning, Tomsk State University, Saratov, Russia
Laboratory of Laser Diagnostics of Technical and Living Systems, Institute of Precision Mechanics and Control, FRC "Saratov Scientific Centre" of the Russian Academy of Sciences, Saratov, Russia
A.N. Bach Institute of Biochemistry, FRC "Fundamentals of Biotechnology" of the Russian Academy of Sciences, Moscow, Russia.

tuchinvv@mail.ru

ABSTRACT

The concepts of multimodality and temporal formation or expansion of optical transparency windows of biological tissues are fruitful tools of the method of immersion optical clearing (IOC) of tissues. The method is based on a controlled and reversible modification of the optical properties of a tissue when exposed to a biocompatible optical clearing agent (OCA). At present, the basics of the method have been studied and the leading mechanisms of IOC have been described [1-4]. These mechanisms determine a significant increase in the efficiency of imaging of almost all known optical imaging tools and laser impact on living tissues. This versatility is due to the fact that the method is aimed at temporary suppression of the fundamental cause that limits the transparency of the tissue and blurs the image of its structures, namely, elastic light scattering in the tissue. As a result, the IOC method makes it possible to enhance the contrast of pathological foci in depth of tissue when imaging living tissues using various optical modalities operating in an ultra-wide wavelength range from deep UV to terahertz. Figure 1 illustrates the main optical methods that benefit significantly from the optical clearing method [1-17].

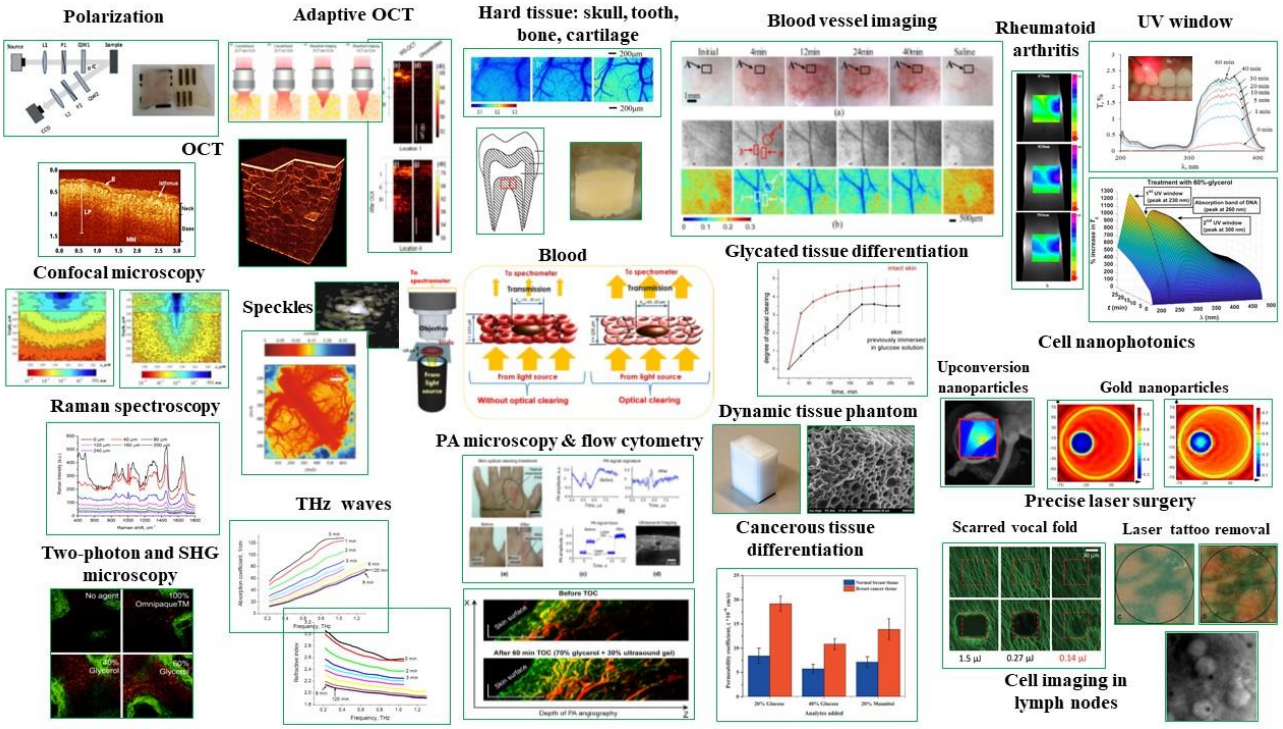

Figure 1: Different optical tools beneficial from the immersion optical clearing method.

It is important to note that the method is well compatible with other widely used imaging modalities such as computed tomography, MRI and ultrasound [6,15,17].

Recently, there has been activity in the field of application of the method in therapeutic technologies, including photodynamic, photocatalytic and photothermal therapies [5, 18, 19].

Unique applications may be in transplantology, since OCAs are known as cryopreservative fluids for transplant storage [3, 20] and can provide a better optical communication channel with smart implants in the human body [21].

ACKNOWLEDGMENTS

The study was funded by the grant under the Degree of the Government of the Russian Federation No. 220 of 09 April 2010 (Agreement No. 075-15-2021-615 of 04 June 2021).

REFERENCES

[1] A.Yu. Sdobnov, M.E. Darvin, E.A. Genina, A.N. Bashkatov, J. Lademann, V.V. Tuchin, Recent progress in tissue optical clearing for spectroscopic application, *Spectrochim. Acta Part A: Mol. Biomol. Spectr.* **197**, 216–229 (2018).

[2] A. N. Bashkatov, K. V. Berezin, K. N. Dvoretskiy, M. L. Chernavina, E. A. Genina, V. D. Genin, V. I. Kochubey, E. N. Lazareva, A. B. Pravdin, M. E. Shvachkina, P. A. Timoshina, D. K. Tuchina, D. D. Yakovlev, D. A. Yakovlev, I. Yu. Yanina, O. S. Zhernovaya, V. V. Tuchin, Measurement of tissue optical properties in the context of tissue optical clearing, *J. Biomed. Opt.* **23**(9), 091416 (2018).

[3] L. Oliveira and V.V. Tuchin, *The Optical Clearing Method: A New Tool for Clinical Practice and Biomedical Engineering*, Springer Nature Switzerland AG, Basel, 2019 – 177 p.

[4] V.V. Tuchin, D. Zhu, and E.A. Genina (Eds.), *Handbook of Tissue Optical Clearing: New Prospects in Optical Imaging*, Taylor & Francis Group LLC, CRC Press, Boca Raton, FL, 2022 – 688 p.

[5] V.V. Tuchin, E.A. Genina, E.S. Tuchina, A.V. Svetlakova, Y.I. Svenskaya, Optical clearing of tissues: issues of antimicrobial phototherapy and drug delivery, *Advanced Drug Delivery Reviews* **180**(1), 114037 (2022).

[6] N.I. Kazachkina, V.V. Zherdeva, I.G. Meerovich, A.N. Saydasheva, I.D. Solovyev, D.K. Tuchina, A.P. Savitsky, V.V. Tuchin, A.A. Bogdanov Jr., "MR and fluorescence imaging of gadobutrol-induced optical clearing of red fluorescent protein signal in an in vivo cancer model, *NMR Biomed.* e4708-1–13 (2022).

[7] A. Jaafar, R. Holomb, A.Y. Sdobnov, Z. Ocskay, Z. Jakus, V.V. Tuchin, M. Veres, Ex vivo confocal Raman microspectroscopy of porcine *dura mater* supported by optical clearing, *J. Biophotonics* **15** (1), e202100332 (2022).

[8] S.M. Zaytsev, M. Amouroux, G. Khairallah, A.N. Bashkatov, V.V. Tuchin, W. Blondel, E.A. Genina, Impact of optical clearing on ex vivo human skin optical properties characterized by spatially resolved multimodal spectroscopy, *J. Biophotonics* **15**(1), e202100202 (2022).

[9] Z. Wei, Q. Lin, E.N Lazareva, P.A. Dyachenko (Timoshina), J. Yang, Y. Duan and V.V Tuchin, Optical clearing of laser-induced tissue plasma, *Laser Phys. Lett*. **18**, 085603-1–7 (2021).

[10] P. Listewnik, M. Ronowska, M. Wasowicz, V.V. Tuchin, M. Szczerska, Porous phantoms mimicking tissues—Investigation of optical parameters stability over time, *Materials* **14**, 423-1–11 (2021).

[11] P.A. Dyachenko, L.E. Dolotov, E.N. Lazareva, A.A. Kozlova, O.A. Inozemtseva, R.A. Verkhovskii, G.A. Afanaseva, N.A. Shushunova, V.V. Tuchin, E.I. Galanzha, and V.P. Zharov, Detection of melanoma cells in whole blood samples using spectral imaging and optical clearing, *IEEE J. Selec. Tops Quant. Electr.* **27** (4), 7200711-1–11 (2021).

[12] I. Carneiro, S. Carvalho, R. Henrique, A. Selifonov, L. Oliveira, V.V. Tuchin, Enhanced ultraviolet spectroscopy by optical clearing for biomedical applications, *IEEE J. Selec. Tops Quant. Electr.* **27** (4), 7200108-1–8 (2021).

[13] Q. Lin, E.N. Lazareva, V.I. Kochubey, Y. Duan, V.V. Tuchin, Kinetics of optical clearing of human skin studied in vivo using portable Raman spectroscopy, *Laser Physics Letters* **17** (10), 105601(2020).

[14] G.R. Musina, I.N. Dolganova, N.V. Chernomyrdin, A.A. Gavdush, V.E. Ulitko, O.P. Cherkasova, D.K. Tuchina, P.V. Nikitin, A.I. Alekseeva, N.V. Bal, G.A. Komandin, V.N. Kurlov, V.V. Tuchin, K.I. Zaytsev, Optimal hyperosmotic agents for tissue immersion optical clearing in terahertz biophotonics, *J. Biophotonics* **13**(12), e202000297 (2020).

[15] D.K. Tuchina, I.G. Meerovich, O.A. Sindeeva, V.V. Zherdeva, A.P. Savitsky, A.A. Bogdanov Jr, V.V. Tuchin, Magnetic resonance contrast agents in optical clearing: Prospects for multimodal tissue imaging, *J. Biophotonics* **13**(11), e201960249 (2020).

[16] M.V. Novoselova, T.O. Abakumova, B.N. Khlebtsov, T.S. Zatsepin, E.N. Lazareva, V.V. Tuchin, V.P. Zharov, D.A. Gorin, E.I. Galanzha, Optical clearing for photoacoustic lympho- and angiography beyond conventional depth limit in vivo, *Photoacoustics* **20**, 100186 (2020).

[17] E.A. Genina, Y.I. Surkov, I.A. Serebryakova, A.N. Bashkatov, V.V. Tuchin, V.P. Zharov, Rapid ultrasound optical clearing of human light and dark skin, *IEEE Trans. Med. Imag.* **39** (10), 3198–3206 (2020).

[18] L. Pires, V. Demidov, B.C. Wilson, A.G. Salvio, L. Moriyama, V.S. Bagnato, I.A. Vitkin, C. Kurachi, Dual-agent photodynamic therapy with optical clearing eradicates pigmented melanoma in preclinical tumor models, *Cancers* **12**, 1956 (2020).

[19] A. Bucharskaya, N. Khlebtsov, B. Khlebtsov, G. Maslyakova, N. Navolokin, V. Genin, E. Genina, V. Tuchin, Photothermal and photodynamic therapy of tumors with plasmonic nanoparticles: Challenges and prospects, *Materials* **15**, 1606 (2022).

[20] S. Bojic, A. Murray, B.L. Bentley, R. Spindler, P. Pawlik, J.L. Cordeiro, R. Bauer, and J. Pedro de Magalhães, Winter is coming: the future of cryopreservation, *BMC Biology* **19**, 56 (2021).

[21] J. Kim, J. Seo, D. Jung, T. Lee, H. Ju, J. Han, N. Kim, J. Jeong, S. Cho, J. H. Seol, and J. Lee, Active photonic wireless power transfer into live tissues, *PNAS* **117** (29), 16856–16863 (2020).